



Università degli Studi della Basilicata

Dottorato di Ricerca in
“Ingegneria per l’innovazione e lo sviluppo sostenibile”

TITOLO DELLA TESI

“Use of innovative technologies and nanomaterials in the hydrocarbon production and processing cycle”

Specific area: application of expanded graphite materials in adsorption of organic pollutants and oily content of produced water

Settore Scientifico-
Disciplinare
“ICAR/03”
Nov-2023

Coordinatrice del Dottorato: Prof. Aurelia Sole

Relatore: Prof. Donatella Caniani

Dottorando: Dott. Alireza Faraji

Ciclo XXXV

Abstract

The issue of managing oil-contaminated aqueous solutions has received considerable attention in recent years, primarily because of its environmental and industrial implications. The pollution of aquatic ecosystems resulting from oil spills, industrial effluents, and produced water has emerged as a significant concern, presenting risks to both the natural environment and human well-being. To overcome these challenges, there has been a focus on research endeavors aimed at the advancement of efficient and ecologically viable techniques for the removal of oil. In the offshore oil fields, the produced water is often transferred by pipes to offshore infrastructure, where it passes various treatment processes. Produced water is often managed by either re-injection into wells and oil fields or reusing it to enhance oil recovery (EOR) purposes. The composition of produced water often includes hydrocarbons (oil and gas), as well as a mixture of salts, inorganic compounds, and organic substances. Typically, it includes a varying range of total organic carbon (TOC) compounds. In the context of pre-treatment for membrane processes, it is typical to carry out three stages of hydrocarbon-removal operations. These phases include primary oil-water separation, where the oil concentration is typically below 500 mg L^{-1} , followed by secondary oil-water separation. Finally, tertiary oil-water separating is conducted to achieve an oil concentration level below $15\text{-}30 \text{ mg L}^{-1}$. If considered necessary, further post-processes, including advanced methods such as reverse osmosis (RO) or nanofiltration (NF) membrane separation, can be implemented.

Among different removal methods and adsorbents, expanded graphite (EG) is a low-density and mesoporous carbon-based material. It can adsorb organic compounds selectively owing to its hydrophobic nature and weak polarity. This work aimed at the evaluation and application of expanded graphite materials for tackling the oily hydrocarbon in an aqueous solution. Different materials based on EG were applied to organic dye and oil contents differently (dissolved and floating on the water) by employing batch and fixed bed column approaches. EG materials were characterized physically, such as BET surface area, and the results were discussed accordingly.

DEDICATION

I dedicate my dissertation work:

To my wife, **Shiva Radfar**, for her love, support, and belief in me.
Without her, I would not be the person I am today.

To my **parents and my family**

For their infinite support and love

ACKNOWLEDGMENTS

I want to express my sincere appreciation to my advisor Prof. Donatella Caniani, for her help, guidance, and enthusiasm. Also, I would like to thank Prof. Salvatore Masi and Prof. Tanju Karanfil for their expertise and support and Dr. Gamze Ersan and Prof. Giovanni Esposito for serving as reviewers of my thesis. My sincere thanks to Dr. Marco Cuccarese and all colleagues at the University of Basilicata and Clemson University for our life and research discussion.

There are not enough words to express my feelings for following people. I am also very grateful to Dr. Shiva Radfar for always being there for me and helping me in many ways. I am very grateful to my parents and sisters for their support and knowledge and time.

I want to say thank you to all ENI staff and colleagues (Dr and PhDs: Delfina Bersano, Lucilla Del Gaudio, Michela De Simoni, Vera Di Finizio, Olga Shapran, Sara Scagliotti, Luciano Montanari, and Stefano Andrea Nava) for their support and funding this work.

Last but not least, I would like to thank all the engineering department members of UNIBAS and the EEES staff of Clemson University for their help and friendship.

Table of Contents

List of abbreviations	14
Chapter 1: Introduction	16
1.1 Background and Context.....	17
1.2 Constituents of Produced Water	18
1.3 Environmental effect of PW components	20
1.4 Research Problem	21
1.5 Research goals	21
1.5.1 Assessment of adsorption efficiency:	22
1.5.2 Optimization of Operating Parameters:	22
1.5.3 Mechanistic Understanding:	22
1.5.4 Comparative study of various EG types:	23
1.6 Research hypotheses and questions	23
1.7 Significance of the study.....	24
Chapter 1 References	26
Chapter 2: Literature review	28
2.1 PW components	29
2.1.1 Inorganic Salts:	29
2.1.2 Oil and BTEX:	29
2.1.3 Organic acids:	30
2.1.4 Metals and radioisotopes:	30
2.2 Adsorption conception and process	32
2.3 The basic principles of adsorption	34
2.4 Expanded graphite (EG)	35
2.4.1 Summary of graphite exfoliation:	36
2.5 Efficient parameters in the adsorption process of carbon materials for oily contents and organic contaminations and mechanism of adsorption	38

2.5.1 Porosity:	38
2.5.2 Surface area:.....	38
2.5.3 Bulk density and pore volume:	38
2.5.4 Target pollutant characteristic:	39
2.5.5 The temperature of oil contents:	39
2.5.6 Contact time:.....	40
2.5.7 Initial concentration of adsorbate:	40
2.5.8 Salinity:.....	40
2.6 Literature Review on the Removal of PW Components.....	42
2.6.1. Oily contents and hydrocarbon removal:.....	42
2.6.2 Literature review on adsorption of heavy metals, BTEX, and organic acids:	47
2.6.2.1 Heavy metals removal.....	47
2.6.2.2 BTEX removal	48
2.6.2.3 Removal of organic acids.....	49
2.7 Experimental Methodology for the Synthesis of EG.....	50
2.8. organic pollutant and dye removal literature review	52
Chapter 2 References	57
Chapter 3: Material and Methodology	64
3.1 Model molecules, adsorption materials, and chemicals.....	64
3.1.1 Methylene Blue:.....	65
3.1.2 Crude oil:	65
3.1.3 Adsorbent and materials used:	66
3.1.3.1 Encapsulation process of EG powder and making granular forms.....	66
3.1.3.2 Experimental plan of G-EG preparation	67
3.1.4 Materials and reagents	68
3.2 Fourier Transform Infrared Spectrometer (FT-IR) analysis	68
3.3 Elemental Analysis	70

3.4 BET surface area and pore size distribution analysis	71
3.5 UV-VIS spectrophotometer	72
3.6 Ion chromatography (IC)	72
3.7 HACH colorimeter.....	74
3.8 Oil concentration detection	75
3.9 Elemental analysis: Inductively Coupled Plasma Optical Emission Spectroscopy (ICP-OES).....	76
3. 10 Response Surface Methodology (RSM)	77
3. 11 Adsorption Isotherm Models	78
3. 11. 1 Langmuir Isotherm model:	78
3.11.2 Freundlich Isotherm:	79
3.12 Adsorption Kinetics Models	81
3.13 Adsorption Thermodynamics.....	82
3.14 Batch adsorption experiments.....	82
3.15 Process variables (RSM).....	83
3.16. Regeneration and reusing of MW-EG	84
3.17. Materials and experimental design of oil removal.....	84
3.18.1 Dissolved oil adsorption conditions.....	84
3.18.1.1 Batch tests:	84
3.18.1.2 Experimental Design for the Removal of Dissolved Crude Oil Using EG in a Fixed Bed Column	85
3.18.2 Floating oil removal conditions	87
Chapter 3 References	88
Chapter 4: Results and discussion	93
4.1 Evaluation of granular EG adsorption performance for removal of Methylene Blue as model contamination.....	94
4.1.1 Introduction.....	94
4.1.2 Specific surface area and pore volume	94

4.1.3 FT-IR analysis.....	95
4.1.4 Chemical characteristics of adsorbent materials.....	96
4.2 Preliminary study: Effect of different experimental factors on MB adsorption onto Granular EG.....	97
4.2.1 Factors Examined in the Preliminary Investigation.....	97
4.2.1.1 Contact time.....	97
4.2.1.2 Adsorbent dosage:.....	97
4.2.1.3 Initial concentration.....	97
4.2.1.4 Sodium alginate amounts.....	98
4.2.2 Preliminary results.....	98
4.3 Microwave (MW)-assisted production and regeneration of granular EG for adsorption of MB from aqueous solution.....	106
4.3.1 Optimization of adsorption process parameters using RSM.....	106
4.3.2 Evaluation of the one-factor effect on adsorption features.....	110
4.3.3 Response surface plots.....	114
4.3.4 Adsorption isotherms.....	119
4.3.5 Kinetics studies.....	123
4.3.6 Thermodynamics output.....	125
4.3.7 Regeneration studies.....	126
4.3.8 The performance of adsorption of MB from surface water.....	127
4.3.9. Conclusion.....	130
Removal of oil contents from aqueous solution by Expanded graphite materials.....	131
4.4.1 Adsorption of dissolved oil.....	131
4.4.1.1 The Impact of Oil Concentration.....	131
4.4.1.2 The Impact of Varying Dosages of EG Powder:.....	132
4.4.1.3 The Mechanism of Adsorption.....	134
4.4.2 Adsorption of oil (floating) on the water surface by using powder EG.....	135
4.4.3 Column study.....	140

4.4.4 Conclusion of oil removal.....	143
5. Overall conclusion	145
Future work and suggestions	146
Chapter 4 References	147

List of Figures

- Fig. 1.1 The total components of PW (Faraji et al., 2021).
- Fig. 1.2 PW components from Norwegian offshore production platforms in 2019 (Data source: Norwegian Oil and Gas and the Norwegian Environment Agency & (Beyer et al., 2020))
- Fig 2.1 Comparing the average amounts of various elements and inorganic ions in PWs worldwide to average concentrations in 35‰ seawater (Collins 1975)
- Fig 2.2 BTEX from three offshore production facilities in Indonesia and different platforms in Gulf of Mexico USA (from Neff 2002)
- Fig 2.3 Organic acids have been discovered in the PW from four production facilities on the Norwegian continental shelf (Re Utvik 1999) compared to the Gulf of Mexico (USA offshore) (MacGowan and Surdam 1988).
- Fig 2.4 PW metal contents compared to seawater (PW: northwestern Gulf of Mexico and the Norwegian sector of the North Sea)
- Fig 2.5 Exfoliation/Expansion of graphite
- Fig 3.1 The stages of MW-EG preparation
- Fig 3.2. Separation of oil from solution
- Fig 3.3. Column system and connection to a pump for removal of dissolved oil
- Fig 3.4. Column design for removal of dissolved oil
- Fig 3.5. Experimental design adsorption process of oil contents in PW
- Fig 4.1 pore width and pore volume relationship for adsorbent materials
- Fig 4.2. FTIR analysis of MW-EG and EG
- Fig 4.3. Removal efficiency of MB through Granular EG (Effect of time)
- Fig 4.4 Adsorption capacity of granular EG by removing MB (Effect of time)
- Fig 4.5. Final concentration of MB remained in solution using granular EG (Effect of time)
- Fig 4.6 Pseudo-first order fitted on experimental data of MB adsorption onto granular EG (effect of time in preliminary study).
- Fig 4.7 Pseudo-2nd-Order model fitted on experimental data of MB adsorption onto granular EG (effect of time in preliminary study).
- Fig 4.8 Intra-particle diffusion model model fitted on experimental data of MB adsorption onto

- Fig 4.9. Effect of adsorbent dose in preliminary studies of MB removal onto granular EG.
- Fig 4.10 Adsorption rate and capacity for preliminary step of MB removal onto granular EG considering different initial concentrations.
- Fig 4.11. Langmuir, Freundlich models fitted on preliminary step of experiment for MB removal onto granular EG.
- Fig 4.12. Temkin and Dubinin-Radushkevich models fitted on preliminary step of experiment for MB removal onto granular EG.
- Fig 4.13. The effect of different sodium alginate additions on adsorption performance of granular EG in MB removal.
- Fig 4.14 Actual (experimental) versus predicted (models) values by RSM for adsorption rate (%) (MW-EG plus MB removal)
- Fig 4.15 Actual (experimental) versus predicted (models) values by RSM for adsorption amount (q) (MW-EG plus MB removal)
- Fig. 4.16 Effects of time on q performance
- Fig 4.17. Effects of initial concentration on q performance
- Fig 4.18 Effects of pH on q performance
- Fig 4.19 Effects of adsorbent dose on q performance
- Fig 4.20 Effects of time on adsorption rate
- Fig 4.21 Effects of initial concentration on adsorption rate
- Fig 4.22 Effects of pH on adsorption rate
- Fig 4.23 Effects of adsorbent dose on adsorption rate
- Fig. 4.24. 3D surface of the adsorption capacity (q) of MB versus the contact time and dose
- Fig 4.25. 3D surface of the adsorption capacity (q) of MB versus the contact time and initial concentration
- Fig. 4.26. 3D surface of the adsorption capacity (q) of MB versus the contact time and pH
- Fig 4.27. 3D surface of the adsorption rate of MB versus the contact time and initial concentration
- Fig 4.28. 3D surface of the adsorption rate of MB versus the contact time and dose
- Fig 4.29. 3D surface of the adsorption rate of MB versus the contact time and pH
- Fig 4.30 Linear and non-linear Langmuir models fitted on experimental data

- Fig 4.31 Linear and non-linear Freundlich models on experimental data
- Fig 4.32 Temkin and Dubinin-Radushkevich models on experimental data
- Fig 4.33 kinetics and equilibrium outlines of MB removal onto MW-EG
- Fig 4.34. pseudo-first-order, pseudo-second-order, and Intra-particle diffusion models of MB removal experiment using MW-EG adsorbent
- Fig 4.35 Thermodynamics plot of the adsorption process
- Fig 4.36 Regeneration of MW-EG by MW irradiation (MB removal)
- Fig 4.37. isotherm linear plot of MW-EG after 10-cycle regeneration
- Fig 4.38. The effect of initial concentration on dissolved oil removal
- Fig 4.39. Effect of adsorbent dose on dissolved oil removal
- Fig 4.40. Adsorption illustration of EG powder (0.1 g L⁻¹) for 200 ppm dissolved oil in water solution
- Fig. 4.41. Adsorption illustration of EG powder (0.2 g L⁻¹) for 200 ppm dissolved oil in water solution
- Fig 4.42. Hydrophobic interaction mechanism between oil and EG powder molecules
- Fig 4.43. Experimental design of floating oil removal by EG powder
- Fig 4.44. The effect of oil amount increases on adsorption capacity (q)
- Fig 4.45. One-factor effect of EG powder amount on adsorption capacity (q)
- Fig 4.46. Interaction between oil amount and EG powder quantities effects on adsorption capacity (q)
- Fig 4.47. Floating oil removal experiment by EG powder (6 g oil, 270 mg EG)
- Fig 4.48. Floating oil removal experiment by EG powder (4 g oil, 90 mg EG)
- Fig 4.49. Floating oil removal experiment by EG powder (4 g oil, 90 mg EG)
- Fig 4.50. performance of packed column1 with EG powder
- Fig 4.51. Flow rate chart for the column 2 adsorption
- Fig 4.52. The final concentration of collected samples by using column 2 (initial concentration)
- Fig 4.53. The removal efficiency of dissolved crude oil adsorption in fixed bed column 2
- Fig 4.54. Before and after adsorption of dissolved crude oil by column 2 (initial concentration)

List of tables

- Table 2.1 pore categories of carbon material (Metcalf & Eddy, 2013).
- Table 2.2. Various oil-on-water removal with different adsorbents (Takeuchi et al., 2017)
- Table 3.1 MB properties
- Table 3.2 Texas raw crude oil (Environment Canada 2016b West Texas Intermediate)
- Table 3.3 Reagents used for HACH calorimetry.
- Table 3.4 Equations and parameters for isothermal models
- Table 3.5 kinetics models used
- Table 3.6. Thermodynamic of adsorption (Eq 9-11)
- Table 3.7. The domain of parameters optimized in the RSM method.
- Table 3.8. Characteristics of two columns used as a fixed-bed filter for dissolved crude oil removal.
- Table 4.1. Physical characterization of adsorbents
- Table 4.2 Chemical characteristics of EG and MW-EG
- Table 4.3. Comparison of Pseudo- second order, Pseudo-first order, and Intra-particle diffusion models in the preliminary study of MB adsorption onto granular EG
- Table 4.4. Kinetics' constants
- Table 4.5 Different runs of MB removal
- Table 4.6 Analysis of variance for three responses in terms of p-value
- Table 4.7 Coefficients of correlation provided by RSM model fitted on experimental data
- Table 4.8 results of optimization of RSM
- Table 4.9 isotherm parameters by different models
- Table 4.10 Kinetics parameters of different models
- Table 4.11 Thermodynamics parameters
- Table 4.12 results of various studies on modified EG versus the result of this study
- Table 4.13. BET and pore size distribution changes for MW-EG
- Table 4.14. Removal efficiency of experimental design for dissolved oil

List of abbreviations

AC	activated carbon
ACTF	amorphous carbon thin film
Bq/L	becquerels/L
BTEX	benzene, toluene, ethylbenzene, and xylenes
CTS-A-MMT	chitosan-activated montmorillonite
EG	expanded graphite
FGIC	fluorinated graphite intercalation compounds
GAC	granular activated carbon
GIC	graphite intercalation compounds
GO	graphite oxide
HEG	highly expanded graphite
IFM	in situ formed magnesium hydroxide
MB	methylene blue
MEG	magnetic expanded graphite
MEG-NH ₂	amino-functionalized magnetic expanded graphite
MI	microwave irradiation
MONPs	manganese oxide nanoparticles
MWCNTs	multi-walled carbon nanotubes
NF	nanofiltration
O & G	oil and grease
PAH	polycyclic aromatic hydrocarbons
pCi/L	picocuries/L
PDMS	polydimethylsiloxane–graphene sponge
PET	polyethylenetere phthalate
PP	polypropylene
PPQA@SiO ₂	silica-supported polyether polysiloxane quaternary ammonium
PW	produced water
RO	reverse osmosis
SEB	sodium exchanged bentonite
SEM	scanning electron microscopy
TDS	total dissolved solids
TEM	transmission electron microscopy
TGA	thermal gravimetric analysis
TOC	total organic carbon

TRG	thermally reduced graphene
WGR	water to gas ratio
WOR	water to oil ratio
XRD	x-ray diffraction

Chapter 1: Introduction

1.1 Background and Context

Over the last decades, the oil and gas sector has been associated with substantial water consumption and the subsequent generation of vast volumes of wastewater during extraction activities ((Jiménez et al., 2018). This wastewater is so-called produced water (PW); the treatment of PW typically involves reducing the oil concentration to a level that meets the effluent regulations of the site, ensuring that the water quality is suitable. Subsequently, the treated water is either released into the sea or injected into the oil layers of the well (Takeuchi et al., 2015). Thereby, partial or inefficient management strategies may cause detrimental effects on environmental communities (Igunnu & Chen, 2012). However, regulations on risk assessment, the adoption of environmentally friendly offshore chemicals, and enhanced cleaning methodologies have effectively diminished the environmental hazards associated with PW discharges.

Nonetheless, PW remains the predominant operational source of oil contamination in marine environments (Beyer et al., 2020). The utilization of untreated PW can engender plant growth (Burkhardt et al., 2015) and increase the risk of contaminating soil, surface water, and underground aquifers (Fakhru'l-Razi et al., 2009). PW originates from different processes and operations, including formation water, re-injection water/steam, and treatment agents employed throughout various phases such as drilling, fracturing, stimulation, production, as well as the processes involving oil-water and oil-sand separation (Igunnu & Chen, 2014; Neff et al., 2011a)

The discharge of PW presents more threats to ocean environments than other habitats due to the increasing volumes of PW in mature offshore production regions. These wastewaters may contain toxic organic compounds and metals that can cause severe damage to aquatic ecosystems (Neff et al., 2011a). The volume of PW is notable, given the water-to-oil ratio (WOR). Globally, the average WOR stands at approximately 2 to 3 (Neff et al., 2011a). Furthermore, the water-to-gas ratio (WGR) resulting from well operations varies across oil and gas fields. To illustrate, the average WOR and WGR associated with oil and gas extraction in the Federal offshore waters of the U.S. is 1.04 and 86, respectively (Clark & Veil, 2009). Besides, the production of PW is increasing, reaching a volume of up to 39.5 million m³ per day. Anticipating a WOR of approximately 12 (v/v) for onshore crude oil resources by 2025

emphasizes the significance of treating PW as an economically viable solution for sustainable resource management (Jiménez et al., 2018).

PW contains various hazardous organic and inorganic compounds, such as salts, oily contentts, benzene, toluene, ethylbenzene, xylenes (BTEX), polyaromatic hydrocarbons, and organic acids, and so on (Neff, 2002; Arthur et al., 2011). However, the specific properties of PW depend on factors such as the geographical location of the field, the geological formation, the extraction technique, and the nature of the hydrocarbon product. Consequently, efficient PW treatment is essential, transforming it into a less hazardous by-product that can meet various water needs such as irrigation, livestock watering, aquifer storage, and municipal and industrial purposes (Guerra et al., 2011). For these purposes, it is crucial to identify the PW constituents. Additionally, selecting the most suitable treatment approach for PW is essential in effective PW management, accounting for environmental considerations, economic factors, and local regulatory frameworks (Jiménez et al., 2018).

1.2 Constituents of Produced Water

PW contains different chemical constituents influenced by reservoir depth, hydrocarbon-bearing formation geochemistry, chemical interactions within the reservoir, additives employed during extraction, and the lifespan of the reservoir itself. Inorganic salts, O&G, a wide range of organic chemicals, organic acids, primarily hydrocarbons, metals, and radioisotopes, can be found in PW (Neff et al., 2011).

The salinity concentration of PW, ranging from a few parts per thousand (%) to 300%, dramatically surpasses that of seawater (between 32 and 36%) (Rittenhouse et al., 1969). Notably, sodium and chloride, which are the predominant components of PW's saline content, have concentrations varying from 23,000 to 141,000 (mg L^{-1}) (Neff et al., 2011). Various components within PW, including total organic acids, total organic carbon (TOC), total saturated hydrocarbons, total BTEX, and total polycyclic aromatic hydrocarbons (PAH), have been reported from 0.1 to 11,000, 0.001 to 10,000, 17 to 30, 0.068 to 578, and 0.04 to 3.0 mg L^{-1} , respectively (Neff, 2002). Formic acid stands as the most abundant acid, changing from 26 to 584 mg L^{-1} ((MacGowan & Surdam, 1988). Furthermore, the concentration of BTEX, representing petroleum hydrocarbons, approaches 600 mg L^{-1} , potentially dispersing into groundwater and leading to critical environmental and health concerns (Su et al., 2010).

Metals are also present within PW, depending on geological age and formations where oil and gas extraction occurs (Collins, 1975). However, the occurrence of metals within PW samples is infrequent. Other elements forming the PW components are radioisotopes, such as radium (Ra). Ra originates from the radioactive decay of uranium-238 and thorium-232 from specific rock formations and clays within the hydrocarbon reservoir (Kraemer & Reid, 1984). The quantification of radionuclides in environmental media is typically expressed in units of the radioactive decay rate, conventionally denoted picocuries/L (pCi/L) or becquerels/L (Bq/L) (Neff 2002). For example, the activity of ^{226}Ra and ^{238}U ranges between 0.054 – 32,400 pCi/L and 0.008 – 2.7 pCi/L, respectively. Comparatively, these quantities are 0.04 pCi/L and 1.1 pCi/L for seawater. Some studies discussed PW characteristics (Fakhru'l-Razi et al. 2009; Jiménez et al. 2018; Neff et al. 2011). Fig. 1.1 illustrated PW components' details (Collins 1975; Neff 2002; Neff et al. 2011). Besides, Fig. 1.2 showed PW substances discharged from Norwegian offshore production platforms in 2019.

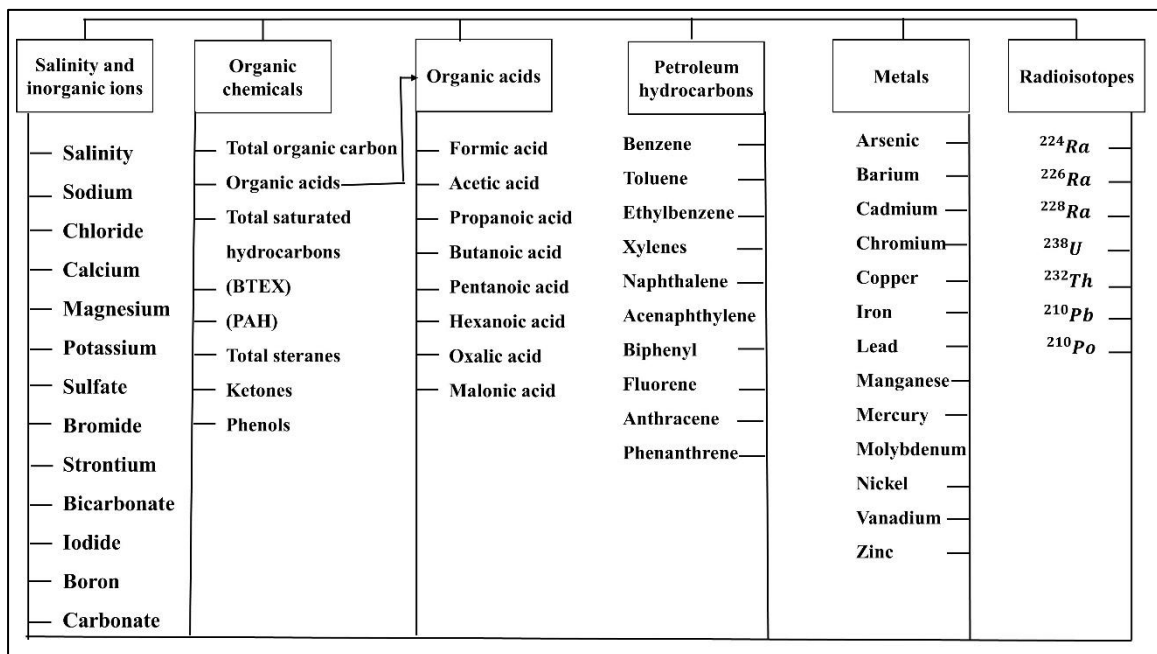


Fig. 1.1 The total components of PW (Faraji et al., 2021).

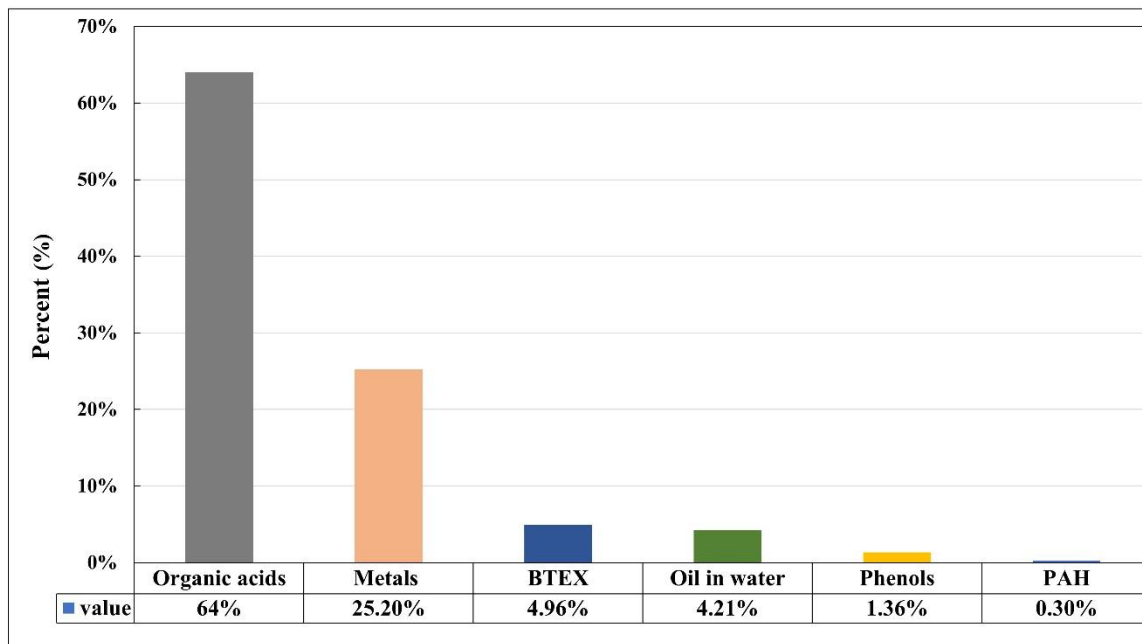


Fig. 1.2 PW components from Norwegian offshore production platforms in 2019 (Data source: Norwegian Oil and Gas and the Norwegian Environment Agency & (Beyer et al., 2020))

1.3 Environmental effect of PW components

Adverse effects can arise from the different PW elements, which can be categorized into six distinct groups:

- i) Impact of high salinity levels
- ii) Implications arising from heavy metals
- iii) Contamination from soluble organic
- iv) Influence from insoluble organic components
- v) Pollution linked to oil-field toxic materials
- vi) Radioactivity (Allen & Robinson, 1993)

Potential adverse impacts can include marine pollution, river contamination, lake pollution, aquifer pollution, soil degradation, and harm to aquatic plants and animals. Recent studies are increasingly focusing on examining the impact of dissolved organic compounds, heavy metals, and chemicals used in production on living organisms. This attention results from the lack of documentation and understanding of prolonged effects on the environment. Research findings

indicate that metals and hydrocarbons driven from oil platforms exhibit significant ecosystem toxicity. Moreover, fish subjected to alkyl phenols experience disruptions in both organ functionality and reproductive capabilities (Grant & Briggs, 2002; Igunnu & Chen, 2014).

Acute toxicity may be limited to the area nearest where produced water discharges into offshore waters, considering the concentrations and relative toxicities of chemicals generally observed in most produced waters and predictions concerning dispersion and the rates of biodegradation/transformation in the end points of water. Sensitive biotests, mainly consisting of regulatory acute toxicity evaluations and the created water plume's quick dispersion and disintegration within the recipient waters, support this idea (Neff et al., 2011). Holdway (2002) suggested that to adequately evaluate the possible long-term environmental effects of PW releases, the chronic effects connected to permanent exposures must be measured. This chronic exposure over an extended period can result in sub-lethal shifts in populations and communities, such as reduced community and genetic diversity, reduced growth and fecundity, respiratory issues, behavioral and physiological conditions, reduced developmental success, and disruptions to the endocrine system (Holdway, 2002).

1.4 Research Problem

Given PW's detrimental effects on the environment and human health, producing organic contaminants in PW is a significant concern. The issue with this research is how effectively current treatment techniques can reduce the effects of these contaminants. Creative and environmentally friendly alternatives are necessary because of the compositional complexity of organic contaminants and the variety of their sources. Although the use of carbon materials as adsorbent has potential, there are still questions about its viability, effectiveness, and optimization. Furthermore, a comprehensive study is needed to understand the interactions between carbon materials and the complex concoction of organic chemicals. The scientific challenge also includes bridging the gap between carbon materials' theoretical promise and actual implementation in PW treatment. This research aims to further the understanding of sustainable solutions for eliminating organic contaminants from PW and consequently promote environmental and water resource sustainability by tackling these complex problems.

1.5 Research goals

The thesis aims to gain an extensive comprehension of expanded graphite (EG) potential as a helpful carbon material and an adsorbent for removing organic pollutants from PW. The main objective of this research is to provide practical knowledge as well as feasible solutions to the critical problems associated with the treatment of PW, especially concerning its organic pollutants, oil in water, and organic acids concentration in lab-scale studies. Besides, a part of this research focused on regeneration technology for EG materials. To realize this goal, the following research objectives have been meticulously formulated:

1.5.1 Assessment of adsorption efficiency:

The main goal of this study is to evaluate EG materials' adsorption capacity for eliminating a range of organic contaminants from aqueous solution. The adsorption capability, kinetics, and equilibrium behavior of EG will be examined by experimental research. To guarantee the applicability and relevance of the findings, representative organic components frequently discovered in produced water will be carefully chosen.

1.5.2 Optimization of Operating Parameters:

This thesis aims to optimize critical operating parameters to improve the effectiveness of EG as an adsorbent. To ascertain their impact on adsorption, variables will be changed, including pH, contact time, adsorbent dose, and initial pollutant concentration. Developing effective and practical treatment solutions for PW, including organic contaminants, would benefit from discovering ideal conditions. Besides, response surface methodology (RSM) will be used to facilitate the optimization process and save on the number of runs and time requirement.

1.5.3 Mechanistic Understanding:

Another essential study goal is to have a thorough mechanistic comprehension of the interactions between organic contaminants and EG. The adsorption mechanisms, sites, and molecule interactions will be clarified using characterization techniques, including surface area and porosity analysis. This understanding will support the theory underlying the adsorption phenomena and aid in creating prediction models.

1.5.4 Comparative study of various EG types:

In order to assess efficiency and practicality, regeneration capabilities, and cost-effectiveness, EG powder and granular shapes will be compared. This goal is to ensure that the suggested solution aligns with environmentally friendly methods and sustainable practices.

In conclusion, the study's goals described in this thesis are intended to advance our knowledge of using EG to remove organic contaminants from PW. This thesis aims to build a solid basis for sustainable and efficient PW adsorption strategies, significantly advancing environmental protection and water treatment. This is accomplished through experimentation, mechanistic insights, comparative analysis, and regenerative assessments.

1.6 Research hypotheses and questions

A collection of established research questions and assumptions facilitates the thesis. These questions act as critical points, directing the course of the research and providing a comprehensive framework for analysis.

RQ1: To what extent does EG effectively absorb different organic pollutants from produced water?

EG is predicted to have effective adsorption properties and a substantial removal rate for various organic contaminants found in PW owing to its hydrophobic nature and morphological structure containing mesopore sites.

RQ2: What effects do different operational factors, such as pH, , adsorbent dose, contact time, and initial pollutant concentration, have on the EG adsorption process?

The best adsorption efficiency will be achieved by systematic parameter changes, which will clarify how each parameter affects adsorption performances, as well as using the statistical optimization model will clarify the optimization process.

RQ3: What fundamental principles underlie the molecular interactions between organic contaminants and expanding graphite?

Theoretically, more profound characterization tools will identify certain surface functional groups and chemical interactions that aid in the adsorption process, revealing details about the interaction's mechanism.

RQ4: How influential are different EG form capabilities in the removal of selected contaminants?

Theoretically, granular EG (G-EG) will be more practical in terms of regeneration purposes than powder in removing organic. However, a trade-off between the adsorption capacities of different forms and their performance, plus the possibilities of recycling, should be taken into account.

RQ5: Is it feasible to transform EG into a more affordable and environmentally friendly adsorbent using innovative regeneration technologies like microwave irradiation?

It is anticipated that the feasibility study will demonstrate that involving regeneration studies is both economically and technically possible and in accordance with environmental considerations.

RQ 6: How are adsorption technologies effective? Is there a need for coupled or synergistic strategies? Specifically, the strategic combination of different methods of treatment may improve the effectiveness of pollution removal.

1.7 Significance of the study

The significance of this study is increased by the convergence of three crucial criteria, all of which fall under the category of adsorption for PW treatment: the regeneration benefits of EG, its environmental benefits, and the possibility for cost-effectiveness. The potential of using EG for pollutant adsorption is highlighted by these interconnected features, which also accomplish the more general requirements of sustainability, economic viability, and environmental responsibility.

One of these research aspects is the G-EG's ability to be regenerated when exposed to microwave irradiation. EG granules may be effectively regenerated, restoring their adsorption ability, unlike traditional adsorbents, which frequently require replacement after usage. Pollutants, especially organic dyes that have been adsorbed to the G-EG's surface, can be released by microwave irradiation, regaining the adsorbent's effectiveness for continued use. This regenerating ability reduces the need for frequent replacements, which substantially reduces costs while also extending the life of the adsorbent. This component is consistent with the general objective of resource optimization and advances produced water treatment practices in a more sustainable direction.

Additionally, using microwave irradiation for regeneration is entirely in line with sustainable practices. Compared to traditional thermal regeneration techniques, its energy-efficient nature lowers the use of energy throughout regeneration, therefore reducing the carbon impact. Additionally, the potential for cost-effectiveness of treated PW is increased by the advantages of its natural adsorption capabilities.

In conclusion, this study's profound significance lies in its multifaceted effects, where the novel regeneration potential of EG granules through microwave irradiation converges with its cost-effective treatment methods, environmental practices, and inherent adsorption features. This research seeks to redefine the parameters of PW processing by highlighting these interconnected advantages. It expects an approach that is not only practical from an economic standpoint but also one that is sustainable and environmentally friendly.

Chapter 1 References

- Allen, R. M., & Robinson, K. (1993, April 3). *Environmental Aspects of Produced Water Disposal*. Middle East Oil Show. <https://doi.org/10.2118/25549-MS>
- Arthur JD, Dillon LW and Drazan DJ (2011) Management of Produced Water from Oil and Gas Wells. Working Document of the NPC North American Resource Development Study, p. 32.
- Beyer, J., Goksøyr, A., Hjermmann, D. Ø., & Klungsøyr, J. (2020). Environmental effects of offshore produced water discharges: A review focused on the Norwegian continental shelf. *Marine Environmental Research*, 162, 105155. <https://doi.org/10.1016/j.marenvres.2020.105155>
- Burkhardt, A., Gawde, A., Cantrell, C. L., Baxter, H. L., Joyce, B. L., Stewart, C. N., & Zheljzkov, V. D. (2015). Effects of Produced Water on Soil Characteristics, Plant Biomass, and Secondary Metabolites. *Journal of Environmental Quality*, 44(6), Article 6. <https://doi.org/10.2134/jeq2015.06.0299>
- Clark, C. E., & Veil, J. A. (2009). *Produced water volumes and management practices in the United States*. (ANL/EVS/R-09-1; Issue ANL/EVS/R-09-1). Argonne National Lab. (ANL), Argonne, IL (United States). <https://doi.org/10.2172/1007397>
- Collins, A. (1975). *Geochemistry of oil-field waters, Volume 1—1st Edition*. <https://www.elsevier.com/books/geochemistry-of-oilfield-waters/collins/978-0-444-41183-9>
- Fakhru'l-Razi, A., Pendashteh, A., Abdullah, L. C., Biak, D. R. A., Madaeni, S. S., & Abidin, Z. Z. (2009). Review of technologies for oil and gas produced water treatment. *Journal of Hazardous Materials*, 170(2), Article 2. <https://doi.org/10.1016/j.jhazmat.2009.05.044>
- Faraji, A., Cuccarese, M., Masi, S., Mancini, I. M., & Caniani, D. (2021). Use of carbon materials for produced water treatment: A review on adsorption process and performance. *International Journal of Environmental Science and Technology*. <https://doi.org/10.1007/s13762-021-03395-y>
- Grant, A., & Briggs, A. D. (2002). Toxicity of sediments from around a North Sea oil platform: Are metals or hydrocarbons responsible for ecological impacts? *Marine Environmental Research*, 53(1), 95–116. [https://doi.org/10.1016/S0141-1136\(01\)00114-3](https://doi.org/10.1016/S0141-1136(01)00114-3)
- Guerra K, Dahm K and Dundorf S (2011) Oil and Gas Produced Water Management and Beneficial Use in the Western United States. Science and Technology Program Report, p. 157.
- Holdway, D. A. (2002). The acute and chronic effects of wastes associated with offshore oil and gas production on temperate and tropical marine ecological processes. *Marine Pollution Bulletin*, 44(3), 185–203. [https://doi.org/10.1016/s0025-326x\(01\)00197-7](https://doi.org/10.1016/s0025-326x(01)00197-7)
- Igunnu, E. T., & Chen, G. Z. (2012). Produced water treatment technologies. *International Journal of Low-Carbon Technologies*, 9(3), Article 3. <https://doi.org/10.1093/ijlct/cts049>

- Igunnu, E. T., & Chen, G. Z. (2014). Produced water treatment technologies. *International Journal of Low-Carbon Technologies*, 9(3), 157–177. <https://doi.org/10.1093/ijlct/cts049>
- Jiménez, S., Micó, M. M., Arnaldos, M., Medina, F., & Contreras, S. (2018a). State of the art of produced water treatment. *Chemosphere*, 192, 186–208. <https://doi.org/10.1016/j.chemosphere.2017.10.139>
- Jiménez, S., Micó, M. M., Arnaldos, M., Medina, F., & Contreras, S. (2018b). State of the art of produced water treatment. *Chemosphere*, 192, 186–208. <https://doi.org/10.1016/j.chemosphere.2017.10.139>
- Kraemer, T. F., & Reid, D. F. (1984). The occurrence and behavior of radium in saline formation water of the U.S. Gulf Coast region. *Chemical Geology*, 46(2), Article 2. [https://doi.org/10.1016/0009-2541\(84\)90186-4](https://doi.org/10.1016/0009-2541(84)90186-4)
- MacGowan, D. B., & Surdam, R. C. (1988). Difunctional carboxylic acid anions in oil-field waters. *Organic Geochemistry*, 12(3), Article 3. [https://doi.org/10.1016/0146-6380\(88\)90262-8](https://doi.org/10.1016/0146-6380(88)90262-8)
- Neff, J. (2002). *Bioaccumulation in Marine Organisms—1st Edition*. <https://www.elsevier.com/books/bioaccumulation-in-marine-organisms/neff/978-0-08-043716-3>
- Neff, J., Lee, K., & DeBlois, E. M. (2011a). Produced Water: Overview of Composition, Fates, and Effects. In K. Lee & J. Neff (Eds.), *Produced Water: Environmental Risks and Advances in Mitigation Technologies* (pp. 3–54). Springer. https://doi.org/10.1007/978-1-4614-0046-2_1
- Neff, J., Lee, K., & DeBlois, E. M. (2011b). Produced Water: Overview of Composition, Fates, and Effects. In K. Lee & J. Neff (Eds.), *Produced Water: Environmental Risks and Advances in Mitigation Technologies* (pp. 3–54). Springer. https://doi.org/10.1007/978-1-4614-0046-2_1
- Rittenhouse, G., Fulton, R. B., Grabowski, R. J., & Bernard, J. L. (1969). Minor elements in oil-field waters. *Chemical Geology*, 4(1), Article 1. [https://doi.org/10.1016/0009-2541\(69\)90045-X](https://doi.org/10.1016/0009-2541(69)90045-X)
- Su, F., Lu, C., & Hu, S. (2010). Adsorption of benzene, toluene, ethylbenzene and p-xylene by NaOCl-oxidized carbon nanotubes. *Colloids and Surfaces A: Physicochemical and Engineering Aspects*, 353(1), Article 1. <https://doi.org/10.1016/j.colsurfa.2009.10.025>
- Takeuchi, K., Fujishige, M., Kitazawa, H., Akuzawa, N., Medina, J. O., Morelos-Gomez, A., Cruz-Silva, R., Araki, T., Hayashi, T., Terrones, M., & Endo, M. (2015). Oil sorption by exfoliated graphite from dilute oil–water emulsion for practical applications in produced water treatments. *Journal of Water Process Engineering*, 8, 91–98. <https://doi.org/10.1016/j.jwpe.2015.09.002>

Chapter 2: Literature review

2.1 PW components

A diverse blend of dissolved and dispersed organic and inorganic substances constitute PW composition. The geologic age, depth, geochemistry, chemistry of the oil and gas components in the reservoir, and production-related chemicals used for processing all have a significant impact on the chemical and physical characteristics of the PW. Since no two PWs are the same, research tailored to a particular location is required to tackle the environmental issues associated with their disposal. These chemicals and compounds can be grouped into salts and inorganic ions, Organic compounds, metals, and radioisotopes (K. Lee & Neff, 2011).

PW is a complex aqueous combination that results from interactions between geological formations, drilling and production additives, reservoir fluids, and other by-products of the extraction of oil and gas. Based on elements including geographic location, geological features, extraction techniques, and the particular hydrocarbon resource, its composition varies greatly.

2.1.1 Inorganic Salts:

The presence of inorganic salts mainly causes the salinity of PW. The three main salts included in PW are sodium, chloride, and sulfate. PW frequently has salinities greater than those of seawater, with concentrations varying from a few parts per thousand (‰) to that of a saturated brine (~300‰; (Rittenhouse et al., 1969). Particularly, the range of sodium and chloride values, which range from 23,000 to 141,000 mg L⁻¹ (Neff et al., 2011), is rather wide. These salts are produced by the water used during rock formation and rock-reservoir interactions (Fig 2.1).

2.1.2 Oil and BTEX:

Oil and grease (O&G) are two common organic substances found in PW together with hydrocarbons. According to Neff et al. (2011), O&G concentrations might fluctuate, often falling between 17 and 30 mg L⁻¹. PW frequently contains certain organic substances, including benzene, toluene, ethylbenzene, and xylenes (BTEX). Total BTEX chemical concentrations have been shown to range widely, from 0.068 to 578 mg L⁻¹ (Neff et al., 2011) (Fig 2.2).

2.1.3 Organic acids:

With quantities ranging from 26 to 584 mg L⁻¹, organic acids like formic acid contribute to the organic component of PW (MacGowan & Surdam, 1988) (Fig 2.3).

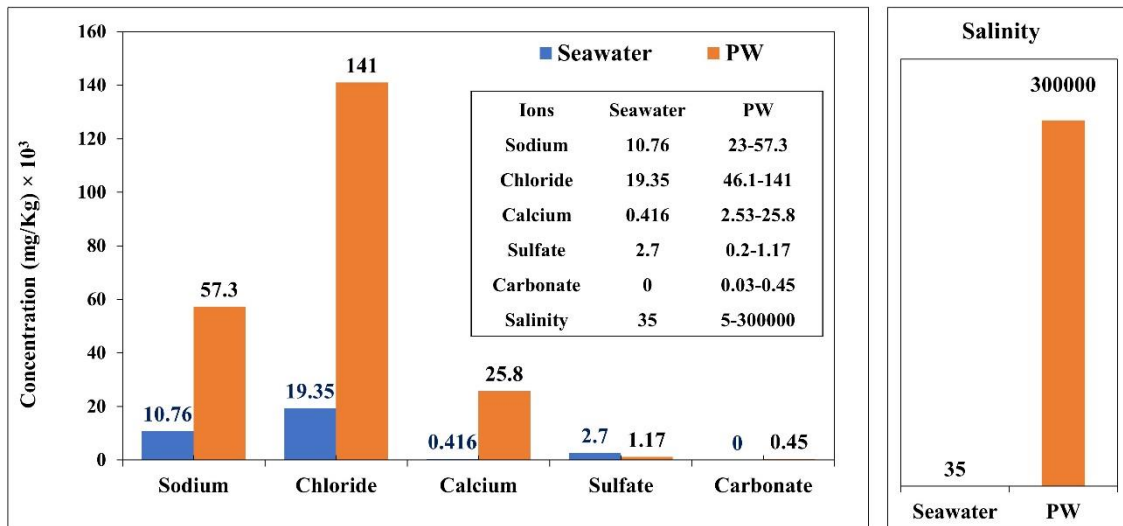


Fig 2.1 Comparing the average amounts of various elements and inorganic ions in PWs worldwide to average concentrations in 35‰ seawater (Collins 1975)

2.1.4 Metals and radioisotopes:

Metals, both heavy and trace elements, contribute to the PW's varied components. The age of the reservoir and the surrounding geology both affect the amounts of these metals. PW also contains radioisotopes like Ra and U. According to Neff et al. (2002), the activity of Ra ranges from 0.054 to 32,400 (pCi L⁻¹), whereas that of U is between 0.008 and 2.7 (pCi L⁻¹). The possible radiological effect from PW waste is apparent even if these quantities are significantly lower than those in seawater (Neff et al., 2002) (Fig 2.4).

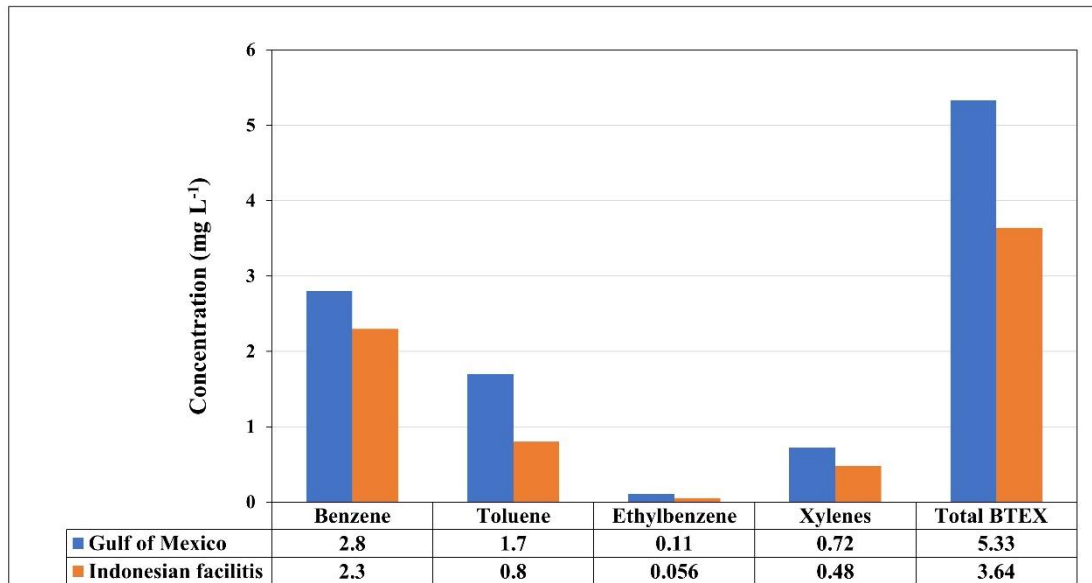


Fig 2.2 BTEX from three offshore production facilities in Indonesia and different platforms in the Gulf of Mexico USA (from Neff 2002)

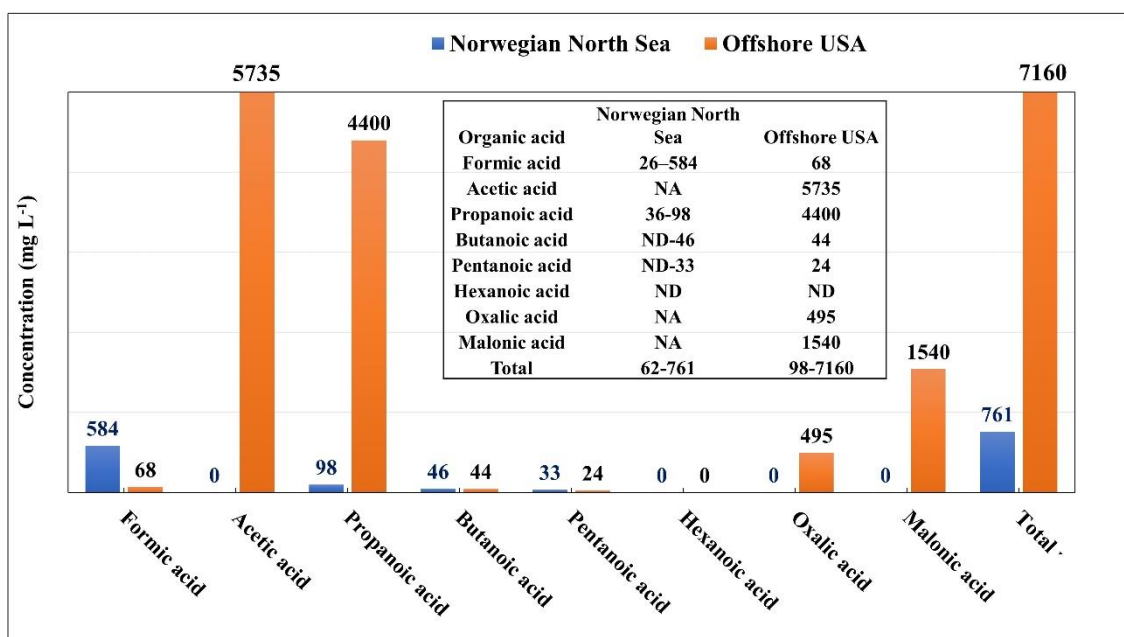


Fig 2.3 Organic acids have been discovered in the PW from four production facilities on the Norwegian continental shelf (Re Utvik 1999) compared to the Gulf of Mexico (USA offshore) (MacGowan and Surdam 1988).

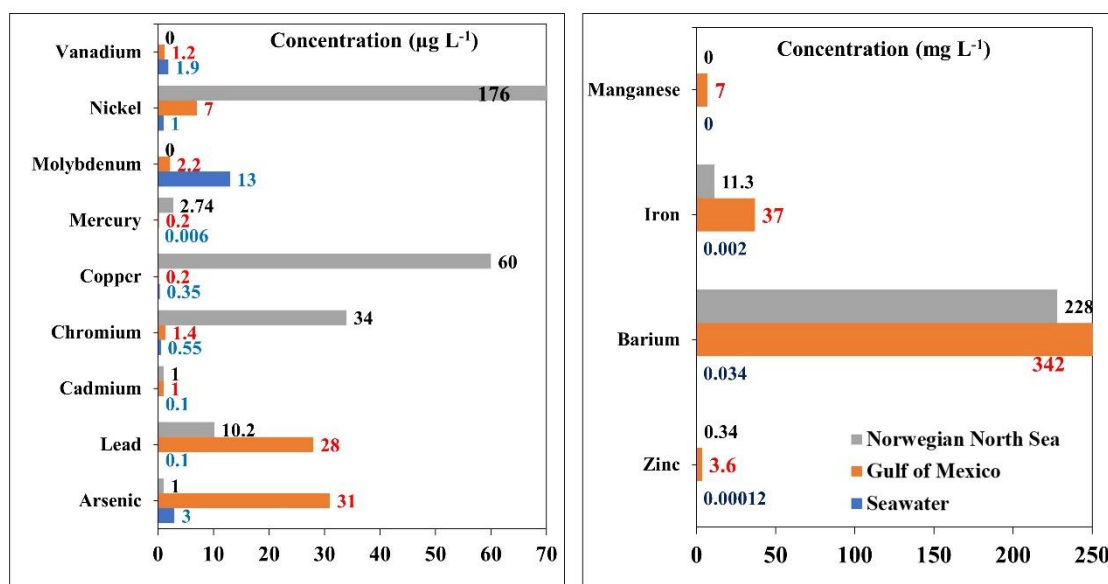


Fig 2.4 PW metal contents compared to seawater (PW: northwestern Gulf of Mexico and the Norwegian sector of the North Sea)

2.2 Adsorption conception and process

The Removal of organic pollutants from aqueous systems has been the subject of many studies using a variety of approaches, including adsorption, coagulation, filtration, and precipitation (Gopinath et al., 2021). Adsorption has emerged as the least expensive and environmentally friendly strategy among these strategies, demonstrating greater performance in removing contaminants from aquatic environments. The remaining approaches, however, have several disadvantages, including expensive operating expenses, the production of sludge, and a substantial initial investment (Bashir et al., 2019; Mashkoo et al., 2020; Vieira et al., 2020). Adsorption refers to the phenomenon whereby chemicals present in a solution accumulate on a compatible surface. Adsorption is a process of mass transfer when a component present in the liquid phase is transported to the solid part. The adsorbate refers to the molecule that is being extracted from the liquid state at the contact. The adsorbent is to the phase, whether it be gas, liquid, or solid, upon which the adsorbate collects. While adsorption is employed in the flotation process at the air-liquid interfaces, this chapter focuses on the scenario of adsorption occurring at the liquid-solid contact. However, the increasing need for a better quality of treated wastewater discharge, particularly in terms of toxicity decreasing, has prompted an in-depth study and application of the adsorption process with activated carbon (AC) and carbon

materials. The use of AC for the treatment of wastewater is often seen as a supplementary procedure aimed at refining water quality subsequent to undergoing conventional biological treatment. In the present case, carbon is used to eliminate a proportion of the residual dissolved organic materials. The objective of this part is to provide an introduction to the fundamental principles of adsorption and to examine the application of carbon material adsorption (Metcalf & Eddy, 2013).

Adsorption is regarded as a highly suited solution compared to traditional approaches owing to its low operational difficulty, efficacy, cost-effectiveness, and low by-product. Because of its outstanding regeneration characteristics, adsorption is particularly preferred in industrial settings (Rathi et al., 2021). Different categories of adsorbents, such as AC, synthetic polymeric, and silica-based adsorbents, have been used for water and wastewater treatment. However, owing to their costly prices, synthetic polymeric and silica-based adsorbents are rarely employed for wastewater adsorption treatment. AC is one of the most prevalent adsorbents employed in advanced wastewater treatment technologies.

The production of AC involves the first conversion of organic resources, such as almond, coconut, and walnut hulls, into char. Additionally, The production of ACs with a significant surface area and the capacity to adsorb substantial quantities of gas from biomass sources, such as lignin, corncob, fungus, chitosan, gelatine, and starch, has drawn considerable interest (Alhwaige et al., 2013; Chen et al., 2013; Sun et al., 2012; Sun & Webley, 2011; H. Wang et al., 2009; J. Wang et al., 2012). Additionally, in order to enhance their energy-storage capabilities, many investigations are turned to plant wastes like leaf, sawdust, seaweed, and peel, along with cellulose, lignin, glucose, and starch to create carbonaceous adsorbents with advantageous nanostructures and functionalization structures by hydrothermal carbonization (Alabadi et al., 2015; Falco et al., 2011; Song et al., 2012). The process involves subjecting the base material to high temperatures, typically below 700°C, inside a retort. This thermal treatment facilitates the removal of hydrocarbons while intentionally limiting the availability of oxygen to prevent continuous burning. The process of carbonization or char production can be described as a pyrolysis mechanism. The char particle is then activated by its contact with oxidizing gases, including steam and CO₂, at elevated temperatures, reaching from 800 to 900 °C (Alabadi et al., 2015; Metcalf & Eddy, 2013). The formation of these gases results in the development of a structure with pores inside the char, therefore leading to the creation of a significantly expanded internal surface area. The pore diameters that are obtained can be characterized as follows (Table 2.1).

Table 2.1 The pore categories of carbon material (Metcalf & Eddy, 2013).

Pores	Width (nm)
Micropore	<2 nm
Mesopore	Between 2 and (25-50) nm
Macropore	>50 nm

The resulting surface qualities are influenced by both the raw material used and the process of preparation technique, thus creating many potential variations. The pore size distribution and regeneration properties of AC can be influenced by the base material from which it is produced. Following the process of activation, the carbon material can be divided or produced into various dimensions, each with distinct adsorption capabilities. Powdered activated carbon (PAC), which generally has a diameter of less than 0.074 mm (200 sieves), and granular activated carbon (GAC) are the two size classes.

2.3 The basic principles of adsorption

The adsorption process may be divided into four distinct steps: (1) transportation of the bulk solution, (2) transportation via the film diffusion, (3) transportation through the pores, and (4) the actual adsorption or sorption. The process of bulk solution refers to the transfer of an organic substance under adsorption from the bulk liquid to the boundaries of a stationary liquid film that surrounds the adsorbent. This transfer is often achieved by advection and diffusion inside carbon contactors (Metcalf & Eddy, 2013). The film diffusion process implies the movement of organic substances across a stationary liquid film, ultimately reaching the entry point of the adsorbent's pores through diffusion. Pore transport entails the movement of the substance through the pores by a mix of molecular diffusion inside the pore liquid and/or adhesion on the surface of the adsorbent. Adsorption is a process whereby the item to be adsorbed adheres to an adsorbent at a location of adsorption that is readily accessible (Snoeyink & Summers, 1999). Adsorption may take place on the external surface of the adsorbent as well as inside various pore sizes, including macropores, mesopores, micropores, and sub-micropores. However, it is worth noting that the total area of the macro- and mesopores is rather limited compared to the surface area of the micropores and sub-micropores. Metcalf & Eddy (2013) identify adsorption forces as a key component, including coulombic-unlike charges, point charge and a dipole, dipole-dipole interactions, point charge neutral species, Van der Waals forces, covalent bonding with reaction and hydrogen bonding. According to Kecili

and Hussain (2018), adsorption is also a surface-oriented mechanism in which the adsorbate is attached to the adsorbent's surface either by physisorption or chemisorption, in other words, physical and chemical adsorption are the two main adsorption processes (Kecili & Hussain, 2018). Physical adsorption, also known as physisorption, is characterized by weak bonding between the adsorbent and adsorbate that result in reversible adsorption. Van der Waals forces, hydrogen binding and dipole interactions are a few of the driving mechanisms behind physical adsorption.

However, with chemical adsorption, stronger chemical interactions are created between the molecules of the adsorbate and the adsorbent surface, leading to irreversible adsorption. Furthermore, electrons perform a crucial part in chemical adsorptions involving the adsorbent and the adsorbate, and as a result, the adsorbent's electrons' characteristics will alter upon adsorption. Adsorbent and adsorbate react in two different ways: through covalent bonds and ionic bonds, which refer to weak chemical and strong chemical adsorption, respectively. Physical forces and weak chemical bonds, such as changes to functional groups, hydrogen bonding, electrostatic interaction, and electron donor-acceptor interactions, facilitate the contact between the adsorbate and adsorbent (Natarajan et al., 2022).

2.4 Expanded graphite (EG)

EG (expanded graphite) is made from natural mineral graphite flakes by intercalating molecules between the layers. The process usually employs acids, such as sulfuric acid, facilitating the conversion of the natural graphite into EG (Lu, 2012).

EG has a layered structure accompanied by interlayer space, which allows its expansion over 150 times. Thus, macromolecules can penetrate porosities and interlayer voids of EG. Good electrical and thermal conductivity plus the layered structure makes it a good option for adsorption and as well as polymer studies (Zheng et al., 2002). Natural graphite is added to nitric acid and sulfuric acid in the first step, followed by filtration of the reacted mixture after one day, washed with water, and oven-dried at low temperature. Then, the expandable graphite is put in a furnace (about 900°C) to expand up to 100 to 300 times without oxidation (Taherian, 2019).

The usage of graphite and different types of composites made from it, such as graphite intercalation compounds (GICs), is widespread in a number of scientific, technological, and industrial domains. Thermally, EG (TEG), which has the appearance of a foamed carbon structure and is utilized to create low-density carbon substances and products (Yakovlev et al.,

2006), is produced by treating certain GICs with acids and salts. TEG is chemically inert and heat-resistant, just like graphite. The material's porosity determines its electrical and thermal conductivity, which can vary greatly. High chemical and thermal stability, adjustable electrical and thermal conductivity, porosity, and developed specific surface area all set the stage for the creation of multi-functional EG (Saikam et al., 2023).

GIC production has been accomplished using a variety of techniques, including chemical (which involves liquid-phase intercalation and vapor- or gas-phase manner) and electrochemical processes, such as galvanostatic or potentiostatic oxidation (You et al., 2023). The progressive intercalation and need for an oxidizer are the vital distinctive characteristics of the procedure. Because most added acids have low redox potentials and are unable to eliminate electrons from the graphite structure, the addition of an oxidizing agent is crucial. Nitric and perchloric acids, which are self-intercalating agents, offer an exception. The form of oxygen-containing surface functional groups at the terminal atoms of graphite layers is first altered by oxidants. Numerous substances, including KMnO_4 , H_2O_2 , CrO_3 , HNO_3 , $\text{K}_2\text{Cr}_2\text{O}_7$, O_3 , $(\text{NH}_4)_2\text{S}_2\text{O}_8$, etc., can function as oxidizers (Kitaoka et al., 2011; Sykam et al., 2015). Inorganic and organic acid compounds, including H_2SO_4 , HClO_4 , HReO_4 , H_2SeO_4 , HNO_3 , HCOOH , and CF_3COOH , are utilized in an electrochemical process to create GICs (Kong et al., 2010). Anodic oxidation of graphite in H_2SO_4 solutions with an adequate amount provides the basis for the electrochemical formation of graphite bisulphate. The remaining quantities of acids and oxidizing agents are present in GICs made chemically and electrochemically, both directly in their composition and as adducts on the surface. GIC are rinsed with water to pH range 5-7 to get rid of the acid and oxidizer traces. There is significant debate over the GIC's expansion by heat process. Theoretically, nearby layers dissolve as carbon structures quickly loses a specific proportion of intercalating fragments from the graphite host's interlayer gap. The heat-induced expansion of graphite was thought to be a phase shift brought on by the elimination of the intercalating reagent from GIC.

2.4.1 Summary of graphite exfoliation:

The layered network of graphite facilitates chemical interactions by permitting intercalates—guest chemical species—to lodge themselves between its layers, forming graphite intercalation compounds (GICs). Because of their high electrical conductivity, acid salts of graphite, which are created when graphite reacts with acids, have attracted interest. Graphite bi-sulphate (graphite- H_2SO_4) and graphite nitrate (graphite- HNO_3) are two significant acid salts (Kong et al., 2010). Utilizing fuming nitric acid along with additional oxidizers, the latter can be created.

As seen in Fig 2.5, the intercalation procedure includes introducing layers of chemical species between graphite layers. Concentrated nitric acid and graphite are easily combined to create a variety of phases, including graphite nitrate complexes. Since it is more controllable than liquid-phase nitration, the use of fuming nitric acid at various pressures is preferred. Electrochemical approaches employ graphite as the baseline electrode, fuming nitric acid as an electrolyte, and intercalation as a source of layer growth (M. Li et al., 2008; Saikam et al., 2023).

A very porous, worm-like structure with low density is one of EG's special characteristics. Three different types of pores may be found in the porous structure of EG: internal pores, surface holes, and pores between worm-like particles. The characteristics of EG, including its weak polarity, hydrophobicity, and lipophilicity, make it a very effective adsorbent with excellent potential for selectively sorbing large, weakly polar organic compounds from aqueous (Minitha et al., 2017). Changes to the intercalation chemicals or thermal sources will affect the synthesis of EG and produce diverse end products. The page offers a schematic diagram explaining the creation process and possible uses for EG. Fig 2.5 shows schematic instructions for creating EG.

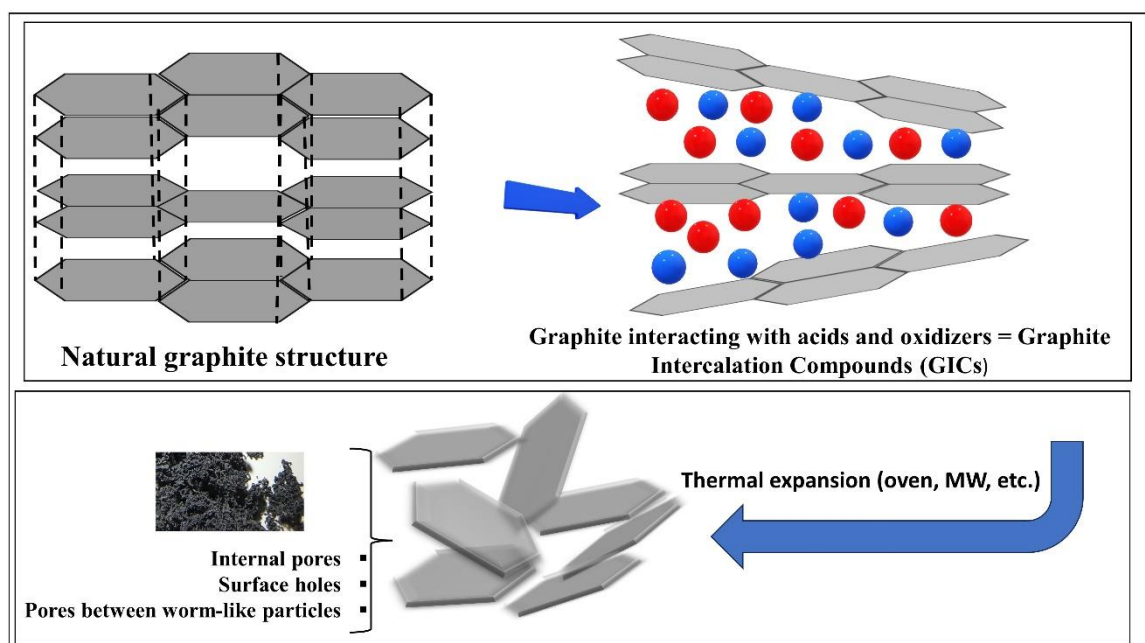


Fig 2.5 Exfoliation/Expansion of graphite

2.5 Efficient parameters in the adsorption process of carbon materials for oily contents and organic contaminations and mechanism of adsorption

2.5.1 Porosity:

In terms of adsorbent, one of the main properties can be pore structure and porosity. There are three general categories for pores: micropore, mesopore, and macropore (Table 2.1). Depending on the molecular size of organic pollutants, different porosity behaviors are possible. For example, smaller size and molecular organic can reach the micropore structure. However, EG presented a mesopore structure ranging between 2 to 50 nm in width.

2.5.2 Surface area:

The surface area is another feature of an adsorbent that presents the capacity and applicability of its adsorption process. There are internal and external surfaces in an adsorbent where most of the micropores take place on the internal surface, and mesoporous and macropores form the external areas. In terms of AC, the surface area ranges between 500 to 1200 m² g⁻¹ (Ersan et al., 2017; Liao et al., 2008). However, different types of ACs can be mesoporous or microporous. Besides microporous, which plays the main role in AC adsorption due to their high energy site, meso- and macropores are also important by connecting the micropores or, in other words, acting as highways in the adsorbent. However, the surface area of EG was reported to be lower than AC, ranging from 35 to 50 (m² g⁻¹) (Cuccarese et al., 2021)

2.5.3 Bulk density and pore volume:

The bulk density is one of the important factors influencing the adsorption characteristics of EG. Numerous investigations noted a substantial reduction in adsorbed quantities because of a greater bulk density. The main cause of this could be pore volume reduction at increasing bulk densities. It is also important to note that the structure of EG's pore volume impacts the quantity of adsorbed pollutants. For instance, Iqbal et al. (2013) underlined the idea that it is reasonable to believe that Macro-pores (>50 nm) are effective for oil sorption in addition to the surface area of graphene (Iqbal & Abdala, 2013).

Therefore, capillary condensation causes large particles in heavy oils to be sorbed into macropores in EG (Toyoda et al., 2000a). Inagaki et al. (2001) demonstrated that the adsorbed quantity is proportional to the total pore volume of EG. As a result, they determined that an appropriate pore size for heavy oil sorption is between 1 and 600 μm (Inagaki et al., 2001). This EG's morphology is characterized by a notably balloon-like structure (Inagaki, Konno, et al., 2000), which is documented in most adsorption investigations. Furthermore, this balloon-like or worm-like property of EG has been found to persist after both heavy oil sorption and desorption by filtering followed by suction or xylene treatment (Inagaki, Shibata, et al., 2000). The thermal shock that causes intercalating vaporization consequently creates this worm-like EG formation (Bayat et al. 2008). Wang et al. (2010) demonstrated that the myrmekitic textures and multilevel pore architectures of MEG were significantly increased when compared to EG. However, intense stirring during preparation destroyed the typical worm-like shape, resulting in a decreased absorption capacity (G. Wang et al., 2010). As a result, finding an appropriate adsorption technique is critical in worm-like morphology adsorption research.

2.5.4 Target pollutant characteristic:

Another important factor impacting the adsorption rate is the properties of pollution molecules, for example, the viscosity of heavy oil or the oil content of PW, the molecular weight of organic pollutants, chemical characteristics such as hydrophilicity and hydrophobicity, and so on. Multiple investigations have found that more viscous oil requires a longer period to be adsorbed (Wang et al. 2010), such as 8 hours (Toyoda et al. 2000). The amount of oil absorbed into the unoccupied spaces between EG's entangled particles is controlled by oil viscosity in addition to adsorption duration. According to Bayat et al. (2008), the sorption capacity of EG decreases as oil viscosity increases (Bayat et al., 2008). According to Iqbal and Abdala (2013), the higher viscosity of heavy oil is connected to the higher concentration of long-chain hydrocarbons in highly viscous oil (Iqbal & Abdala, 2013).

2.5.5 The temperature of oil contents:

The adsorption quantities are affected by the temperature of the oil. The higher the temperature, the less viscous the oil becomes, which might result in more adsorption. However, due to the evaporation of light components, heavy oil recycling at high temperatures is impractical. (Toyoda et al., 2000). Furthermore, raising the temperature of genuine PW in real adsorption circumstances is difficult. Bach et al. (2016) performed their experiments at temperatures

between 10 and 30 degrees Celsius. Findings revealed that the elimination of diesel oil increased with rising temperatures. Furthermore, the primary reason can be attributed to better oil diffusion into the pore of EG/CoFe₂O₄ at high temperatures (Bach et al. 2016).

2.5.6 Contact time:

The amount of time necessary for reaching maximum adsorbed quantities under specific circumstances is determined by the viscosity of the heavy oil or pollutant (Inagaki et al. 2000b). Bayat et al. (2008) discovered that gas oil was adsorbed in one minute. However, light crude oil and heavy crude oil required 5 and 90 minutes, respectively, due to the viscosity of heavy crude oil (Bayat et al. 2008). Other investigations observed varying contact times needed to finish the adsorption procedure. The adsorbed quantities, for example, remained steady after 2 minutes (Wang et al., 2010), 6 minutes (Bach et al., 2016), and 60 minutes (Takeuchi et al., 2015). The quantity of EG introduced, however, affects the stabilization time.

2.5.7 Initial concentration of adsorbate:

The influence of the initial dose (concentration) of adsorbate on the adsorbed quantities is dependent on the experimental condition. Bach et al. (2016), for example, investigated the effect of varying oil content dose (15, 20, 25, 30, and 35 g) on adsorption effectiveness. They discovered that adding floating oil reduced the quantity of adsorbed oil because the adsorbent results in less oil dosage on the surface by giving greater porosity (Bach et al. 2016). However, Tuan Nguyen et al. (2019) found that the adsorption properties of MnFe₂O₄ in diesel oil did not change greatly; the crude oil removal had a modest variation in the condition upon adding a variable dosage of oil (15 to 45 g) (Tuan Nguyen et al., 2019).

2.5.8 Salinity:

Bach et al. (2016) observed that salinity (varying from 0.5% to 3.5%) might facilitate adsorption by reducing diesel solubility in water with higher salinity (Bach et al. 2016). Additionally, Tuan Nguyen et al. (2019) examined the influence of salinity on adsorption. They increased the concentration of NaCl from 1% to 3%. The study findings demonstrated the effective elimination of heavy oil in a saline water environment by modest variations in

adsorbed quantities (Tuan Nguyen et al. 2019). Other parameters, such as pH and adsorbent dose, can affect adsorbent capacity. However, the influence of such factors on oil sorption behavior must be further studied (Takeuchi et al. 2017).

Khang et al. (2020) discuss the intricate interactions between organic dye molecules and available adsorption sites. Their paper highlights that the adsorption rate was predominantly governed by a single-step mechanism at low pollutant concentrations, determined by the underlying reaction mechanism. However, at higher concentrations, the adsorption processes exceeded the confines of a single-step mechanism, prompting the consideration of a multistep elementary reaction mechanism. These complex reactions involve lateral interactions, multiple binding sites, and/or non-random contributions from the adsorbate. Recently, it has been increasingly acknowledged that multi-step adsorption significantly influences the determination of the adsorption rate.

2.6 Literature Review on the Removal of PW Components

2.6.1. Oily contents and hydrocarbon removal:

EG presented a patent proposal to cure heavy oil in Japan for the first time in 1979 (Inagaki et al., 2001). Following that, in 1996, another team provided a brief study on the potential of employing EG in heavy oil adsorption. Their findings revealed that the amount of EG adsorption was 25 (g g⁻¹). Finally, Inagaki and his colleagues conducted various tests on EG in 1998. They reported that EG might be a potential carbon-based substance by adsorbed quantities in weight of approximately 80 (g g⁻¹) of heavy oil dispersed on water surface in a span of one minute (Toyoda et al., 2000b).

In a series of papers, Inagaki and his colleagues investigated the adsorption and recovery of heavy oils employing EG. They first investigated the adsorption quantities utilizing four heavy oils with varying viscosities and EG with different bulk densities. The results showed that the adsorption characteristics of EG are significantly dependent on its bulk density and pore volume. Furthermore, the contact time related to maximum adsorption was affected by the grade of heavy oil. After 1 minute of adsorption, these researchers achieved maximum adsorption of 83 (g g⁻¹). They proposed that the greater the viscosity of the oil used for the experiment, the longer the adsorption takes (about 8 hours) (Toyoda & Inagaki, 2000).

Inagaki et al. (2000a) investigated the extraction of heavy oil and EG regeneration using filtering after mild suction in another investigation. They indicated that when EG regenerates, its adsorbed quantities drop significantly. Furthermore, it has been shown that the collected oils have essentially identical properties to those of the original. It is noteworthy to notice that the bulk density exceeded the density of the original EG and was subsequently disrupted during compression. Consequently, the authors suggested the need for a less aggressive approach, such as using moderate suction filtration (Inagaki, Konno, et al., 2000).

In their third publication, Inagaki et al. (2000b) performed research examining the feasibility of compressing EG into a plastic bag for practical reasons. The objective of this research was to achieve a significantly enhanced sorption capacity using a metallic mesh and clamp. However, the findings yielded similar quantities of adsorbed pollutants in terms of weight compared to the earlier study conducted by Inagaki, Shibata, et al. (2000).

Moreover, the authors Toyoda et al. (2003) provided a discussion on the significant oil adsorption capabilities of EG in their fourth experimental study. The researchers evaluated the correlation between the quantified adsorbed quantities and the pore dimensions determined using a mercury porosimeter. This was the first instance in which investigations focused on the assessment of the composition and porosity of EG. The researchers demonstrated that the presence of large pores, which can be understood as inter-particle pores between the entangled worm-like particles of the EG material, played a significant role in facilitating the high adsorption capabilities of EG. The U-type cell's volume estimation demonstrated a strong agreement with the calculated adsorbed volumes for A-grade heavy oil, as reported by Toyoda et al.(2003).

Inagaki et al. (2001) conducted a study in 2001 to examine the use of EG for the remediation of spilled heavy oil. The objective of this study was to conduct a comparative analysis of the adsorption capacities of EG with several other adsorbents. The quantities of adsorbed substances were much greater in comparison to the polypropylene (PP) and polyurethane mats that have been used recently. Inagaki et al. (2001) reported that EG can absorb heavy oils selectively. In order to assess the relative selectivity of EG sorption compared to other materials, the researchers conducted a parallel experiment using commercially available PP mats.

In contrast to EG, the PP mats exhibited a notable water adsorption capacity of around $4 \text{ (g g}^{-1}\text{)}$, while EG had a lower water adsorption capacity of $1.8 \text{ (g g}^{-1}\text{)}$. Upon the introduction of A-grade heavy oil onto the water-saturated PP mat, no observable expulsion of water from the PP mat was detected. As a result, this particular attribute is exclusively identified in EG, conferring upon it a comparative advantage over other materials.

In addition, previous studies have directed their attention to the practical use of graphite in the context of heavy oil and PW adsorption. An evaluation was conducted by Bayat et al. (2008) to determine the oil sorption capacity of synthesized EG using both static and dynamic techniques. The results were then compared to those of other adsorbents. They emphasized the fact that graphite's thermal shock causes intercalate to evaporate and GICs to decompose. The thermal shock resulted in a significant increase in the size of natural graphite flakes by a factor of 80, thereby leading to the formation of a distinctive worm-like structure in EG. The results showed that EG exhibited the greatest oil adsorption within the range of $65 \text{ to } 73 \text{ (g g}^{-1}\text{)}$, followed by PP nonwoven web with an adsorption capacity of $7\text{-}9 \text{ (g g}^{-1}\text{)}$. In addition, the

influence of oil viscosity on the adsorption processes was found to be substantial. Specifically, a greater oil viscosity led to decreased oil uptake into the pores of vermicular particles and the empty spaces between the entangled particles of the EG material (Bayat et al., 2008).

In their study, Wang et al. (2010) used a novel magnetic property in order to evaluate the adsorption and recovery of magnetic EG (MEG). In order to effectively manage, remediate, and use environmentally harmful oil spills of a significant magnitude, a magnetic field is established around the affected region. As a result, MEG promptly aggregated, collected, and facilitated the efficient recovery of the oil. The findings indicated that the adsorption percentage increased by 18.01% and 5.65% for engine oil and crude oil, respectively, in the case of MEG. In contrast, a decrease of 10.95% for diesel oil and 4.63% for gasoline was reported. This loss may be attributed to the higher levels of glutinosity and density found in both crude and engine oil (Wang et al. 2010).

In the context of a lab investigation, researchers from Shinshu University conducted an analysis of the efficacy of EG in the oil-water emulsion. The use of micron-sized iron particles facilitated the easy recovery of the oil that had been absorbed into the EG. According to Takeuchi et al. (2015), the treatment efficiency of EG in reducing the oil content in the emulsion from 100 mg L^{-1} to a range of 0.1 mg L^{-1} was found to be comparable to the performance of nanofiltration (NF) or reverse osmosis (RO) membrane treatment (Takeuchi et al., 2015). Moreover, Takeuchi et al. (2017) used EG in the practical treatment of PW. This research is one of the first examples of practical PW treatment conducted by EG. In their study, They used a laboratory-scale adsorption column containing EG to effectively reduce the oil concentration from initial levels of 278 and 66 (mg L^{-1}) to $1.2 \text{ (mg L}^{-1}\text{)}$ and undetectable levels, respectively (Takeuchi et al., 2017).

The issue of managing oil-contaminated aqueous solutions has received considerable attention in recent years, because of its environmental and industrial implications. The pollution of aquatic ecosystems resulting from oil spills, industrial effluents, and produced water has emerged as a significant concern, presenting risks to both the natural environment and human well-being. To overcome these challenges, there has been a focus on research endeavors aimed at the advancement of efficient and ecologically viable techniques for the removal of oil.

In the offshore oil fields, the produced water is often transferred by pipes to offshore infrastructure, where it passes various treatment processes. Produced water is often managed by either re-injection into wells and oil fields or reusing it to enhance oil recovery (EOR)

purposes. The composition of produced water often includes hydrocarbons (oil and gas), as well as a mixture of salts, inorganic compounds, and organic substances. Typically, it includes a varying range of total organic carbon (TOC) compounds. In the context of pre-treatment for membrane processes, it is typical to carry out three stages of hydrocarbon-removal operations. These phases include primary oil-water separation, where the oil concentration is typically below 500 mg L⁻¹, followed by secondary oil-water separation. Finally, tertiary oil-water separating is conducted to achieve an oil concentration level below 15-30 mg L⁻¹. If considered necessary, further post-processes, including advanced methods such as reverse osmosis (RO) or nanofiltration (NF) membrane separation, can be implemented (Takeuchi et al., 2015).

Besides, the growing need for petroleum-based goods over the last several decades has led to an increase in the frequency with which incidents involving oil spills have happened at all stages of the supply chain, from extraction to final disposal. The marine ecosystem and its living organisms have been negatively impacted by water pollution resulting from oil spill events. This is mostly attributed to the presence of hydrocarbons and trace metals found in the components of oil (Ordinioha & Brisibe, 2013; Tuan Nguyen et al., 2019).

Polypropylene and polyurethane are two examples of porous polymers that have been employed for oil spill absorption; their maximum absorption capacity is 20-30 g of heavy oil per 1 g of polymer. However, it is worth noting that the majority of polymers can absorb water and heavy oil. It is important to highlight that these polymers do not exhibit any specific selectivity towards heavy oils, which ultimately results in a reduced absorption capacity for heavy oils (Toyoda & Inagaki, 2003).

The study group led by Inagaki and Toyoda first discovered the efficacy of EG in sorbing heavy oil, whether in the form of "oil floating on water" or "pure oil (Inagaki et al., 2001; Inagaki, Konno, et al., 2000; Inagaki, Shibata, et al., 2000; Toyoda et al., 1998, 2000, 2003)". According to the research, the A-grade heavy oil had a sorption capability exceeding 80 times the weight of the EG (Toyoda et al., 1998). Moreover, a multitude of research endeavours were undertaken, including studies on the impact of the bulk density of EG on its adsorption behavior, the collection of heavy oil and the reuse of EG, experimental trials aimed at real-world implementation, and investigations into the mechanisms behind oil sorption on EG (Inagaki et al., 2001; Inagaki, Konno, et al., 2000; Inagaki, Shibata, et al., 2000; Toyoda et al., 1998, 2000, 2003).

Additionally to EG, carbon materials like carbon nanotube (nanofiber) or its composites, EG oxide, hollow carbon fibers, hollow carbon beads, polyurethane-activated carbon composite, etc., have been studied for their oil sorption behavior. This research primarily focuses on the sorption of oil in the context of floating oil on the water, with a specific emphasis on addressing oil spills. In contrast, this chapter specifically targeted the selective sorption of oil-water emulsions (dissolved) since it is often observed that oil in produced water is mostly present in emulsified form. Furthermore, studies on oil on water (floating) were conducted as well for comparison purposes.

Takeuchi et al., 2017 compared and summarized the performance of different types of oil removal, mainly oil-on-water (Table 2.2).

Table 2.2. Various oil-on-water removal with different adsorbents (Takeuchi et al., 2017)

Adsorbent	Type of oil	Uptake capacity	Reference
EG	Heavy oil	80	(Toyoda et al., 1998)
EG	Heavy oil	86	(Inagaki, Shibata, et al., 2000), (Toyoda & Inagaki, 2000)
EG	Heavy oil	86	(Inagaki et al., 2002)
EG	Heavy oil	80	(Zheng et al., 2004)
EG	Heavy oil	73	(Bayat et al., 2008)
EG	Crude oil	49	(G. Wang et al., 2010)
EG	Crude oil	36	(Ding et al., 2014)
EG-MnFe₂O₄	Crude oil	33	(Tuan Nguyen et al., 2019)
Carbon nanotube	Kerosene	69	(Fan et al., 2010)
Carbon nanotube	Kerosene	35	(Zhao et al., 2012)

Carbon fibers	Crude oil	79	(B. Wang et al., 2013)
Carbon fibers	Motor oil	40	(Zeng et al., 2014)
Carbon nanofiber aerogels	Diesel oil	52-139	(Wu et al., 2014)
Powdered activated carbon	Crude oil	50	(Medjahdi et al., 2016)

2.6.2 Literature review on adsorption of heavy metals, BTEX, and organic acids:

2.6.2.1 Heavy metals removal

The existence of heavy metal ions poses a significant risk to both living organisms and the environment, consequently posing a substantial threat to human well-being. According to Yurtsever and Şengül (2012), a significant quantity of silver is hazardous to human cells. Ma et al. (2017) utilized amino-functionalized magnetic EG (MEG-NH₂) Nano-hybrids in their study to remove Ag (I) from water (Yurtsever & Şengül, 2012). This study aimed to assess the impact of different factors on the adsorption performance of MEG-NH₂ nano-hybrids through batch experiments. Specifically, the effects of Fe₃O₄ content, pH, initial concentration, contact time, and dosage on the adsorption properties of the MEG-NH₂ nano-hybrids were investigated. They demonstrated the conversion of Ag to elemental silver by the adsorption process. In an experimental study, Do et al. (2019) employed EG coated with manganese oxide nanoparticles (MONPs-EG) to eliminate lead and nickel. The findings revealed that the highest quantities of adsorbed substances were determined to be 0.278 mmol g⁻¹ and 0.113 mmol g⁻¹ for Pb²⁺ and Ni²⁺ ions, respectively. They proposed the utilization of MONPs-EG as an adsorbent for elimination of heavy metals from aqueous solutions (Do et al., 2019)

Furthermore, some research investigations have employed EG oxide (GO) adsorbing heavy metals along with the use of EG. In a study conducted by Lee and Yang (2012), flower-like TiO₂ particles on GO effectively eliminated heavy metal ions. The researchers demonstrated that the formation of a GO-TiO₂ hybrid by the growing of TiO₂ flowers on GO can result in the development of effective adsorbent for heavy metal cations. This work proposes that the incorporation of metal oxide (e.g., TiO₂) decoration onto graphene oxide (GO) has potential as an effective adsorbent material to remove heavy metal ions from aqueous solutions, surpassing

the conventional application of photocatalysts. The findings of the study indicated a notable enhancement in the removal efficiency of the GO-TiO₂ hybrid structures as the duration of treatment extended from 6 hours to 12 hours. Specifically, the removal capacities for Zn²⁺, Cd²⁺, and Pb²⁺ increased from initial values of 44.8, 65.1, and 45 mg g⁻¹ to final values of 88.9, 72.8, and 65.6 mg g⁻¹, respectively (Y.-C. Lee & Yang, 2012). In their study, Gong et al. (2015) employed a fixed-bed column to investigate the continuous adsorption of Pb (II) and methylene blue (MB) using GO-coated sand. The experiment utilized a cylindrical glass column with a diameter of 2 cm and a length of 30 cm, which was maintained at a temperature of 25°C, adjusting four key factors, namely the initial concentration, flow rate, bed depth, and pH. The GO-sand filter exhibited a maximum adsorption capacity of 0.63 (mg g⁻¹) for Pb (II). In contrast to other adsorbents, such as algae delirium (Shahbazi et al., 2013) with a Pb adsorption capacity of 0.083 mg g⁻¹, dye-loaded coir fiber (Mondal, 2009) with a capacity of 0.020 mg g⁻¹, and functionalized SBA-15 mesoporous silica with polyamidoamine groups (Vilar et al., 2008) with a capacity of 0.269 mg g⁻¹, GO-sand exhibited a higher adsorption capacity for Pb. Furthermore, the values for MB (0.74 mg g⁻¹) were much greater in comparison to the values published for other adsorbents, such as cottonalk (0.024 mg g⁻¹) (Ding et al., 2014; Gong et al., 2015). Olanipekun et al. (2014) utilized GO to eliminate lead. The adsorption rates for the different concentrations of Pb (50, 100, and 150 mg L⁻¹) were found to be 98%, 91%, and 71% correspondingly. The authors emphasized the potential superiority of GO over graphite (Olanipekun et al., 2014). In their study, Sheet et al. (2014) conducted a batch adsorption experiment that employed nanostructured GO, silica/GO composites, and silica nanoparticles to remove heavy metal ions from aqueous solutions. They suggested that a higher concentration of heavy metals in the solution (200 mg L⁻¹) led to a decrease in the removal rate of the heavy metals. The removal rates for nickel, cadmium, zinc, lead, and chromium were found to be 89.90%, 88.33%, 85.60%, 85.0%, and 63.0%, respectively, in a solution containing 30 mg L⁻¹ of these metals (Sheet et al., 2014).

2.6.2.2 BTEX removal

According to Aivalioti et al. (2012), BTEX is more likely to seriously harm both human health and the lives of aquatic and other organisms. owing to the severe health risks related with BTEX, the Removal of these compounds from diverse water sources, including groundwater, wastewater, and PW, has emerged as a major issue. The recovery and regeneration of the adsorbent and adsorbate in the adsorption process are significant considerations in the treatment of BTEX removal from aqueous solutions (Aivalioti et al., 2012). Numerous studies

have been carried out to find out the adsorption of BTEX compounds from aqueous solutions. These studies have utilized various adsorbents, including zeolite (Seifi et al., 2011; Szala et al., 2015), resins (Makhathini & Rathilal, 2017, 2018), carbon nanotubes (Su et al., 2010, 2016; Yu et al., 2016), organoclay (Jaynes & Vance, 1996; Nourmoradi et al., 2012; Vianna et al., 2005), and activated carbon (Aleghafouri et al., 2015; Daifullah & Girgis, 2003).

The study conducted by Li et al. (2010) involved an assessment of the efficacy of three complex materials using EG in the Removal of toluene. The primary objective of this study was to ascertain the optimal oil composition for the development of a sophisticated absorbent material using three commonly utilized oil types: plant oil, animal oil, and mineral oil. The quantities of oils adsorbed onto EG for every gram of pure plant oil, animal oil, and vaseline were found to be 1068 mg g^{-1} , 966 mg g^{-1} , and 817 mg g^{-1} , respectively (S. Li et al., 2010). In their study, Yu et al. (2016) utilized a magnetic nano-composite material consisting of multi-walled carbon nanotubes (MWCNTs) known as APCNT-KOH to investigate its effectiveness in adsorbing toluene, ethylbenzene, and xylene. The results of the study conducted by Yu et al. (2016) showed that the composites of APCNTs-KOH had significant adsorption capacities for ethylbenzene, m-xylene, o-xylene, p-xylene, and toluene. The particular conditions resulted in adsorbed quantities of around 227.05, 138.04, 63.34, 249.44, and 105.59 (mg g^{-1}) for each respective compound (Yu et al., 2016).

2.6.2.3 Removal of organic acids

In their study, Kamio et al. (2004) investigated the utilization of highly porous PEI chitosan beads (PEI-Ch), which possess a high level of porosity, for the purpose of adsorbing organic acids such as acetic acid, formic acid, and pyroglutamic acid. These organic acids were derived from various sources, including the fermentation process, sub-critical water hydrolysis process, and other industrial methods. According to Kamio et al. (2004), it was proposed that the transportation of organic acids within the particle occurs by surface and pore diffusions (Kamio et al., 2004). Morad et al. (2014) conducted an additional experiment to investigate the adsorption of acetic acid into AC. The researchers utilized batch techniques in order to estimate the contact time required to achieve a removal rate of 16.5% within a time frame of 4 hours. Morad et al. (2014) observed that the adsorption rate is enhanced when the starting concentration is elevated. In contrast, the quantity of acetic acid adsorbed decreased with increasing amount of activated carbon (AC). The ideal mass of AC for this process was determined to be 0.5 g (Morad et al., 2014). The study conducted by Pradhan et al. (2017)

examined the adsorption behavior of lactic acid, with a concentration of less than 10 g L^{-1} , on several adsorbents. These adsorbents included GAC, weak base anion exchange resin (Reillex® 425 or RLX425), and strong base anion exchange resin (Amberlite® IRA-400 or AMB400). The researchers explored the effects of several running situations on the adsorption process. According to the findings of Pradhan et al. (2017), the quantities of adsorbed amounts for GAC, AMB400, and RLX425 were determined to be 38.2, 31.2, and 17.2 mg g^{-1} , respectively (Pradhan et al., 2017). In addition, previous studies have employed other adsorbents, such as magnetite nanoparticles (Tombácz et al., 2013) and alginate/clay composites (Achazhiyath Edathil et al., 2020).

2.7 Experimental Methodology for the Synthesis of EG

The process of graphite exfoliation is considered to be a highly effective method for achieving cost-effective large-scale manufacturing. In order to get high-quality graphene by improving exfoliation processes, it is essential to have a thorough understanding of the exfoliation mechanism. Yi and Shen (2015) have presented a collection of reviews related to exfoliation graphite (Yi & Shen, 2015). EG is commonly produced by applying thermal shock to chemically intercalated graphite, as observed by Yakovlev et al. in 2006. In addition, graphite intercalation compounds (GICs) are acquired by the introduction of various chemical compounds, known as intercalants, between the layers of natural graphite flakes (Dresselhaus & Dresselhaus, 2002). The exfoliation process is influenced by several aspects, as discussed by Makotchenko et al. (2011). These parameters include (1) the characteristics of the graphite flakes used in the creation of GICs, (2) the properties of the intercalant, (3) the efficiency of heat transmission throughout the process, and (4) the rate at which heating is applied. Sulfuric acid is commonly employed as a precursor for EG production, typically by its addition to GIC in the presence of an oxidizing agent (Makotchenko et al., 2011). Examples of such oxidizers include nitric acid (HNO_3) (Inagaki et al., 2004), hydrogen peroxide (H_2O_2) (Tryba et al., 2003), potassium permanganate (KMnO_4) and ferric chloride (FeCl_3) (Hristea & Budrugaec, 2008), and ozone (O_3) and chlorine (Cl_2) (Avdeev et al., 1996). The utilization of GIC (Graphite Intercalation Compound) in conjunction with nitric acid is a standard method (Yakovlev et al., 2006). In addition, previous research has proposed bromine (Chung, 1987) and formic acid (Kang et al., 1997) as alternative precursors for the synthesis of EG.

A range of techniques and methodologies are utilized to evaluate the morphology EG and demonstrate the effectiveness of the exfoliation process. These include powder X-ray diffraction (XRD), Raman spectroscopy, mercury porosimetry, elemental analysis, transmission electron microscopy (TEM), scanning electron microscopy (SEM), nitrogen adsorption-desorption, thermal gravimetric analysis (TGA), and dilatometer (specifically N-type cell and U-type cell). Various research suggested multiple EG synthesis methods. As an illustration, Bayat et al. (2008) conducted a procedure to synthesize EG by submerging graphite flakes in a solution containing sulfuric and nitric acids in a 4:1 ratio for 24 hours at ambient temperature. The prepared GIC was afterward rinsed with distilled water in order to achieve a pH level ranging from 3 to 4. Following this, it was placed in an oven with a temperature of 100 °C for 1 hour. Finally, the GIC residue was subjected to thermal shock at a temperature of 1000 °C for 5 seconds, resulting in its conversion to EG (Bayat et al. 2008).

In addition, the inclusion of iron particles enhances the process of preparing MEG, as demonstrated by Wang et al. (2010), who successfully dissolved iron nitrate, cobalt nitrate, and citric acid in a beaker, maintaining a molar ratio of 1:2:4. Subsequently, an aqueous solution of ammonia was used in order to achieve a pH range of 7.0 to 8.0. After that, the beaker was placed into a water bath set at a temperature of 90 °C, and the solution combination was vigorously agitated. The addition of the weighted EG was followed by the application of aqueous ammonia in order to adjust and maintain the pH level within the range of 7.0 to 8.0. The agitation stopped until a significant number of colloidal particles became visible. The sample was subjected to a drying process at a temperature of 100 °C for a duration of 12 to 15 hours in order to remove all moisture prior to proceeding to the subsequent stage. Following that, the MEG sample experienced rapid calcination in a muffle furnace operating at a temperature of 900 °C for 90 seconds. The structure of EG can be destroyed by solid stirring (Wang et al. 2010). In a research, Takeuchi et al. (2015) suggested that the incorporation of iron particles into EG results in a superparamagnetic characteristic, which enables the use of magnetic fields to effectively retrieve oil-filled EG particles from the treated emulsion. A two-step process conducted the preparation of MEG. Initially, EG was subjected to immersion in a solution of iron citrate that had been dissolved in water at at 90 degrees Celsius. EG was dried at 600°C in a hydrogen environment to embed iron ions in the structure. Furthermore, the synthesis of graphite-iron chloride intercalation compounds involved the introduction of EG to iron chloride within a glass tube under vacuum conditions. Subsequently, the resulting mixture was exposed to heat treatment at a temperature of 300 °C for 24 hours.

The samples were subsequently subjected to a drying process at a temperature of 600 °C in the presence of a hydrogen environment, as described by Takeuchi et al. (2015).

In their study, Pham et al. (2019) employed a novel technique known as microwave irradiation (MI) for the purpose of exfoliating EG. In this experimental procedure, graphite flake, KMnO_4 , HClO_4 , and $(\text{CH}_3\text{COO})_2\text{O}$ were combined in specific weight ratios of 1:0.5:1:0.4 (g g^{-1}). The mixture reacted for 10 seconds, resulting in the formation of GICs. The GICs were subjected to a 360 (W) MW oven for less than one minute. The EG was designated as EG-MI.

Additionally, the researchers organized a conventional experiment in order to establish a basis for comparison with their novel methodology. In the conventional approach, a combination of 20 mL of H_2SO_4 (serving as an intercalating agent) and H_2O_2 (acting as an oxidizing agent) was combined with 1 gram of graphite flake. The mixture was subjected to a continuous water wash on the Buchner funnel until it reached a pH of 5-6. The mixture passed filtration and was subjected to heating at a temperature of 80 °C. Then, for one minute, it was treated in the furnace at 1100 °C. The findings of Pham et al. (2019) indicate that the MI technique yields a larger surface area and micropore volume than the conventional process. Consequently, this results in increased adsorption capacity for heavy oil (Pham et al., 2019).

Makotchenko et al. (2011) used a variety of intercalated composites based on fluorinated graphite to insert high EGs (HEGs) in order to evaluate the present EG from graphite nitrate with another exfoliation process. The researchers utilized fluorinated graphite intercalation compounds (FGICs) weighing between 40-50 mg. These compounds were placed inside a quartz tube with dimensions of around 30-40 mm in diameter and 200-300 mm in height. Subsequently, the tube was subjected to a heating process in a furnace at a temperature of around 800 °C for 30 seconds. Following the heat shock, the HEG process yielded a significantly reduced quantity of graphene sheets compared to the conventional methods utilizing graphite bisulfate or nitrate. The production of HEG resulted in the expansion of interlayer distances, specific surface areas (measured at $370 \text{ m}^2 \text{ g}^{-1}$). It reduced bulk densities ranging from 0.4 to 0.7 (g L^{-1}), thus leading to a higher amount of adsorbed quantities (Makotchenko et al., 2011).

2.8. organic pollutant and dye removal literature review

In recent years, the harmful impacts of organic pollution originating from different industries have become more evident, posing significant threats to both human and aquatic ecosystems.

These organic pollutants are hazardous, which results in increased chemical and biological oxygen demands, reduced light penetration into surface waters, and disruptions in the growth of aquatic life's microorganisms (Hoang et al., 2019). The Environmental Protection Agency (EPA) is actively working towards improving water resource safety and safeguarding human health via the classification of waste generated by the dyes and pigments sector as hazardous. EPA classifies waste resulting from the disposal of certain dyes, pigments, food, drugs, and cosmetic colorants (FD&C) as hazardous waste under classification K181. The management of these wastes is within the jurisdiction of the Resources Conservation and Recovery Act (RCRA). However, the EPA primarily prioritizes the assessment of chemical components of concern in the waste that pose the greatest danger (USEPA, 2005). Various physical and chemical techniques have been used to eliminate organic dye effluents. These methods include adsorption, coagulation, flocculation, ozonation, membrane filtration, ion exchange, and chemical precipitation (Avetta et al., 2015). Adsorption is a very advantageous process from an environmental perspective because of its low production of by-products, superior performance, and cost-effectiveness, making it a viable solution for mitigating the presence of dye pollutants. Activated carbon (AC) has attracted significant interest as an adsorbent owing to its notable characteristics, including a large specific surface area and a very rapid adsorption rate. However, the increased expenses associated with AC applications pose some difficulties in certain contexts (Pang et al., 2014).

EG is a carbon-based material with a low density ranging from 0.002 to 0.010 g cm⁻³. It is characterized by its mesoporous structure (Xu et al., 2018). Due to its hydrophobicity and weak polarity, it can preferentially adsorb organic molecules (Zhang et al., 2016). A multitude of layers and interlayer space characterizes the structure of EG. The manufacturing process involves first combining natural graphite with nitric acid and sulfuric acid. After the reaction between graphite and acids, the resulting slurry is subjected to water washing and subsequent drying in an oven. The end product is prepared for expansion in a 900 °C furnace up to 100–300 times without oxidation (Taherian, 2019). The utilization of EG has been documented in various studies for the purpose of removing heavy and diesel oil (Bayat et al., 2008; Ding et al., 2014a; Hristea & Budrugaec, 2008; Inagaki et al., 2001; Takeuchi et al., 2017), biomedical wastes (Cuccarese et al., 2021), heavy metals, and organic dyes (Carvallho et al., 2016; Linh et al., 2019).

Furthermore, it should be noted that EG exhibits recyclability and can be easily disposed of when required, as shown by previous studies (Caniani et al., 2018). The research conducted by

Li et al. (2008) examined the efficacy of EG in eliminating dyes from water solutions. However, the investigation revealed that EG exhibited a prolonged adsorption time for the targeted pollutants (M. Li et al., 2008). In a separate investigation, Zhao and Liu (2009) used a technique involving the utilization of modified EG (MEG). This was achieved by introducing a mixture of sulfuric and nitric acid (in a ratio of 4:1, v/v) to graphite powders at ambient temperature. The resulting mixture was then subjected to agitation for 16 hours, followed by a complete washing using water and subsequent drying at a temperature of 100 °C. The graphene oxide (GO) was subjected to thermal expansion at a temperature of 600 °C for 90 minutes in a nitrogen environment. According to (M. Zhao & Liu, 2009), the findings of their study indicated that the adsorption effectiveness of MB removal can be enhanced by factors such as basic pH, increased starting dye concentration, and elevated temperature. However, the potential for regeneration of MEG was not addressed in this work. In their study, Hoang et al. (2019) used MW technology to generate the EG material. The composition of the GIC consisted of natural graphite, KMnO_4 , HClO_4 , and $(\text{CH}_3\text{CO})_2\text{O}$ in a ratio of 1:0.5:1:0.4. The reaction was kept for 10 seconds. Subsequently, the mixtures were subjected to microwave irradiation at a power of 720 W for 40 seconds, resulting in the production of EG. The measured surface area of EG was around $30 \text{ M}^2 \text{ g}^{-1}$. Ethanol was used as a solvent for the purpose of desorbing the MB that had been adsorbed in the EG pores and then regenerating the material. However, the findings of Hoang et al. (2019) indicated that the solvent regeneration technique led to a notable decrease in the adsorption efficiency. In their study, Wu et al. (2021) used an explosive combustion approach using black powder to synthesize an EG/ Fe_3O_4 composite. The authors emphasized that this particular approach yielded no hazardous waste by-products. However, the study conducted by (Wu et al., 2021) did not include any discussion on regeneration research related to dye removal.

In order to address the issue of low density in EG, one potential solution from a practical standpoint is the granulation and impregnation of EG powder using CaCl_2 and sodium alginate, as discussed in the material and method section. This approach is advantageous since granular forms can be removed from the solution without the need for additional processes. In addition, the use of microwave irradiation during the manufacturing of granular forms can lead to the modification of the resulting material and facilitate the improvement of the adsorption process. The use of MW irradiation is justified by its ability to effectively eliminate substances inside pores and enhance macro-porosity, therefore facilitating the connection between mesopores.

Additionally, the use of granular form not only has the potential to enhance the adsorption process but also facilitates the regeneration of materials due to their distinctive shape.

Chemical reagents have been used in many research as a means of regeneration, including the use of ethanol (Hoang et al., 2019), 1% HCl, H₂SO₄, and NaOH (Pathania et al., 2017) for desorption purposes. The findings of Hoang et al. (2019) show that the use of solvents may have a notable impact on the adsorption capacity of regenerated EG, resulting in a considerable reduction. Furthermore, it was observed that the process of employing solvents is both time-consuming and energy-intensive. Moreover, the management of solvents after the process of regeneration poses a remarkable concern within the field of chemical regeneration.

On the other hand, thermal regeneration can act as a viable option due to facilitating a more efficient procedure. However, the heat regeneration process encounters a notable reduction in material weight owing to friction, burn-off, and washout, leading to a decline in adsorption capacity (Gagliano et al., 2021). Moreover, the issue of energy consumption is a significant consideration in the context of thermal regeneration. The typical approach, which involves pre-heating using an oven, has limited practical and theoretical usefulness, as previously discussed. Gagliano et al. (2021) recently did research whereby they investigated the regeneration of AC-saturated PFAS with the use of MW irradiation. The findings of their study demonstrated the potential efficacy of microwave irradiation in revitalizing activated carbon adsorbents.

Therefore, these challenges emphasize the need for innovative technology and cost-effective recycling methods in the context of extensive dye removal applications. The use of MW irradiation has been recognized as a very effective method for the aim of thermal regeneration due to its rapid heating rate, exceptional heat transfer efficiency, and minimal contact durations (Gagliano et al., 2021). The MW system exhibits a heat direction from the inside to the outside, which has been seen to effectively remove impurities that are trapped inside carbon materials (Zaker et al., 2019), particularly mesoporous EG,

The objective of this chapter was to enhance the use of MW granular EG (MW-EG) as an effective adsorbent and evaluate its efficacy in the removal of organic dye (methylene blue (MB)) from aqueous solutions as a model system.

The effectiveness of a MW step to dry the G-EG soaked in DDW was investigated in order to improve the final product of G-EG. The implementation of this process was intended for application during the regeneration phase, where G-EG spent for organic dye was irradiated by an MW to recycle the material and to be used for the second cycle. Interestingly, after

regeneration, there was a significant decrease in the time needed to remove MB, from 1 day to 30 minutes in the second cycle of the application of adsorbent. Due to the observed decrease in adsorption contact time following microwave regeneration, the utilization of MW in synthesizing G-EG was suggested. Consequently, the adsorbent material was designated as MW-EG. Therefore, 2 types of granular forms were applied in this study: firstly, G-EG, which is produced without MW application in one step, and MW-EG, which was produced in two steps by using MW setup.

Chapter 2 References

- Achazhiyath Edathil, A., Pal, P., Kannan, P., & Banat, F. (2020). Total organic acid adsorption using alginate/clay hybrid composite for industrial lean amine reclamation using fixed-bed: Parametric study coupled with foaming. *International Journal of Greenhouse Gas Control*, *94*, 102907. <https://doi.org/10.1016/j.ijggc.2019.102907>
- Aivalioti, M., Pothoulaki, D., Papoulias, P., & Gidarakos, E. (2012). Removal of BTEX, MTBE, and TAME from aqueous solutions by adsorption onto raw and thermally treated lignite. *Journal of Hazardous Materials*, *207–208*, 136–146. <https://doi.org/10.1016/j.jhazmat.2011.04.084>
- Alabadi, A., Razzaque, S., Yang, Y., Chen, S., & Tan, B. (2015). Highly porous activated carbon materials from carbonized biomass with high CO₂ capturing capacity. *Chemical Engineering Journal*, *281*, 606–612. <https://doi.org/10.1016/j.cej.2015.06.032>
- Aleghafouri, A., Hasanzadeh, N., Mahdyarfar, M., SeifKordi, A., Mahdavi, S. M., & Zoghi, A. T. (2015). Experimental and theoretical study on BTEX removal from aqueous solution of diethanolamine using activated carbon adsorption. *Journal of Natural Gas Science and Engineering*, *22*, 618–624. <https://doi.org/10.1016/j.jngse.2015.01.010>
- Alhwaige, A. A., Agag, T., Ishida, H., & Qutubuddin, S. (2013). Biobased chitosan hybrid aerogels with superior adsorption: Role of graphene oxide in CO₂ capture. *RSC Advances*, *3*(36), 16011–16020. <https://doi.org/10.1039/C3RA42022A>
- Avdeev, V. V., Martynov, I. U., Nikol'skaya, I. V., Monyakina, L. A., & Sorokina, N. E. (1996). Investigation of the Graphite-H₂SO₄-gaseous oxidizer (Cl₂, O₃, SO₃) system. *Journal of Physics and Chemistry of Solids*, *57*(6), Article 6. [https://doi.org/10.1016/0022-3697\(96\)00359-9](https://doi.org/10.1016/0022-3697(96)00359-9)
- Bach LG, Linh NTN, Thuong NT, Quynh BTP, Hoang NM and Ho VTT (2016) Studying of the effect of adsorption conditions for the Removal of diesel oil from wastewater using the magnetic exfoliated graphite/CoFe₂O₄. *Journal of Multidisciplinary Engineering Science and Technology (JMEST)* *3*(5): 4870-4873. <http://www.jmest.org/wp-content/uploads/JMESTN42351603.pdf>
- Bashir, A., Malik, L. A., Ahad, S., Manzoor, T., Bhat, M. A., Dar, G. N., & Pandith, A. H. (2019). Removal of heavy metal ions from aqueous system by ion-exchange and biosorption methods. *Environmental Chemistry Letters*, *17*(2), 729–754. <https://doi.org/10.1007/s10311-018-00828-y>
- Bayat, A., S.f, A., & A, M. (2008). *OIL SORPTION BY SYNTHESIZED EXFOLIATED GRAPHITE (EG)* (1). *5*(1), Article 1.
- Chen, X. Y., Chen, C., Zhang, Z. J., & Xie, D. H. (2013). Gelatin-derived nitrogen-doped porous carbon via a dual-template carbonization method for high performance supercapacitors. *Journal of Materials Chemistry A*, *1*(36), 10903–10911. <https://doi.org/10.1039/C3TA12328F>
- Chung, D. D. L. (1987). Intercalate vaporization during the exfoliation of graphite intercalated with bromine. *Carbon*, *25*(3), Article 3. [https://doi.org/10.1016/0008-6223\(87\)90007-8](https://doi.org/10.1016/0008-6223(87)90007-8)
- Cuccarese, M., Brutti, S., De Bonis, A., Teghil, R., Mancini, I. M., Masi, S., & Caniani, D. (2021). Removal of diclofenac from aqueous solutions by adsorption on thermo-plasma expanded graphite. *Scientific Reports*, *11*(1), Article 1. <https://doi.org/10.1038/s41598-021-83117-z>

- Daifullah, A. A. M., & Girgis, B. S. (2003). Impact of surface characteristics of activated carbon on adsorption of BTEX. *Colloids and Surfaces A: Physicochemical and Engineering Aspects*, 214(1), Article 1. [https://doi.org/10.1016/S0927-7757\(02\)00392-8](https://doi.org/10.1016/S0927-7757(02)00392-8)
- Ding, Z., Hu, X., Zimmerman, A. R., & Gao, B. (2014). Sorption and cosorption of lead (II) and methylene blue on chemically modified biomass. *Bioresource Technology*, 167, 569–573. <https://doi.org/10.1016/j.biortech.2014.06.043>
- Do, Q. C., Choi, S., Kim, H., & Kang, S. (2019). Adsorption of Lead and Nickel on to Expanded Graphite Decorated with Manganese Oxide Nanoparticles. *Applied Sciences*, 9(24), Article 24. <https://doi.org/10.3390/app9245375>
- Ersan, G., Apul, O. G., Perreault, F., & Karanfil, T. (2017). Adsorption of organic contaminants by graphene nanosheets: A review. *Water Research*, 126, 385–398. <https://doi.org/10.1016/j.watres.2017.08.010>
- Falco, C., Baccile, N., & Titirici, M.-M. (2011). Morphological and structural differences between glucose, cellulose and lignocellulosic biomass derived hydrothermal carbons. *Green Chemistry*, 13(11), 3273–3281. <https://doi.org/10.1039/C1GC15742F>
- Gong, J.-L., Zhang, Y.-L., Jiang, Y., Zeng, G.-M., Cui, Z.-H., Liu, K., Deng, C.-H., Niu, Q.-Y., Deng, J.-H., & Huan, S.-Y. (2015). Continuous adsorption of Pb(II) and methylene blue by engineered graphite oxide coated sand in fixed-bed column. *Applied Surface Science*, 330, 148–157. <https://doi.org/10.1016/j.apsusc.2014.11.068>
- Gopinath, K. P., Vo, D.-V. N., Gnana Prakash, D., Adithya Joseph, A., Viswanathan, S., & Arun, J. (2021). Environmental applications of carbon-based materials: A review. *Environmental Chemistry Letters*, 19(1), 557–582. <https://doi.org/10.1007/s10311-020-01084-9>
- Hristea, G., & Budrugaec, P. (2008). Characterization of exfoliated graphite for heavy oil sorption. *Journal of Thermal Analysis and Calorimetry*, 91(3), Article 3. <https://doi.org/10.1007/s10973-006-7465-x>
- Inagaki, M., Konno, H., Toyoda, M., Moriya, K., & Kihara, T. (2000). sorption and recovery of heavy oils by using exfoliated graphite Part II: Recovery of heavy oil and recycling of exfoliated graphite. *Desalination*, 128(3), Article 3. [https://doi.org/10.1016/S0011-9164\(00\)00035-7](https://doi.org/10.1016/S0011-9164(00)00035-7)
- Inagaki, M., Shibata, K., Setou, S., Toyoda, M., & Aizawa, J. (2000). sorption and recovery of heavy oils by using exfoliated graphite Part III: Trials for practical applications. *Desalination*, 128(3), Article 3. [https://doi.org/10.1016/S0011-9164\(00\)00036-9](https://doi.org/10.1016/S0011-9164(00)00036-9)
- Inagaki, M., Tashiro, R., Washino, Y., & Toyoda, M. (2004). Exfoliation process of graphite via intercalation compounds with sulfuric acid. *Journal of Physics and Chemistry of Solids*, 65(2), Article 2. <https://doi.org/10.1016/j.jpics.2003.10.007>
- Inagaki, M., Toyoda, M., Iwashita, N., Nishi, Y., & Konno, H. (2001). Exfoliated Graphite for Spilled Heavy Oil Recovery. *Carbon Letters*, 2(1), Article 1.
- Iqbal, M. Z., & Abdala, A. A. (2013). Oil spill cleanup using graphene. *Environmental Science and Pollution Research*, 20(5), Article 5. <https://doi.org/10.1007/s11356-012-1257-6>

- Jaynes, W. F., & Vance, G. F. (1996). BTEX Sorption by Organo-Clays: Cosorptive Enhancement and Equivalence of Interlayer Complexes. *Soil Science Society of America Journal*, 60(6), Article 6. <https://doi.org/10.2136/sssaj1996.03615995006000060019x>
- Kamio, E., Yoshida, H., & Saiki, Y. (2004). Adsorption Mechanism of Organic Acids on Highly Porous PEI Chitosan Beads—Adsorption Isotherm and Adsorption Rate—. *Asian Pacific Confederation of Chemical Engineering Congress Program and Abstracts, 2004*, 999–999. <https://doi.org/10.11491/apcche.2004.0.999.0>
- Kang, F., Leng, Y., & Zhang, T.-Y. (1997). Electrochemical synthesis and characterization of formic acid-graphite intercalation compound. *Carbon*, 35(8), Article 8. [https://doi.org/10.1016/S0008-6223\(97\)00065-1](https://doi.org/10.1016/S0008-6223(97)00065-1)
- Kecili, R., & Hussain, C. M. (2018). Chapter 4—Mechanism of Adsorption on Nanomaterials. In C. M. Hussain (Ed.), *Nanomaterials in Chromatography* (pp. 89–115). Elsevier. <https://doi.org/10.1016/B978-0-12-812792-6.00004-2>
- Khang, D. S., Hai, T. D., Thi, T. D., & Tuan, P. D. (2020). Dye removal using cashew nut shell activated carbon. *Vietnam Journal of Chemistry*, 58(6), 832–840. <https://doi.org/10.1002/vjch.202000096>
- Kitaoka, S., Wada, M., Nagai, T., Osa, N., & Konno, T. (2011). Increasing the thermal diffusivity of flexible graphite sheets by superheated steam treatment. *Journal of Materials Science*, 46(4), 1132–1135. <https://doi.org/10.1007/s10853-010-4991-5>
- Kong, Y., Chen, X., Ni, J., Yao, S., Wang, W., Luo, Z., & Chen, Z. (2010). Palygorskite-expanded graphite electrodes for catalytic electro-oxidation of phenol. *Applied Clay Science*, 49(1), 64–68. <https://doi.org/10.1016/j.clay.2010.04.003>
- Lee, K., & Neff, J. (2011). *Produced Water: Environmental Risks and Advances in Mitigation Technologies*. Springer Science & Business Media.
- Lee, Y.-C., & Yang, J.-W. (2012). Self-assembled flower-like TiO₂ on exfoliated graphite oxide for heavy metal removal. *Journal of Industrial and Engineering Chemistry*, 18(3), Article 3. <https://doi.org/10.1016/j.jiec.2012.01.005>
- Li, M., Li, J.-T., & Sun, H.-W. (2008). Decolorizing of azo dye Reactive red 24 aqueous solution using exfoliated graphite and H₂O₂ under ultrasound irradiation. *Ultrasonics Sonochemistry*, 15(5), 717–723. <https://doi.org/10.1016/j.ultsonch.2007.10.001>
- Li, S., Tian, S., Feng, Y., Lei, J., Wang, P., & Xiong, Y. (2010). A comparative investigation on absorption performances of three expanded graphite-based complex materials for toluene. *Journal of Hazardous Materials*, 183(1), Article 1. <https://doi.org/10.1016/j.jhazmat.2010.07.052>
- Liao, Q., Sun, J., & Gao, L. (2008). The adsorption of resorcinol from water using multi-walled carbon nanotubes. *Colloids and Surfaces A: Physicochemical and Engineering Aspects*, 312(2), 160–165. <https://doi.org/10.1016/j.colsurfa.2007.06.045>
- Lu, Y. (2012). Size Effect of Expandable Graphite. *Advanced Materials Research*, 499, 72–75. <https://doi.org/10.4028/www.scientific.net/AMR.499.72>
- MacGowan, D. B., & Surdam, R. C. (1988). Difunctional carboxylic acid anions in oilfield waters. *Organic Geochemistry*, 12(3), Article 3. [https://doi.org/10.1016/0146-6380\(88\)90262-8](https://doi.org/10.1016/0146-6380(88)90262-8)

- Makhathini, T. P., & Rathilal, S. (2017). Investigation of BTEX compounds adsorption onto polystyrenic resin. *South African Journal of Chemical Engineering*, 23, 71–80. <https://doi.org/10.1016/j.sajce.2017.03.001>
- Makhathini, T. P., & Rathilal, S. (2018). Modelling competitive BTEX compounds removal from industrial wastewater in packed-bed columns using polystyrenic resin. *Journal of Water Reuse and Desalination*, 8(3), Article 3. <https://doi.org/10.2166/wrd.2017.045>
- Makotchenko, V. G., Grayfer, E. D., Nazarov, A. S., Kim, S.-J., & Fedorov, V. E. (2011). The synthesis and properties of highly exfoliated graphites from fluorinated graphite intercalation compounds. *Carbon*, 49(10), Article 10. <https://doi.org/10.1016/j.carbon.2011.03.049>
- Mashkooor, F., Nasar, A., & Inamuddin. (2020). Carbon nanotube-based adsorbents for the Removal of dyes from waters: A review. *Environmental Chemistry Letters*, 18(3), 605–629. <https://doi.org/10.1007/s10311-020-00970-6>
- Metcalf, & Eddy. (2013). *Wastewater Engineering: Treatment and Reuse*. McGraw-Hill Higher Education.
- Minitha, M., L., Y.I., J., L., S., & R.t., R. K. (2017). Adsorption behavior of reduced graphene oxide towards cationic and anionic dyes: Co-action of electrostatic and $\pi - \pi$ interactions. *Materials Chemistry and Physics*, 194, 243–252. <https://doi.org/10.1016/j.matchemphys.2017.03.048>
- Mondal, M. K. (2009). Removal of Pb(II) ions from aqueous solution using activated tea waste: Adsorption on a fixed-bed column. *Journal of Environmental Management*, 90(11), Article 11. <https://doi.org/10.1016/j.jenvman.2009.05.025>
- Morad, M., Hilali, M., Bazzi, L., & Chaouay, A. (2014). Adsorption of Organic Molecule (acetic acid) on Activated Carbon in Aqueous. *Moroccan Journal of Chemistry*, 2(5), Article 5.
- Natarajan, R., Saikia, K., Ponnusamy, S. K., Rathankumar, A. K., Rajendran, D. S., Venkataraman, S., Tannani, D. B., Arvind, V., Somanna, T., Banerjee, K., Mohideen, N., & Vaidyanathan, V. K. (2022). Understanding the factors affecting adsorption of pharmaceuticals on different adsorbents – A critical literature update. *Chemosphere*, 287, 131958. <https://doi.org/10.1016/j.chemosphere.2021.131958>
- Nourmoradi, H., Khiadani, M., & Nikaeen, M. (2012, July 12). *Multi-Component Adsorption of Benzene, Toluene, Ethylbenzene, and Xylene from Aqueous Solutions by Montmorillonite Modified with Tetradecyl Trimethyl Ammonium Bromide* [Research Article]. *Journal of Chemistry*; Hindawi. <https://doi.org/10.1155/2013/589354>
- Olanipekun, O., Oyefusi, A., Neelgund, G. M., & Oki, A. (2014). Adsorption of lead over graphite oxide. *Spectrochimica Acta Part A: Molecular and Biomolecular Spectroscopy*, 118, 857–860. <https://doi.org/10.1016/j.saa.2013.09.088>
- Pham, T. V., Nguyen, T. T., Nguyen, D. T., Thuan, T. V., Bui, P. Q. T., Viet, V. N. D., & Bach, L. G. (2019). The Preparation and Characterization of Expanded Graphite via Microwave Irradiation and Conventional Heating for the Purification of Oil Contaminated Water. *Journal of Nanoscience and Nanotechnology*, 19(2), Article 2. <https://doi.org/10.1166/jnn.2019.15926>
- Pradhan, N., Rene, E. R., Lens, P. N. L., Dipasquale, L., D'Ippolito, G., Fontana, A., Panico, A., & Esposito, G. (2017). Adsorption Behavior of Lactic Acid on Granular Activated Carbon and Anionic

Resins: Thermodynamics, Isotherms and Kinetic Studies. *Energies*, 10(5), Article 5.
<https://doi.org/10.3390/en10050665>

Rathi, B. S., Kumar, P. S., & Show, P.-L. (2021). A review on effective Removal of emerging contaminants from aquatic systems: Current trends and scope for further research. *Journal of Hazardous Materials*, 409, 124413. <https://doi.org/10.1016/j.jhazmat.2020.124413>

Saikam, L., Arthi, P., Senthil, B., & Shanmugam, M. (2023). A review on exfoliated graphite: Synthesis and applications. *Inorganic Chemistry Communications*, 152, 110685.
<https://doi.org/10.1016/j.inoche.2023.110685>

Seifi, L., Torabian, A., Kazemian, H., Bidhendi, G. N., Azimi, A. A., Nazmara, S., & AliMohammadi, M. (2011). Adsorption of BTEX on Surfactant Modified Granulated Natural Zeolite Nanoparticles: Parameters Optimizing by Applying Taguchi Experimental Design Method. *CLEAN – Soil, Air, Water*, 39(10), Article 10. <https://doi.org/10.1002/clen.201000390>

Shahbazi, A., Younesi, H., & Badiei, A. (2013). Batch and fixed-bed column adsorption of Cu(II), Pb(II) and Cd(II) from aqueous solution onto functionalised SBA-15 mesoporous silica. *The Canadian Journal of Chemical Engineering*, 91(4), Article 4. <https://doi.org/10.1002/cjce.21691>

Sheet, I., Kabbani, A., & Holail, H. (2014). Removal of Heavy Metals Using Nanostructured Graphite Oxide, Silica Nanoparticles and Silica/ Graphite Oxide Composite. *Energy Procedia*, 50, 130–138.
<https://doi.org/10.1016/j.egypro.2014.06.016>

Snoeyink, V. L., & Summers, R. S. (1999). Adsorption of Organic Compounds. In *Water Quality and Treatment: A Handbook of Community Water Supplies*. (5th ed.). American Water Works Assn./McGraw Hill.

Song, X., Zhang, Y., & Chang, C. (2012). Novel Method for Preparing Activated Carbons with High Specific Surface Area from Rice Husk. *Industrial & Engineering Chemistry Research*, 51(46), 15075–15081. <https://doi.org/10.1021/ie3012853>

Su, F., Lu, C., & Hu, S. (2010). Adsorption of benzene, toluene, ethylbenzene and p-xylene by NaOCl-oxidized carbon nanotubes. *Colloids and Surfaces A: Physicochemical and Engineering Aspects*, 353(1), Article 1. <https://doi.org/10.1016/j.colsurfa.2009.10.025>

Su, F., Lu, C., & Tai, J.-H. (2016). Separation of Benzene, Toluene, Ethylbenzene and P-Xylene from Aqueous Solutions by Carbon Nanotubes/Polyvinylidene Fluoride Nano-composite Membrane. *Journal of Water Resource and Protection*, 8(10), Article 10.
<https://doi.org/10.4236/jwarp.2016.810075>

Sun, Y., & Webley, P. A. (2011). Preparation of Activated Carbons with Large Specific Surface Areas from Biomass Corn cob and Their Adsorption Equilibrium for Methane, Carbon Dioxide, Nitrogen, and Hydrogen. *Industrial & Engineering Chemistry Research*, 50(15), 9286–9294.
<https://doi.org/10.1021/ie1024003>

Sun, Y., Yang, G., Zhang, J., Wang, Y., & Yao, M. (2012). Activated Carbon Preparation from Lignin by H₃PO₄ Activation and Its Application to Gas Separation. *Chemical Engineering & Technology*, 35(2), 309–316. <https://doi.org/10.1002/ceat.201100309>

Sykam, N., Gautam, R. K., & Kar, K. K. (2015). Electrical, mechanical, and thermal properties of exfoliated graphite/phenolic resin composite bipolar plate for polymer electrolyte membrane fuel cell. *Polymer Engineering & Science*, 55(4), 917–923. <https://doi.org/10.1002/pen.23959>

- Szala, B., Bajda, T., Matusik, J., Zięba, K., & Kijak, B. (2015). BTX sorption on Na-P1 organo-zeolite as a process controlled by the amount of adsorbed HDTMA. *Microporous and Mesoporous Materials*, 202, 115–123. <https://doi.org/10.1016/j.micromeso.2014.09.033>
- Taherian, R. (2019). 7 - Application of Polymer-Based Composites: Bipolar Plate of PEM Fuel Cells. In R. Taherian & A. Kausar (Eds.), *Electrical Conductivity in Polymer-Based Composites* (pp. 183–237). William Andrew Publishing. <https://doi.org/10.1016/B978-0-12-812541-0.00007-0>
- Takeuchi, K., Fujishige, M., Kitazawa, H., Akuzawa, N., Medina, J. O., Morelos-Gomez, A., Cruz-Silva, R., Araki, T., Hayashi, T., Terrones, M., & Endo, M. (2015). Oil sorption by exfoliated graphite from dilute oil–water emulsion for practical applications in produced water treatments. *Journal of Water Process Engineering*, 8, 91–98. <https://doi.org/10.1016/j.jwpe.2015.09.002>
- Takeuchi, K., Kitazawa, H., Fujishige, M., Akuzawa, N., Ortiz-Medina, J., Morelos-Gomez, A., Cruz-Silva, R., Araki, T., Hayashi, T., & Endo, M. (2017). Oil removing properties of exfoliated graphite in actual produced water treatment. *Journal of Water Process Engineering*, 20, 226–231. <https://doi.org/10.1016/j.jwpe.2017.11.009>
- Tombácz, E., Tóth, I. Y., Nesztor, D., Illés, E., Hajdú, A., Szekeres, M., & L.Vékás. (2013). Adsorption of organic acids on magnetite nanoparticles, pH-dependent colloidal stability and salt tolerance. *Colloids and Surfaces A: Physicochemical and Engineering Aspects*, 435, 91–96. <https://doi.org/10.1016/j.colsurfa.2013.01.023>
- Toyoda, M., & Inagaki, M. (2000). Heavy oil sorption using exfoliated graphite: New application of exfoliated graphite to protect heavy oil pollution. *Carbon*, 38(2), 199–210. [https://doi.org/10.1016/S0008-6223\(99\)00174-8](https://doi.org/10.1016/S0008-6223(99)00174-8)
- Toyoda, M., Moriya, K., Aizawa, J., Konno, H., & Inagaki, M. (2000a). Sorption and recovery of heavy oils by using exfoliated graphite Part I: Maximum sorption capacity. *Desalination*, 128(3), Article 3. [https://doi.org/10.1016/S0011-9164\(00\)00034-5](https://doi.org/10.1016/S0011-9164(00)00034-5)
- Toyoda, M., Moriya, K., Aizawa, J., Konno, H., & Inagaki, M. (2000b). Sorption and recovery of heavy oils by using exfoliated graphite Part I: Maximum sorption capacity. *Desalination*, 128(3), Article 3. [https://doi.org/10.1016/S0011-9164\(00\)00034-5](https://doi.org/10.1016/S0011-9164(00)00034-5)
- Toyoda, M., Nishi, Y., Iwashita, N., & Inagaki, M. (2003). Sorption and recovery of heavy oils using exfoliated graphite Part IV: Discussion of high oil sorption of exfoliated graphite. *Desalination*, 151(2), Article 2. [https://doi.org/10.1016/S0011-9164\(02\)00992-X](https://doi.org/10.1016/S0011-9164(02)00992-X)
- Tryba, B., Przepiórski, J., & Morawski, A. W. (2003). Influence of chemically prepared H₂SO₄-graphite intercalation compound (GIC) precursor on parameters of exfoliated graphite (EG) for oil sorption from water. [https://doi.org/10.1016/S0008-6223\(03\)00200-8](https://doi.org/10.1016/S0008-6223(03)00200-8)
- Tuan Nguyen, H. D., Nguyen, H. T., Nguyen, T. T., Le Thi, A. K., Nguyen, T. D., Phuong Bui, Q. T., & Bach, L. G. (2019). The Preparation and Characterization of MnFe₂O₄-Decorated Expanded Graphite for Removal of Heavy Oils from Water. *Materials*, 12(12), Article 12. <https://doi.org/10.3390/ma12121913>
- Vianna, M. M. G. R., Valenzuela-Díaz, F. R., Kozievitch, V. F. J., Dweck, J., & Büchler, P. M. (2005). *Synthesis and Characterization of Modified Clays as Sorbents of Toluene and Xylene*. Materials Science Forum; Trans Tech Publications Ltd. <https://doi.org/10.4028/www.scientific.net/MSF.498-499.691>

- Vieira, W. T., de Farias, M. B., Spaolonzi, M. P., da Silva, M. G. C., & Vieira, M. G. A. (2020). Removal of endocrine disruptors in waters by adsorption, membrane filtration and biodegradation. A review. *Environmental Chemistry Letters*, 18(4), 1113–1143. <https://doi.org/10.1007/s10311-020-01000-1>
- Wang, G., Sun, Q., Zhang, Y., Fan, J., & Ma, L. (2010). Sorption and regeneration of magnetic exfoliated graphite as a new sorbent for oil pollution. *Desalination*, 263(1), Article 1. <https://doi.org/10.1016/j.desal.2010.06.056>
- Wang, H., Dai, Q., Li, Q., Yang, J., Zhong, X., Huang, Y., Zhang, A., & Yan, Z. (2009). Preparation of porous carbon spheres from porous starch. *Solid State Ionics*, 180(26), 1429–1432. <https://doi.org/10.1016/j.ssi.2009.08.006>
- Wang, J., Heerwig, A., Lohe, M. R., Oschatz, M., Borchardt, L., & Kaskel, S. (2012). Fungi-based porous carbons for CO₂ adsorption and separation. *Journal of Materials Chemistry*, 22(28), 13911–13913. <https://doi.org/10.1039/C2JM32139D>
- Yakovlev, A. V., Finaenov, A. I., Zabud'kov, S. L., & Yakovleva, E. V. (2006). Thermally expanded graphite: Synthesis, properties, and prospects for use. *Russian Journal of Applied Chemistry*, 79(11), Article 11. <https://doi.org/10.1134/S1070427206110012>
- Yi, M., & Shen, Z. (2015). A review on mechanical exfoliation for the scalable production of graphene. *Journal of Materials Chemistry A*, 3(22), Article 22. <https://doi.org/10.1039/C5TA00252D>
- You, S., Liu, D.-S., Ye, M., Zhang, Y., Tang, Y., Liu, X., & Chao Li, C. (2023). Graphite intercalation compounds (GICs) based multi-functional interface layer toward highly reversible Zn metal anodes. *Chemical Engineering Journal*, 454, 139907. <https://doi.org/10.1016/j.cej.2022.139907>
- Yu, F., Ma, J., Wang, J., Zhang, M., & Zheng, J. (2016). Magnetic iron oxide nanoparticles functionalized multi-walled carbon nanotubes for toluene, ethylbenzene and xylene Removal from aqueous solution. *Chemosphere*, 146, 162–172. <https://doi.org/10.1016/j.chemosphere.2015.12.018>
- Yurtsever, M., & Şengül, . Ayhan. (2012). Adsorption and desorption behavior of silver ions onto valonia tannin resin. *Transactions of Nonferrous Metals Society of China*, 22(11), Article 11. [https://doi.org/10.1016/S1003-6326\(11\)61541-0](https://doi.org/10.1016/S1003-6326(11)61541-0)
- Zheng, W., Wong, S.-C., & Sue, H.-J. (2002). Transport behavior of PMMA/expanded graphite nano-composites. *Polymer*, 43(25), 6767–6773. [https://doi.org/10.1016/S0032-3861\(02\)00599-2](https://doi.org/10.1016/S0032-3861(02)00599-2)

Chapter 3: Material and Methodology

This chapter initially discusses the attributes of the model pollutants, and the adsorption materials and chemical agents. Subsequently, a comprehensive account of the analytical methodologies employed for both aqueous solutions and solids is provided. Lastly, this section describes the various experimental apparatuses and elaborates on their respective operational modes.

3.1 Model molecules, adsorption materials, and chemicals

The investigation was conducted using an Organic pollutant contaminant known as methylene blue, as well as crude oil.

Different graphite materials were employed for the remediation of these contaminants using the adsorption approach.

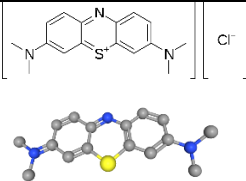
- The application of powder-EG
- The examination of MW-EG was prepared with the thermal method.

A range of chemical substances were utilized in this study. The characteristics of the subject are delineated below:

3.1.1 Methylene Blue:

Methylene blue (MB) is used as a model organic pollutant because of its unique features, which make it a good representation for adsorption and removal investigations. Methylene blue, a cationic thiazine dye, is utilized because of its high-water solubility, low environmental toxicity, and fast detection without colorimetric procedures that employ indicators and create additional by-products that must be handled. For these reasons, it helps develop a standard framework for analyzing adsorption processes across research and sheds light on the efficacy of different adsorbent materials and treatment approaches.

Table 3.1 MB properties

Symbol	Molecular formula	Chemical structure	pKa	Charges	maximum absorption peak	Solubility in water 25 C*
MB	C ₁₆ H ₁₈ ClN ₃ S		3.14	Positive because of N	664 nm	43,600 mg L ⁻¹

3.1.2 Crude oil:

Raw crude oil from Texas was used for this study. Table 3.2 shows the characteristics of the oil.

Table 3.2 Texas raw crude oil ([Environment Canada 2016b West Texas Intermediate](#))

Properties	Values
Sulphur (weigh %)	0.48-0.57
Flash point (C)	-17 to 87
Density (g mL ⁻¹)	0.85-0.89

Kinematic viscosity (mm² S⁻¹)	5
Benzene (mg L⁻¹)	310-1380
Toluene (mg L⁻¹)	2150-2860
Ethylbenzene (mg L⁻¹)	990-1120
Xylenes (mg L⁻¹)	3900-4290

3.1.3 Adsorbent and materials used:

In this work, an adsorbent material known as Commercial EG powder was provided by Innograf (Potenza, Italy). This powder was subsequently utilized to produce G-EG. The procedure of thermal plasma expansion/exfoliation of graphite was conducted by a supply business under strict confidentiality. Following are the stages involved in producing G-EG.

3.1.3.1 Encapsulation process of EG powder and making granular forms

This objective can be accomplished through the use of encapsulation. Encapsulation involves the creation of capsules that include a central core of encapsulated material, which is then surrounded by a layer of material known as encapsulation material or capsular formation material (Blandino et al., 1999). Sodium alginate, chemically represented as NaC₆H₇O₆, has the potential to be employed for this particular application. Alginic acid salt, derived from the cellular structures of brown algae, is extensively utilized in both the food and medicinal sectors. The polymer in question is a non-toxic and biodegradable substance composed of α -L-guluronic acid (block G) and β -D-mannuronic acid (block M) chains. These chains are organized in blocks of homopolymer regions referred to as MM and GG or in an alternating sequence denoted as MG. When subjected to agitation in the presence of water, it transforms its texture, resulting in a gel-like consistency (Cuccarese et al., 2021). The powder substance is introduced into a solution of sodium alginate and subjected to homogenization. The last step involves the formation of intermolecular bonds within the alginate molecules by the interaction of divalent ions, namely Ca²⁺, which are sourced from a solution of calcium chloride (CaCl₂) dissolved in water. The cross-linking process is initiated by introducing a solution containing powdered adsorbent material and sodium alginate into a solution of calcium chloride. The inclusion of the droplet facilitates the development of a granular morphology in the polymer. The adsorbent material in powder form stays trapped inside the polymer matrix of calcium

alginate during the process of cross-linking. Subsequently, the material can undergo a drying process within an oven, resulting in the formation of a granular state for the adsorbent material. The technique ensures a modification in both the morphology and density of the substance. The final parameter is contingent upon the quantity of sodium alginate employed, and it is possible to generate a material with a density greater than that of water.

3.1.3.2 Experimental plan of G-EG preparation

EG was employed as the primary material for the preparation of G-EG. To begin the experiment, a quantity of 20 grams of sodium alginate was dissolved in 1 liter of deionized distilled water (DDW) using a gentle magnetic stirring. This process was carried out for two hours at ambient temperature. A quantity of 2 grams of EG was introduced into the solution while subjecting it to magnetic stirring until a visually transparent mixture was achieved. Subsequently, the solution was placed into a separating funnel. Then, by opening the outlet of the funnel, the solution was added drop by drop into a beaker containing calcium chloride (2% concentration, prepared using distilled deionized water). The particle substance that was generated was separated from the solution by the use of a sieve. Subsequently, the specimens were subjected to an overnight thermal treatment within an oven set at a temperature of 105°C. As a result, the material that was acquired was designated as G-EG. Fig 3.1 depicts the procedure involved in the preparation of the EG granule, as outlined in step 1. In the next step, a commercially available microwave source was employed to eliminate impurities present in the EG granule. A quantity of 2 grams of G-EG was immersed in a vial containing 50 milliliters of DDW.

Subsequently, for one hour, during which the vial was subjected to agitation in an orbital shaker, the saturated EG granule solution underwent filtration in order to eliminate any residual DDW. The moisture level of the material was found to be nearly 100% before undergoing MW treatment. The removal of contaminants that obstruct the channels between pores inside the mesoporous scale is made possible by DDW stored in enlarged graphite pores, which also permits MW heating. As opposed to convection, which is how conventional heating works, MW irradiation allows for the formation of temperature gradients volumetrically across the volume of the material (Zaker et al., 2019). The G-EG solution, saturated with DDW, was subjected to microwave irradiation at several power levels and for varied durations. DDW could be eliminated from pores and the structure of the GTPEG with 510 watts of application

for 2 minutes. The final substance was designated as MW-EG granule and stored in dry for further application.

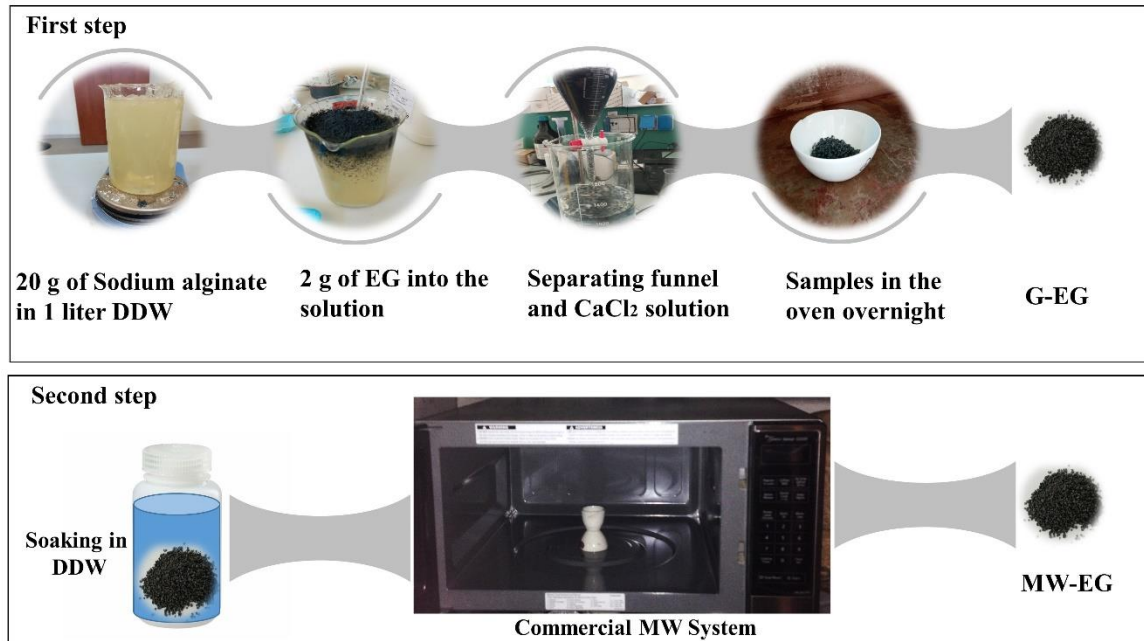


Fig 3.1 The stages of MW-EG preparation

3.1.4 Materials and reagents

Commercial thermo-plasma EG (EG) was supplied by Innograf (Potenza, Italy). Concentrated hydrochloric acid (HCl) and sodium hydroxide (NaOH) were used to adjust the pH values. Methylene blue (molecular weight: 319.86; maximum wavelength: 666 nm) was supplied by Carlo Erba Reagents as employed in this research. Furthermore, sodium alginate and calcium chloride from Carlo Erba Reagents were used.

3.2 Fourier Transform Infrared Spectrometer (FT-IR) analysis

Infrared spectroscopy is an academic discipline that focuses on investigating the intricate interplay between matter and infrared radiation. The primary quantity acquired in the field of infrared spectroscopy is an infrared spectrum, which is a graphical representation of the measured intensity of infrared radiation as a function of the wavelength (or wavenumber) of the light. The device employed for acquiring an infrared spectrum is commonly referred to as an infrared spectrometer. Several types of spectrometers exist worldwide that are employed for

the acquisition of infrared spectra. The predominant sort of spectrometer commonly employed is referred to as an FT-IR. The technique of infrared spectroscopy exhibits sensitivity towards the detection and determination of chemical functional groups inside a given sample. A functional group can be defined as a distinct structural element present inside a molecule. An illustration of a functional group may be observed in the C=O bond of a ketone or the CH₃ group present in a hydrocarbon.

One of the most notable advantages of infrared spectroscopy is its capability to facilitate the identification of unknown substances. The knowledge of wavenumber locations pertaining to the bands shown by a functional group may be effectively employed to identify and classify such functional groups across several samples. Another application of infrared spectra is the verification of identification. The process of identifying the composition of two samples involves comparing their spectra to ascertain if they share the same compositions. Infrared spectra possess the valuable characteristic of exhibiting peak intensities that are directly proportional to concentration. Consequently, these spectra may be effectively employed for quantifying concentrations. (Smith, 1998)

In an FTIR spectrometer, an infrared beam is sent through a sample, and afterward, the transmitted light is evaluated by means of an interferometer. The interferogram obtained is subjected to a Fourier transformation, leading to the generation of an infrared spectrum. In this spectrum, the observed peaks and troughs refer to distinct vibrational modes. The spectrum characteristics of the sample offer significant information about its chemical composition and structural properties. The apparatus generates a beam of infrared radiation, which originates out of a glowing black-body emitter.

Following this, the beam proceeds into the interferometer, where the process of spectrum encoding occurs. The phenomenon of both constructive and destructive interference, also known as an interferogram, is produced by a rearranging of beams that have varying path lengths within the interferometer. The incident beam penetrates the material's compartment, where the sample selectively takes distinct energy frequencies. These frequencies are distinctively indicative of the material's properties and may be identified from the interferogram. Subsequently, the detector proceeds to determine the distinct interferogram signal in terms of time and energy. Across all frequencies concurrently. Meanwhile, a beam is overlaid to serve as a background for the device's functioning. The desired spectra were

generated by subtracting the background spectrum from the obtained spectrum using Fourier transformation computer software (Mohamed et al., 2017).

3.3 Elemental Analysis

The advancement of organic chemistry has led to the emergence of new substances and components. These compounds and materials exhibit a complicated elemental makeup and arrangement, along with a diverse range of characteristics. They possess heat and chemical resistance, are non-combustible, volatile, hygroscopic, and susceptible to degradation in light. The accurate detection and confirmation of the compound's purity need a diagnosis of its constituent elements by organic fundamental analysis procedures (Fadeeva et al., 2008).

Simultaneous elemental analysis needs high-temperature combustion, typically conducted at around 1000 °C furnace temperature, inside an oxygen atmosphere. The combustion process could be conducted in two different ways: static settings, which include introducing a fixed amount of oxygen, and dynamic settings, which involve a continuous flow of oxygen over a while. Currently, instrument makers are utilizing or have employed both types of technology in elemental analysis. In some cases, catalysts are further introduced into the combustion chamber to facilitate the conversion process. Additional elemental combinations can be performed with the element's analysis., including individual analysis of carbon, nitrogen, and sulphur, as well as combined analysis of CN, CHN, and CNS. Historically, CHN analysis has proven widely adopted as the preferred method for elemental evaluation, with all vendors in the microanalytical sector offering that setup. During the burning process, carbon undergoes conversion to carbon dioxide, hydrogen is transformed into water, nitrogen is changed into either nitrogen gas or oxides of nitrogen, and sulphur is transformed into sulphur dioxide or sulphur trioxide. It is important to bear in mind that the presence of other elements, such as chlorine, may result in their conversion into the corresponding combustion compounds, like hydrogen chloride. Various absorbents are employed to eliminate these extra combustion by-products (Analytical Methods Committee, 2006).

After their formation, the combustion by-products are expelled from the furnace using an inert carrier gas, such as helium, and afterward directed onto a hot copper surface of high purity. The copper is positioned either at the bottom of the combustion tube or within an individual furnace, operating at around 600 °C. The primary purpose of this copper is to eliminate remaining oxygen that has not been utilized during the combustion process, as well

as to transform all nitrogen oxides into nitrogen gas. Subsequently, the exhaust gases pass via absorbent trapping with the purpose of separating carbon dioxide, water, nitrogen, and sulphur dioxide. The process of quantifying the elements entails calibrating the device on every occasion of its utilization. Several methods are employed to accomplish this objective; nevertheless, in essence, it needs to measure reaction factors, denoted as K factors, for all components utilizing high-purity substances known as ‘microanalytical standard’ substances, such as acetanilide and benzoic acid (Analytical Methods Committee, 2006).

3.4 BET surface area and pore size distribution analysis

The measurement of surface area and pore distribution is an essential component of material characterization, especially in the case of porous substances such as catalysts, adsorbents, and nanoparticles. The ASAP device, developed by Micromeritics, is a commonly employed instrument for performing surface area and porosimetry investigations. This section will provide a comprehensive exploration of the concepts, techniques, and applications of surface area and pore distribution studies with the ASAP Micromeritics device. Examining surface area and pore distribution has its basis in the key concepts of gas adsorption. The device employs the Brunauer-Emmett-Teller (BET) theory and the Density Function Theory (DFT) technique for calculating surface area and pore size distribution.

At lower pressures, gas molecules undergo the process of adsorption onto the surface of the substance. The BET hypothesis establishes a correlation between the quantity of gas adsorbed at various pressures and the surface area of a substance. Prior to analysis, it is common to subject the material being tested to a degassing (outgassing) process under vacuum conditions in order to eliminate any gases or moisture that may have been adsorbed or stuck. This practice guarantees precise and reliable measurement (ASAP plus 2020 user manual).

The sample is subjected to a known gas, often nitrogen, under various pressures and temperatures. Gas molecules undergo the process of adsorption, wherein they adhere to the surface of the substance and penetrate its pores. The apparatus is designed to gather data pertaining to the quantity of gas that is adsorbed at varying levels of pressure. The provided data is utilized for creating adsorption isotherms, illustrating the correlation between gas adsorption and pressure. The BET theory is utilized for the analysis of adsorption isotherm information in order to determine the specific surface area of the material. The standard unit of measurement for this is commonly denoted as square meters per gram ($\text{m}^2 \text{g}^{-1}$). The

determination of pore size distribution using the DFT approach involves using the desorption branch of the adsorption isotherm. The outcome yields a distribution of pore diameters within the material.

3.5 UV-VIS spectrophotometer

The utilization of selective absorption UV/VIS for online inspection of the contents of samples has been employed in the tracking and monitoring of operations for a period exceeding 60 years. The standards of design for UV/VIS processing analyzers vary from those of laboratory equipment due to the necessity of operating under challenging environmental circumstances, including vibration, significant temperature fluctuations, corrosive environments, and similar factors. Currently, advancements in UV and VIS light sources, detectors, interference filters, and optical components have facilitated the broadening of applications for UV/VIS analytical instruments. Consequently, the utilization of photodiode detectors and holographic gratings in the analyzer procedures enables the possibility of conducting multicomponent assessment, which was previously impractical. The utilization of absorption measurements of UV/VIS light has shown to be highly valuable in the quantitative analysis of diverse species, encompassing both inorganic and organic compounds (Ojeda & Rojas, 2009). The radiation under consideration has a wavelength spectrum spanning about 190-800 nm. It is essential to consider that this range is characterized by variations in energy levels and excitation mechanisms, distinguishing it from other related areas. The attenuation phenomenon arises from several factors, including reflection, scattering, absorption, or interferences.

Nevertheless, precise attenuation measurements can be achieved by simply measuring the absorbance. The relationship between absorbance and the concentration of the analyte, as well as the distance taken by light across the sample while radiation, is generally proportional but with some limitations. The phenomenon being referred to is often known as Beer's law. The primary purpose of a UV-Vis detector is to change an optical signal into an electrical signal. Therefore, the perfect sensor should exhibit a broad spectral response, possess excellent sensitivity and low noise characteristics, provide a linear response over a wide range, exhibit a rapid reaction time, enable downsizing, and require little sample usage (L.C. Passos & M.F.S. Saraiva, 2019).

3.6 Ion chromatography (IC)

IC analyzer is widely used as a prominent analytical method for measuring both organic and inorganic ions. Since the inception of this method of chromatography by Small (Small et al., 1975), it has drawn significant attention in various analytical domains, including environmental monitoring, food testing, water quality control processes, and the pharmaceutical sector. IC possesses favorable selectivity, robustness, and sensitivity, enabling an efficient division of ions within a given sample. Additionally, IC facilitates the simultaneous detection of inorganic anions and cations, as well as the determination of charge-presenting combinations and organic matter that may be found in ionic form (Moura et al., 2022). The approach relies on electrostatic forces that occur between charged fragments present on the outer layer of molecules and oppositely charged functional groups that are attached to a stationary phase. The phenomenon under consideration is a surface process that takes place when an ionic solid encounters a solution (Grönberg, 2018; Shibukawa et al., 2009). This procedure (IC) can potentially act as an alternative to traditional chemical analysis techniques, such as gravimetry, volumetry, or titration. These traditional techniques decrease sensitivity, are sometimes inaccurate, take much time, and are challenging to automate when used on many data. An ion chromatography (IC) apparatus comprises alternating pump systems that keep a consistent pressure, an injector, a separation column, a chemical suppressor, and a detector for creating chromatograms (Moura et al., 2022). Separation columns, often referred to as chromatographic columns, consist of cylindrical tubes of various sizes and lengths that are filled with a stationary phase. These columns are equipped with intake and exit ports at their respective ends. These columns typically include porous, solid substrate particles with positively or negatively charged ionic functional groups on their surfaces as their interior materials (Moldoveanu & David, 2017).

The selection of the sample-preparing technique ought to aim to provide optimal recovery of the analyte while simultaneously minimizing the presence of interfering substances. The techniques used include a variety of approaches, spanning from simple operations like sample dilution, filtration, or changing pH to more intricate methodologies that entail a series of sequential actions, such as the extraction of analytes from solid substances, analyte pre-concentration and the implementation of sample purification steps to remove impurities (Nuckowski et al., 2018).

In the field of analytical chemistry, it is not possible to directly evaluate samples that include very acidic or basic substances. Therefore, it is necessary to partly neutralize samples that have been processed with acids before they can be injected for analysis in IC. Nevertheless, the

inclusion of a neutralizing base hinders the identification of the introduced cation and results in an elevation of the salt load, hence possibly hindering chromatographic separations (Frenzel & Michalski, 2016).

3.7 HACH colorimeter

The HACH colorimeter is a versatile and commonly employed analytical device utilized for the identification and measurement of diverse compounds in water and other solutions. Colorimetry is a commonly used analytical method that is based on the quantification of light absorption or transmission by a solution exhibiting coloration. The foundational idea is derived from the Beer-Lambert Law, a basic concept in spectroscopy, which proposes that the concentration of a chemical inside a solution exhibits a direct relationship with the absorption of light at a certain wavelength. The HACH colorimeter is used to quantify the concentration of an analyte by assessing any changes in color resulting from an interaction between a reagent and the analyte. This reaction induces a change in absorbance, which can be attributed to the concentration of the analyte.

The first stage in using a HACH colorimeter for the detection of organic acids entails the appropriate preparation of the sample. In the context of identifying organic acids in water, it is customary to obtain a representative sample, which is then subjected to filtration to eliminate any suspended particles.

The sample is subjected to the addition of a particular reagent or a mixture of reagents. The reagents undergo a chemical reaction with the organic acids in the sample, resulting in an obvious shift in color. The reagent selection is dependent upon the specific organic acid being targeted.

The combination of samples and reagents is permitted to undergo incubation for a defined duration in order to facilitate thorough interaction between the reagents and the organic acids. Following the incubation period, the HACH colorimeter is used to quantify the absorbance of the sample at a designated wavelength, which corresponds to the change in color arising from the reaction. The device utilizes the principles of the Beer-Lambert Law to transform absorbance data into corresponding concentration values. Calibration curves are often constructed by using established standards in order to establish a correlation between absorbance and concentration. Table 3.3 shows the reagents required for volatile acid detection by HACH.

Table 3.3 Reagents used for HACH calorimetry.

Reagent	Volume for sample preparation (mL)
Ethylene Glycol	1.5
Ferric Chloride-Sulfuric Acid Solution	10
Hydroxylamine Hydrochloride Solution, 100 g L ⁻¹	0.5
Sodium Hydroxide Standard Solution, 4.5 N	2
Sulfuric Acid Standard Solution, 19.2 N	0.2
Water, deionized	10

The HACH colorimeter has a diverse array of uses, such as Water quality monitoring, where the process of assessing and analyzing the characteristics of water to determine its suitability for various purposes is performed. The chemical industry is a sector that encompasses the production, processing, and distribution of chemicals and chemical products. Organic acids serve as crucial intermediates in chemical synthesis, necessitating the monitoring of their concentration to provide effective process control (DR900 Multiparameter Portable Colorimeter user manual).

3.8 Oil concentration detection

In order to quantify the concentration of oil, several investigations used the assumption that the changes in weight of the adsorbent subsequent to adsorption were indicative of the quantity or capacity of adsorption (Inagaki et al., 2001; Takeuchi et al., 2017; Wu et al., 2021). This thesis examined two distinct forms of oil adsorption and uptake. These include oil floating on the surface of the solution and oil that is dissolved in the solution. It should be noted that accurately determining the concentration of the latter form through the use of weighing the Adsorbent is challenging, as the range of dissolved oil is usually within 100 mg L⁻¹. Consequently, an alternative approach involves the extraction of oil constituents from the solution, followed by quantification of their quantity using UV-vis spectrophotometry. Due to this rationale, the determination of oil concentration was achieved by adding 0.25 g of NaCl to a 50 mL sample containing oil dispersed or dissolved in water. The mixture was then subjected to agitation for a brief period using a magnetic stirrer. Then, the solution was transferred to a separating funnel, following by the addition of 5 mL of CCl₄ and vigorous shaking for 2 minutes. After 10

minutes, the solution was separated into two distinct layers. The bottom layer, which consisted of organic compounds, was selected for absorbance measurement using a UV spectrophotometer set at a wavelength of 313 nm. This analytical approach has been previously documented by (Mintcheva et al., 2022) (Fig 3.2).



Fig 3.2. Separation of oil from solution

3.9 Elemental analysis: Inductively Coupled Plasma Optical Emission Spectroscopy (ICP-OES)

ICP-OES analyzer is a widely used analytical method utilized for the quantitative determination of elemental composition inside a given sample. The idea of ICP-OES is based on the phenomenon of energy absorption by atoms and ions, which results in the transition of electrons from their ground state to an excited state. In ICP-OES, the energy is derived from the thermal excitation of an argon plasma, which is maintained at a temperature of 10,000 kelvin. The ICP-OES is based on the phenomenon where atoms, when stimulated, emit light at distinct wavelengths as they undergo a transition to a lower energy state. When an electron transitions from a higher energy level to a lower energy level, often the ground state, it releases

light with a very precise wavelength. The wavelength of the emitted light is determined by the specific atom or ion, denoting the element, as well as the energy levels that the electron transitions between.

The intensity of emitted light at a given wavelength is directly proportional to the number of atoms or ions undergoing the corresponding transition. The connection between light intensity and element concentration is described by the Beer-Lambert law (ICP-OES, Agilent). Particle size or sample thickness is unimportant since the samples are digested before analysis. ICP-OES provides the ability to detect concentrations within the parts per million (mg L^{-1}). The detection limits for sulphur (S) and selenium (Se), for instance, may reach as low as 0.3 mg L^{-1} and 0.2 mg L^{-1} , respectively. Inductively coupled plasma methods can analyze a substantial number of elements, exceeding 70 in total, at the same time. The presence of several emission wavelengths per element allows for the potential resolution of disruptions resulting from spectral overlaps. ICP-OES further provides the user with the advantage of achieving high sample throughput (Morrison et al., 2020; Nölte, 2021). For this purpose, samples were first put in a furnace at $650 \text{ }^\circ\text{C}$ for 16 hours, and then the residue was digested with nitric acid, and the elements were measured.

3. 10 Response Surface Methodology (RSM)

Previously, the optimization process in the field of analytical chemistry has included the systematic examination of individual factors and their impact on the outcome of experiments. While altering just one variable, the other parameters are maintained at a consistent level. The optimization strategy used in this context is often referred to as the one-variable-at-a-time approach. One significant drawback of this approach is its failure to include the interacting impact within the factors under investigation. Therefore, this methodology does not adequately represent the comprehensive impact of the factor on the response (Lundstedt et al., 1998). One further drawback associated with one-factor optimization is the need for a greater number of experiments to be conducted in order to carry out the study. This results in an increase in both time and financial costs, as well as an increase in the use of reagents and chemicals.

To address this issue, researchers have used multivariate statistical approaches to optimize analytical operations. RSM is considered one of the most significant multivariate approaches employed in the field of analytical optimization. RSM is a comprehensive set of mathematical and statistical approaches that include fitting a polynomial equation to data collected through

experiments. The primary purpose of RSM is to accurately explain the trends of a given data set and enable statistical predictions to be made. This approach is particularly applicable in situations when multiple factors impact the result or outcomes of interest. The aim is to simultaneously improve the levels of these factors in order to achieve optimal system efficiency (Allouss et al., 2019; Bezerra et al., 2008a; Mäkelä, 2017).

The Box team initially introduced RSM throughout the 1950s. The phrase in question has its origins in the graphical representation that emerged as a result of evaluating the fitness of a mathematical model. Its application has been extensively acknowledged in the literature regarding chemometrics (Gilmour, 2006). The RSM methodology includes a collection of mathematical and statistical methods that rely on the fitting of empirical modeling to experimental data acquired via experimental design. In achieving this goal, linear or square polynomial functions are used to characterize the setup under investigation and after that investigate (via modeling and modification) experimental circumstances in order to achieve its optimization.

Implementing RSM as an optimization approach involves several phases, which might be outlined as follows: Firstly, the researcher must carefully choose the independent parameters that have a significant impact on the experiment conditions. This selection is based on evaluation studies and the researcher's expertise. Additionally, the experimental level needs to be defined, taking into consideration the study's objective. Secondly, an appropriate experimental design is chosen, and the experiments are conducted based on the selected experimental matrix. Thirdly, the gathered experimental data is subjected to mathematical and statistical analysis. This involves fitting a polynomial function to the data. Next, the fitness of the model is evaluated to assess its accuracy in representing the system. Furthermore, it is important to determine whether a displacement towards the optimal region is necessary and feasible. Finally, the optimal amounts for each factor under study are determined (Bezerra et al., 2008).

3. 11 Adsorption Isotherm Models

3. 11. 1 Langmuir Isotherm model:

The Langmuir adsorption isotherm was formulated assuming that the adsorbent surface contains a specific quantity of available sites, each retaining identical energy levels. Additionally, the process of adsorption is considered reversible, with equilibrium achieved

when the rate of molecules being adsorbed onto the surface equals the rate of molecules being desorbed from the surface. The adsorption rate is directly related to the driving force, which is determined by a difference between the quantity of adsorbate present at a certain concentration and the maximum amount that can be adsorbed at that concentration. At the point of equilibrium, the difference becomes zero (Ayawei et al., 2017a; Günay et al., 2007a; Langmuir, 1916). The determination of the constants in the Langmuir isotherm can be achieved by Equation (3.1) (table 3.4). The Langmuir monolayer equation is utilized to validate the adsorption of a single component onto a uniformly structured solid surface. This equation assumes that all active sites possess identical attraction capabilities and can attract adsorbate molecules independently, disregarding interactions between the molecules themselves.

3.11.2 Freundlich Isotherm:

Freundlich (1906) suggests an empirical fitting model with heterogeneous surfaces. Adsorption is in a multiplayer manner and exponential placement of active sites and their related energies, where the Adsorbent includes many nearby sites (Freundlich, 1906). The mono-component model proposed by Freundlich is effectively employed to depict the adsorption of multiple layers on a solid surface with a heterogeneous structure featuring adsorption sites of varying activities (Freundlich, 1906). According to this model, numerous active sites are initially engaged, and the activity diminishes as more sites are utilized. Equation 3.2 shows the Freundlich equilibrium (table 3.4)

The Temkin model presumes an indirect adsorbate/adsorbate interaction with linear reductions of the heat of the adsorption process owing to the increased surface coverage. Besides all the models mentioned above, the Dubinin–Radushkevich Provides information regarding the adsorption on the adsorbent sites in terms of physical or chemical interactions as well as assumes the adsorption process in heterogeneous surfaces with a steric hindrance between adsorbed and incoming particles. It contemplates multilayer adsorption by Van Der Waals forces and is based on Gaussian energy distribution onto heterogeneous surfaces (Ayawei et al., 2017). Table 3.4 provides equations and parameters for these models:

Table 3.4 Equations and parameters for isothermal models

Model	Equation	Parameters	Details
Langmuir Eq (3.1)	$\frac{C_e}{q_e} = \frac{1}{q_m K_L} + \frac{C_e}{q_m}$	<p>C_e = concentration of adsorbate at equilibrium (mg L⁻¹)</p> <p>q_m = maximum adsorption capacity (mg g⁻¹)</p> <p>q_e = adsorption capacity at equilibrium (mg g⁻¹)</p> <p>K_L = Langmuir constant related to the free energy of the process (L mg⁻¹)</p>	<ul style="list-style-type: none"> • Adsorption into an adsorbent surface with restricted sites and uniform (Langmuir, 1916) • A monolayer of adsorbate is shaped at saturation on the adsorbent surface. • It assumes the surface coverage by trading off between the relative adsorption and desorption mechanisms. • The adsorption process is related to the amounts of open sites on the adsorbent surface • while desorption corresponds to the covered sites in the Adsorbent (Ayawei et al., 2017b; Günay et al., 2007b).
Freundlich Eq (3.2)	$\ln q_e = \ln K_f + \frac{1}{n_f} \ln C_e$	<p>K_f = Representative of adsorption capacity [(mg g⁻¹) (L mg⁻¹)^{1/n}]</p> <p>n_f = Freundlich constant equal to adsorption intensity</p>	<ul style="list-style-type: none"> • Freundlich (1906) suggests an empirical fitting model with heterogeneous surfaces. • Adsorption in a multiplayer manner and exponential placement of active sites and their related energies. • Where the Adsorbent includes many nearby sites (Freundlich, 1906).
Temkin Eq (3.3)	$q_e = B_1 \ln A + B_1 \ln C_e$	<p>B_1 = heat of adsorption (J mol⁻¹)</p> <p>A = equilibrium binding constant (L g⁻¹)</p>	<ul style="list-style-type: none"> • The Temkin model presumes an indirect adsorbate/adsorbate interaction. • Linear reductions of the heat of the adsorption process owing to the increased surface coverage.
Dubinin–Radushkevich Eq (3.4-3.6)	$\ln q_e = \ln q_s - \beta \varepsilon^2$ $\varepsilon = RT \ln \left(1 + \frac{1}{C_e} \right)$ $E = \frac{1}{-\sqrt{2\beta}}$	<p>q_s = the adsorption capacity (mg g⁻¹)</p> <p>β = the Dubinin–Radushkevich constant (mol² J⁻²)</p> <p>ε = the Polanyi potential</p> <p>R = the ideal gas constant (8.314 J (mol K)⁻¹)</p> <p>T = the temperature (Kelvin)</p> <p>E = related to free energy (kJ mol⁻¹)</p>	<ul style="list-style-type: none"> • The Dubinin–Radushkevich Provides information regarding the adsorption on the adsorbent sites in terms of physical or chemical interactions.’ • It assumes the adsorption process in heterogeneous surfaces with a steric hindrance between adsorbed and incoming particles. • It contemplates multilayer adsorption by Van Der Waal’s forces. — • It is based on Gaussian energy distribution onto heterogeneous surfaces (Ayawei et al., 2017)

3.12 Adsorption Kinetics Models

The kinetics of adsorption have been characterized in the research studies by several models, including the conventional pseudo-first order (PFO) and pseudo-second order (PSO) models, as well as the Elovich, Avrami, Crank, Vermeulen, Weber-Morris, Bangham, linear film, mixed surface reaction and diffusion, intra-particle diffusion, and multi-exponential models (Tan & Hameed, 2017). In recent decades, the conventional PFO, PSO, and intra-particle diffusion (Ersan et al. 2019) rate laws have been widely used in several research as the preferred models for analyzing adsorption kinetics. Both models have been used in a diverse range of adsorption systems, including biomass and nanomaterials as adsorbents, as well as heavy metals and medicines as adsorbates or contaminants. The linear versions of these models gained popularity via the work of Ho and McKay (1999), who analyzed many literature databases. Since then, the models have been increasingly common, with PSO being more favored than PFO (Ho & McKay, 1999). This is because PSO can accurately fit a majority of kinetic experiments, leading to the perception that it is the better model compared to PFO (Revellame et al., 2020).

The research conducted by Ho and McKay revealed that PSO kinetics had the strongest correlation with empirical data across all 12 systems of adsorption that were examined. Similarly, a significant majority of the adsorption studies included in the literature exhibited a similar trend, with around 87% conforming to the PSO model. The effectiveness of PSO was further shown by the observation that a portion of the research (about 12%) did not conduct experiments to evaluate the performance of PFO in their modeling endeavors. Instead, these investigations only used PSO to estimate adsorption kinetic parameters (Ho & McKay, 1999; Revellame et al., 2020).

The popular approach for determining adsorption kinetic parameters or modeling the adsorption mechanism involves employing the linearized version of the models. This is achieved by graphing the natural logarithm of $[q_e - q(t)]$ against t , and t/q versus t for PFO and PSO, as shown in table 3.5. The parameters can then be derived based on the slope and intercept of the optimum regression line. Specifically, if we denote the slope as “ m ” and the intercept as “ b ,” the parameter values for PFO can be determined as follows: $k_1 = -m$, and $q_e = \exp(b)$ for PFO while $k_2 = m^2/b$ and $q_e = 1/m$ for PSO.

Table 3.5 Adsorption kinetics models used

Kinetics model	Equation	Parameters
Pseudo-first order Eq (7)	$\log(q_e - q_t) = \log(q_e) - k_1 t$	q_e = adsorption capacity at equilibrium (mg g ⁻¹) q_t = adsorption capacity at time t (mg g ⁻¹) k_1 = rate constant (min ⁻¹) and t = time (min)
Pseudo-second order Eq (8)	$\frac{t}{q_t} = \frac{1}{k_2 q_e^2} + \frac{t}{q_e}$	k_2 = rate constant of pseudo-second order (g mg ⁻¹ min ⁻¹)
Intra-particle diffusion model	$q_t = k_i (t)^{\frac{1}{2}} + \theta$	k_i = intra-particle diffusion rate constant (mg g ⁻¹ h ^{0.5}) θ = intercept of the linear portion of the plot

3.13 Adsorption Thermodynamics

Assessing the experiments' thermodynamics can help examine the interactions between spontaneity, free energy, and temperature during the process. In order to conduct the thermodynamics evaluation, batch experiments are tested at various temperatures (i.e., 293, 299, and 311 K). Thermodynamics equations are shown in Table 3.6.

Table 3.6. Adsorption Thermodynamic Models (Eq 9-11)

Equation	Parameters
$\Delta G^0 = -RT \ln \frac{q_e}{C_e}$	ΔG^0 = the standard free energy (KJ mol ⁻¹)
$\Delta G^0 = \Delta H^0 - T\Delta S^0$	q_e = the adsorption capacity (mg g ⁻¹) C_e = concentration of adsorbate at equilibrium (mg L ⁻¹)
$\ln \frac{q_e}{C_e} = -\frac{\Delta H^0}{RT} + \frac{\Delta S^0}{R}$	ΔH^0 = the standard enthalpy (KJ mol ⁻¹) T = temperature (K) ΔS^0 = the standard entropy (KJ mol ⁻¹)

Enthalpy and entropy of the adsorption can be obtained by plotting $\ln q_e/C_e$ versus $1/T$

3.14 Batch adsorption experiments

The process of adsorption from a solution is typically carried out using either a column or a batch approach. In the first method, the solution is let flow through a column, which is typically maintained in a vertical orientation. This method is often used for ion exchange columns and is the most popular method. In a batch operation, a predetermined amount of Adsorbent is combined

simultaneously with a fixed amount of solution, and the system is maintained in a state of agitation or stirrer for a suitable time. The separation of the resulting solution is achieved using several methods, such as filtration, centrifugation, or decantation (Brandani, 2021; Loebenstein, 1962).

Adsorption efficiency (R: %) and adsorbent phase concentration after equilibrium or adsorption uptake (q: mg of adsorbate per g of Adsorbent) are calculated using Eq. 1 and 2 (Carvallho et al., 2016; Sham & Notley, 2018).

$$R = \frac{C_i - C_e}{C_i} \times 100 \quad \text{Eq (12)}$$

$$q = \frac{V \times (C_i - C_e)}{M} \quad \text{Eq (13)}$$

C_i and C_e (mg L^{-1}) are initial and equilibrium concentrations. V (L) is the volume of the solution, and M (g) is the mass of the Adsorbent.

3.15 Process variables (RSM)

This chapter employed a flexible optional design structure to accommodate a custom model among the various matrix designs. It considers a more comprehensive range and categoric factors with 23 batch adsorption tests to optimize adsorption efficiency/rate (R: %) and adsorption capacity (q: mg g^{-1}) of MB adsorption into MW-EG. The four independent variables, including contact time (min), initial concentration of MB solution (mg L^{-1}), adsorbent dose (g L^{-1}), and pH of MB solution, were applied to investigate their effects on adsorption. This selection was based on previous lab reports, literature on dye adsorption, and the initial studies carried out in the laboratory (Allouss et al., 2019; Hoang et al., 2019). It is worth mentioning that all batch tests were performed at room temperature (25°C). This chapter calculated the ANOVA and 2D–3D surface plots using Design-Expert 13. The range of parameters optimized in this research is presented in Table 3.7. Since the EG is responsible for adsorption and Na alginate and CaCl_2 are for making granular form. They are not playing as an adsorbent, the material dose was calculated based on EG powder usage.

Table 3.7. The domain of parameters optimized in the RSM method.

Factor	Name	Units	Number of levels	Values
A	Time	min	3	10-20-30

B	The initial concentration of MB	mg L ⁻¹	3	25-50-100
C	pH	-	3	3.6-5.7-11
D	Dose	g L ⁻¹	3	0.9-1.8-3.6

3.16. Regeneration and reusing of MW-EG

Regeneration was conducted to indicate the long-term viability of materials. Consequently, the MW-EG that had been exhausted with MB was subjected to irradiation using a commercial microwave. The adsorbents conducted a regeneration process for a total of 10 cycles. The primary factors in microwave treatment are power and irradiation time. However, it was shown that lower power levels ranging from 500 to 700 watts required a longer duration of 8 to 10 minutes in order to effectively remove the MB from the adsorbent. For this investigation, the experimental parameters of 1100 watts and 5 minutes were selected to facilitate the removal of MB adsorbed inside the pores of MW-EG.

3.17. Materials and experimental design of oil removal

In order to conduct the oil removal process from both states, either oil-water emulsion (dissolved) or floating oil, EG powder, and granule EG were employed.

3.18.1 Dissolved oil adsorption conditions

3.18.1.1 Batch tests:

It is important to develop an experimental methodology aimed at examining the efficacy of EG powder in eliminating dissolved crude oil. This investigation has taken into account two key variables: the concentration of oil and the dosage of EG. By doing so, a comprehensive grasp of the process's effectiveness can be obtained. The following is an experimental design for the intended purpose:

Objective: This part aimed to assess the impact of varying oil concentration and EG dosage on the removal of dissolved crude oil from aqueous solutions using a batch-mode experimental setup.

Factors:

1. The oil concentration in the experiment was adjusted at two levels, 100 and 200 mg L⁻¹.
2. Dosage: different EG powder doses (0.1, 0.2, and 0.4 (g of EG L⁻¹)) were applied from 100 mg L⁻¹ of oil concentration, and 10 g (MW-EG) L⁻¹ (equal to 1 g of (EG) L⁻¹) was applied

Dependent Variable: The percentage of dissolved crude oil that has been removed.

The experimental procedure:

To generate a stock solution of crude oil, a predetermined amount of the substance was dissolved in a DDW, resulting in concentrations of 100 and 200 mg L⁻¹. The known quantity of EG powder was added to each solution, followed by stirring the solution to mix adsorbate and adsorbent. The solutions were allowed to be agitated for 1.5 hours (for EG powder) and 15 hours (MW-EG) in order to enhance the process of adsorption. After the end of the stirring period, the sample was separated from EG powder by using a sieve. Then, 50 ml of solution was extracted based on the oil separation method explained previously. Then, its concentration was detected in a UV-spectrophotometer. To determine the percentage removal of crude oil, differences between initial and final concentrations were calculated.

3.18.1.2 Experimental Design for the Removal of Dissolved Crude Oil Using EG in a Fixed Bed Column

The primary aim of this experimental design was to assess the efficacy of removing dissolved crude oil from an aqueous solution. This was achieved by using a fixed bed column that was packed with EG powder. The primary objective of this work was to provide significant contributions to the understanding of the possible use of EG as an adsorbent in the context of removing crude oil from the PW water treatment procedure and comparing the results with batch mode.

The fixed bed column is a commonly used equipment in several industries and research fields. It consists of a cylindrical column filled with a solid material.

The influent was fed from the top part of the column in a reservoir part to avoid oil losses in tubes and to reduce the number of used tubes. Effluent samples were collected from the column outlet.

UV-Vis spectrophotometry was applied to obtain measurements of crude oil content. Figures 3.3 and 3.4 show the column design and system.



Fig 3.3. Column system and connection to a pump for removal of dissolved oil

This experimental design aimed to evaluate the effectiveness of removing dissolved crude oil from a water solution by employing a fixed bed column filled with EG powder. The primary objective was to contribute significantly to understanding the potential use of EG as an adsorbent for removing crude oil from PW water treatment procedures, comparing outcomes between batch mode and column filtration.

The fixed bed column, a typical apparatus across industries and research domains, is a cylindrical structure packed with a solid material. In this study, two different column sizes were utilized. First, a column with a height of 5 cm and diameter of 3.2 cm was packed with 3 grams of EG powder. The second column had the same height (5 cm) and a smaller diameter (2.44 cm) packed with 0.87 g EG powder. Table 3.8 shows the specification of two columns. To regulate the flow rate inside the column, a Peristaltic Pump was employed at a setting of 5-70 rpm, ensuring sufficient contact

between the influent and the fixed bed. Filtering 100 ml of dissolved oil at a concentration of 100 mg L⁻¹ took approximately 11 hours in total for column 1, and around 2.7 liters of 100 mg L⁻¹ dissolved crude oil passed through column 2 for about 14 hours. Figures 3.3 and 3.4 illustrate the column design and the system setup.

Table 3.8. Characteristics of two columns used as a fixed-bed filter for dissolved crude oil removal.

Column	1	2
Height (cm)	5	5
Diameter (cm)	3.2	2.44
Amount of EG powder packed (g)	3	0.87
Volume of column (cm ³)	40.19	23.36
Density of EG packed (g cm ⁻³)	0.074	0.037
Flowrate (mL min ⁻¹)	0.15	2.7-6.6
Flow rate set on pump (rpm)	5	15-70
Volume of filtered oil in water (L)	0.1	2.7
Overall time of operation (hour)	11	14
Concentration of influent (mg L ⁻¹)	100	100

3.18.2 Floating oil removal conditions

To compare oil states in produced water, various experiments were conducted on the removal of floating oil from the water. Since oil on water is not soluble, the mass calculation was applied for experimental design instead of concentration; therefore, the mass of crude oil added directly to the water ranged from 1 g to 6 g. Besides, different EG powder masses (0.045 to 0.27 g) were added to the solution and stirred for 5 mins. Fig 3.5 summarizes different experimental conditions in this chapter for clarity.

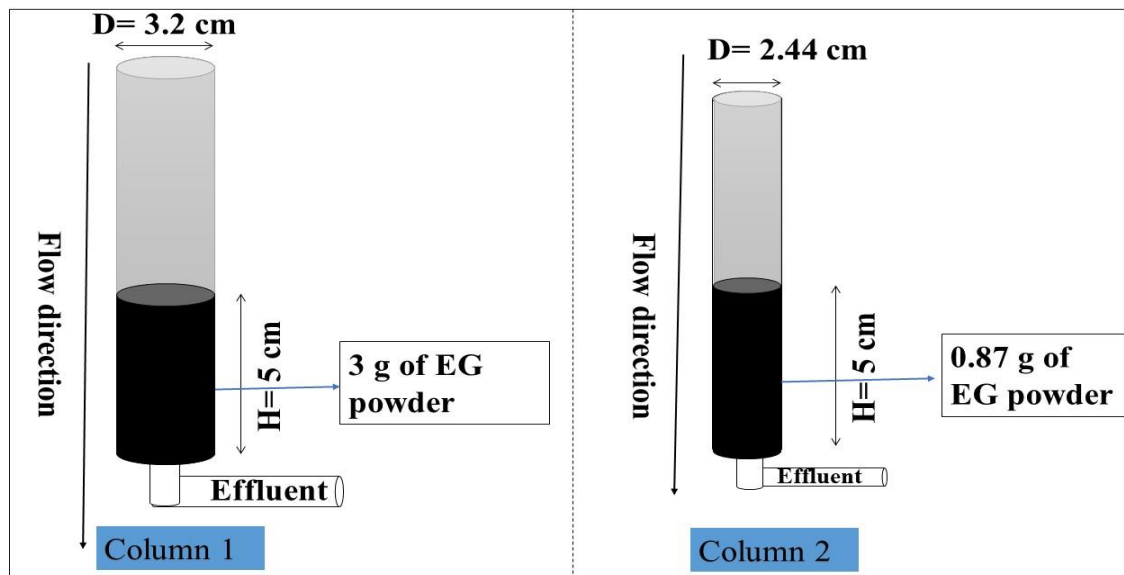


Fig 3.4. Column design for removal of dissolved oil

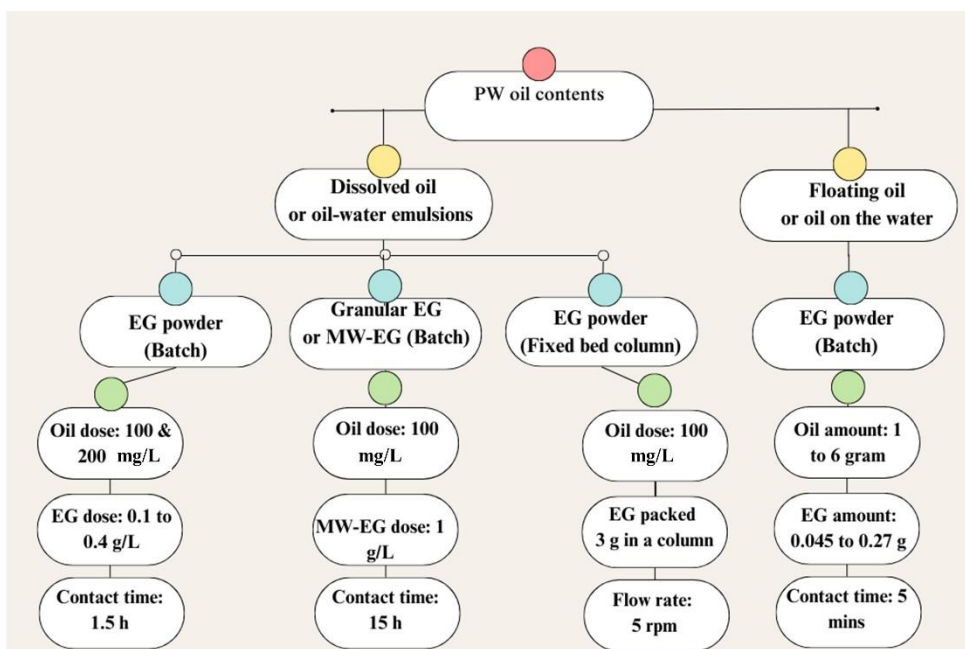


Fig 3.5. Experimental design adsorption process of oil contents in PW

Chapter 3 References

ASAP plus 2020, user manual,
https://www.micromeritics.com/Repository/Files/ASAP_2020_Operator_Manual_Rev_C__1.pdf

Allouss, D., Essamlali, Y., Amadine, O., Chakir, A., & Zahouily, M. (2019). Response surface methodology for optimization of methylene blue adsorption onto carboxymethyl cellulose-based hydrogel beads: Adsorption kinetics, isotherm, thermodynamics and reusability studies. *RSC Advances*, 9(65), 37858–37869. <https://doi.org/10.1039/C9RA06450H>

Analytical Methods Committee. (2006). Evaluation of analytical instrumentation. Part XIX CHNS elemental analysers. *Accreditation and Quality Assurance*, 11(11), 569–576. <https://doi.org/10.1007/s00769-006-0185-x>

Ayawei, N., Ebelegi, A. N., & Wankasi, D. (2017a). Modelling and Interpretation of Adsorption Isotherms. *Journal of Chemistry*, 2017, e3039817. <https://doi.org/10.1155/2017/3039817>

Ayawei, N., Ebelegi, A. N., & Wankasi, D. (2017b). Modelling and Interpretation of Adsorption Isotherms. *Journal of Chemistry*, 2017, e3039817. <https://doi.org/10.1155/2017/3039817>

Bezerra, M. A., Santelli, R. E., Oliveira, E. P., Villar, L. S., & Escaleira, L. A. (2008a). Response surface methodology (RSM) as a tool for optimization in analytical chemistry. *Talanta*, 76(5), 965–977. <https://doi.org/10.1016/j.talanta.2008.05.019>

Bezerra, M. A., Santelli, R. E., Oliveira, E. P., Villar, L. S., & Escaleira, L. A. (2008b). Response surface methodology (RSM) as a tool for optimization in analytical chemistry. *Talanta*, 76(5), Article 5. <https://doi.org/10.1016/j.talanta.2008.05.019>

Blandino, A., Macías, M., & Cantero, D. (1999). Formation of calcium alginate gel capsules: Influence of sodium alginate and CaCl₂ concentration on gelation kinetics. *Journal of Bioscience and Bioengineering*, 88(6), 686–689. [https://doi.org/10.1016/s1389-1723\(00\)87103-0](https://doi.org/10.1016/s1389-1723(00)87103-0)

Brandani, S. (2021). Kinetics of liquid phase batch adsorption experiments. *Adsorption*, 27(3), 353–368. <https://doi.org/10.1007/s10450-020-00258-9>

Carvallho, M. N., da Silva, K. S., Sales, D. C. S., Freire, E. M. P. L., Sobrinho, M. A. M., & Ghislandi, M. G. (2016). Dye removal from textile industrial effluents by adsorption on exfoliated graphite nanoplatelets: Kinetic and equilibrium studies. *Water Science and Technology*, 73(9), 2189–2198. <https://doi.org/10.2166/wst.2016.073>

Cuccarese, M., Brutti, S., De Bonis, A., Teghil, R., Mancini, I. M., Masi, S., & Caniani, D. (2021). Removal of diclofenac from aqueous solutions by adsorption on thermo-plasma expanded graphite. *Scientific Reports*, 11(1), Article 1. <https://doi.org/10.1038/s41598-021-83117-z>

DR900 Multiparameter Portable Colorimeter. (n.d.). Retrieved September 9, 2023, from <https://www.hach.com/p-dr900-colorimeter/9385100>

Environment Canada 2016b West Texas Intermediate http://www.etc-cte.ec.gc.ca/databases/OilProperties/pdf/WEB_West_Texas_Intermediate.pdf

Ersan, G., Kaya, Y., Ersan, M. S., Apul, O. G., & Karanfil, T. (2019). Adsorption kinetics and aggregation for three classes of carbonaceous adsorbents in the presence of natural organic matter. *Chemosphere*, 229, 515–524. <https://doi.org/10.1016/j.chemosphere.2019.05.014>

- Fadeeva, V. P., Tikhova, V. D., & Nikulicheva, O. N. (2008). Elemental analysis of organic compounds with the use of automated CHNS analyzers. *Journal of Analytical Chemistry*, 63(11), 1094–1106. <https://doi.org/10.1134/S1061934808110142>
- Frenzel, W., & Michalski, R. (2016). Sample Preparation Techniques for Ion Chromatography. In *Application of IC-MS and IC-ICP-MS in Environmental Research* (pp. 210–266). John Wiley & Sons, Ltd. <https://doi.org/10.1002/9781119085362.ch8>
- Gilmour, S. G. (2006). Response Surface Designs for Experiments in Bioprocessing. *Biometrics*, 62(2), 323–331. <https://doi.org/10.1111/j.1541-0420.2005.00444.x>
- Grönberg, A. (2018). Chapter 18—Ion Exchange Chromatography. In G. Jagschies, E. Lindskog, K. Łacki, & P. Gallier (Eds.), *Biopharmaceutical Processing* (pp. 379–399). Elsevier. <https://doi.org/10.1016/B978-0-08-100623-8.00018-9>
- Günay, A., Arslankaya, E., & Tosun, I. (2007a). Lead removal from aqueous solution by natural and pretreated clinoptilolite: Adsorption equilibrium and kinetics. *Journal of Hazardous Materials*, 146(1–2), Article 1–2. <https://doi.org/10.1016/j.jhazmat.2006.12.034>
- Günay, A., Arslankaya, E., & Tosun, I. (2007b). Lead removal from aqueous solution by natural and pretreated clinoptilolite: Adsorption equilibrium and kinetics. *Journal of Hazardous Materials*, 146(1–2), 362–371. <https://doi.org/10.1016/j.jhazmat.2006.12.034>
- Ho, Y. S., & McKay, G. (1999). Pseudo-second order model for sorption processes. *Process Biochemistry*, 34(5), 451–465. [https://doi.org/10.1016/S0032-9592\(98\)00112-5](https://doi.org/10.1016/S0032-9592(98)00112-5)
- Inagaki, M., Toyoda, M., Iwashita, N., Nishi, Y., & Konno, H. (2001). Exfoliated Graphite for Spilled Heavy Oil Recovery. *Carbon Letters*, 2(1), Article 1.
- Langmuir, I. (1916a). THE CONSTITUTION AND FUNDAMENTAL PROPERTIES OF SOLIDS AND LIQUIDS. PART I. SOLIDS. *Journal of the American Chemical Society*, 38(11), Article 11. <https://doi.org/10.1021/ja02268a002>
- Langmuir, I. (1916b). THE CONSTITUTION AND FUNDAMENTAL PROPERTIES OF SOLIDS AND LIQUIDS. PART I. SOLIDS. *Journal of the American Chemical Society*, 38(11), 2221–2295. <https://doi.org/10.1021/ja02268a002>
- L.C. Passos, M., & M.F.S. Saraiva, M. L. (2019). Detection in UV-visible spectrophotometry: Detectors, detection systems, and detection strategies. *Measurement*, 135, 896–904. <https://doi.org/10.1016/j.measurement.2018.12.045>
- Loebenstein, W. V. (1962). Batch Adsorption From Solution. *Journal of Research of the National Bureau of Standards. Section A, Physics and Chemistry*, 66A(6), 503–515. <https://doi.org/10.6028/jres.066A.052>
- Lundstedt, T., Seifert, E., Abramo, L., & Thelin, B. (1998). *Experimental design and optimization*. 38.
- Mäkelä, M. (2017). Experimental design and response surface methodology in energy applications: A tutorial review. *Energy Conversion and Management*, 151, 630–640. <https://doi.org/10.1016/j.enconman.2017.09.021>

- Mintcheva, N., Gicheva, G., & Panayotova, M. (2022). Reduction of Heavy Hydrocarbons from Oilfield Produced Water. *Pollutants*, 2(2), Article 2. <https://doi.org/10.3390/pollutants2020016>
- Mohamed, M. A., Jaafar, J., Ismail, A. F., Othman, M. H. D., & Rahman, M. A. (2017). Chapter 1—Fourier Transform Infrared (FTIR) Spectroscopy. In N. Hilal, A. F. Ismail, T. Matsuura, & D. Oatley-Radcliffe (Eds.), *Membrane Characterization* (pp. 3–29). Elsevier. <https://doi.org/10.1016/B978-0-444-63776-5.00001-2>
- Moldoveanu, S. C., & David, V. (2017). Chapter 9—Stationary Phases and Columns for Ion Exchange, Ion-Moderated, and Ligand Exchange Chromatography. In S. C. Moldoveanu & V. David (Eds.), *Selection of the HPLC Method in Chemical Analysis* (pp. 349–362). Elsevier. <https://doi.org/10.1016/B978-0-12-803684-6.00009-3>
- Morrison, C., Sun, H., Yao, Y., Loomis, R. A., & Buhro, W. E. (2020). Methods for the ICP-OES Analysis of Semiconductor Materials. *Chemistry of Materials*, 32(5), 1760–1768. <https://doi.org/10.1021/acs.chemmater.0c00255>
- Moura, A. V., Silva, J. D. S. da, & Gubert, P. (2022). Ion Chromatography: Principles and instrumentation. *Orbital: The Electronic Journal of Chemistry*, 110–115. <https://doi.org/10.17807/orbital.v14i2.15871>
- Nölte, J. (2021). *ICP Emission Spectrometry: A Practical Guide*. John Wiley & Sons.
- Nuckowski, Ł., Kaczmarkiewicz, A., & Studzińska, S. (2018). Review on sample preparation methods for oligonucleotides analysis by liquid chromatography. *Journal of Chromatography B*, 1090, 90–100. <https://doi.org/10.1016/j.jchromb.2018.05.025>
- Ojeda, C. B., & Rojas, F. S. (2009). Process Analytical Chemistry: Applications of Ultraviolet/Visible Spectrometry in Environmental Analysis: An Overview. *Applied Spectroscopy Reviews*, 44(3), 245–265. <https://doi.org/10.1080/05704920902717898>
- Revellame, E. D., Fortela, D. L., Sharp, W., Hernandez, R., & Zappi, M. E. (2020). Adsorption kinetic modeling using pseudo-first order and pseudo-second order rate laws: A review. *Cleaner Engineering and Technology*, 1, 100032. <https://doi.org/10.1016/j.clet.2020.100032>
- Sham, A. Y. W., & Notley, S. M. (2018). Adsorption of organic dyes from aqueous solutions using surfactant exfoliated graphene. *Journal of Environmental Chemical Engineering*, 6(1), 495–504. <https://doi.org/10.1016/j.jece.2017.12.028>
- Shibukawa, M., Shimasaki, T., Saito, S., & Yarita, T. (2009). Superheated Water Ion-Exchange Chromatography: An Experimental Approach for Interpretation of Separation Selectivity in Ion-Exchange Processes. *Analytical Chemistry*, 81(19), 8025–8032. <https://doi.org/10.1021/ac9011864>
- Small, Hamish., Stevens, T. S., & Bauman, W. C. (1975). Novel ion exchange chromatographic method using conductimetric detection. *Analytical Chemistry*, 47(11), 1801–1809. <https://doi.org/10.1021/ac60361a017>
- Smith, B. C. (1998). *Infrared Spectral Interpretation: A Systematic Approach*. CRC Press. <https://doi.org/10.1201/9780203750841>

Takeuchi, K., Kitazawa, H., Fujishige, M., Akuzawa, N., Ortiz-Medina, J., Morelos-Gomez, A., Cruz-Silva, R., Araki, T., Hayashi, T., & Endo, M. (2017). Oil removing properties of exfoliated graphite in actual produced water treatment. *Journal of Water Process Engineering*, *20*, 226–231.

<https://doi.org/10.1016/j.jwpe.2017.11.009>

Tan, K. L., & Hameed, B. H. (2017). Insight into the adsorption kinetics models for the removal of contaminants from aqueous solutions. *Journal of the Taiwan Institute of Chemical Engineers*, *74*, 25–48.

<https://doi.org/10.1016/j.jtice.2017.01.024>

Wu, K.-H., Huang, W.-C., Hung, W.-C., & Tsai, C.-W. (2021). Modified expanded graphite/Fe₃O₄ composite as an adsorbent of methylene blue: Adsorption kinetics and isotherms. *Materials Science and Engineering: B*, *266*, 115068. <https://doi.org/10.1016/j.mseb.2021.115068>

Zaker, A., Chen, Z., Wang, X., & Zhang, Q. (2019). Microwave-assisted pyrolysis of sewage sludge: A review. *Fuel Processing Technology*, *187*, 84–104. <https://doi.org/10.1016/j.fuproc.2018.12.011>

Chapter 4: Results and discussion

4.1 Evaluation of granular EG adsorption performance for removal of Methylene Blue as model contamination

4.1.1 Introduction

Adsorption is a commonly employed method for the elimination of organic contaminants from aqueous solutions in water treatment processes. The primary aim of this chapter was to evaluate the adsorption efficiency of MW-EG. Methylene blue was chosen as a reference model for determining adsorption capacity due to its widespread usage in this context.

4.1.2 Specific surface area and pore volume

The technique of BET measurement via ASAP 2020 plus Micromeritics. Table 4.1 displays the physical attributes of MW-EG and EG powder. The parameters under consideration encompass the BET surface area, micro-porous volume, meso-porous volume, and pore size of materials.

Table 4.1. Physical characterization of adsorbents

Material	BET (m ² g ⁻¹)	Total Pore Volume (cm ³ g ⁻¹)	Average pore diameter (Å)	DFT pore size range (Å)	Porosity Distribution by N ₂ - DFT Model	
					Mesopore (cm ³ g ⁻¹)	Macropore (cm ³ g ⁻¹)
EG	48	0.1329	117	8.5- 343	0.1329 (100 %)	0 (0 %)
MW-EG	10	0.0195	65	14.8- 4003	0.018 (92%)	0.0014 (8%)

The MW-EG composite material incorporated macropores, constituting around 8% of its structure. These macropores are often recognized as the main paths that facilitate the transport of substances into the carbon pores. Additionally, the presence of micropores and mesopores inside the material considerably enhances its internal surface area, as highlighted by Liu et al. in their study conducted in 2020. The granulation of EG resulted in a decrease in the BET surface area from 48 to around 10 (m² g⁻¹), as anticipated. In addition, it was observed that the average pore diameter of EG underwent a reduction from 117 to 65 angstroms following the processes of granulation and

microwave irradiation. Besides, it was observed that the pore size range of MW-EG expanded significantly, reaching up to 4000 Å, which corresponds to the macropores scale.

In general, the formation of pores in MW-EG mostly arises from thermal expansion resulting from the evaporation of a CaCl₂ solution. The observed expansion of the pore diameter range in this work aligns with the findings of Liu et al. (2020), who similarly found that microwave irradiation-induced expansion from the interior to the outside might be a significant factor contributing to the growth of the pore range (both in terms of number and diameter). Figure 4.1 displays the linear isotherm plots showing the relationship between pore width and dV/dlog(W) pore volume.

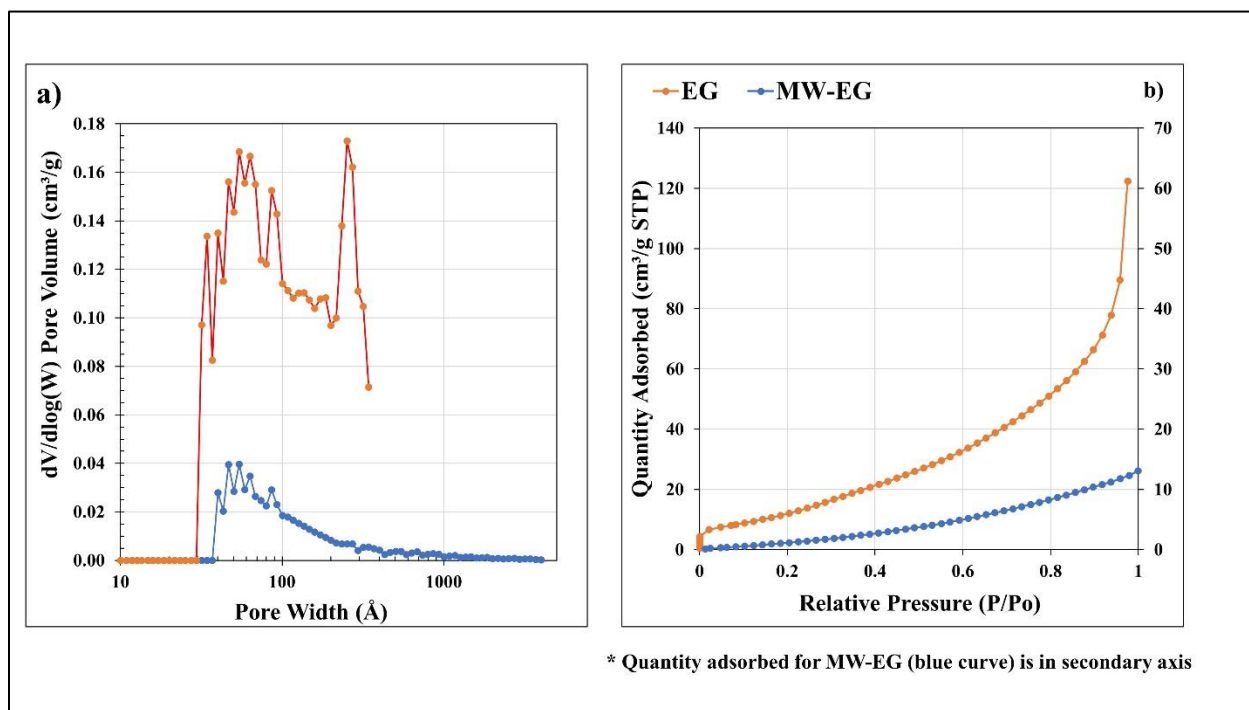


Fig 4.1 Pore width and pore volume relationship for adsorbent materials

4.1.3 FT-IR analysis

Figure 4.2 displays the FTIR spectra corresponding to EG and MW-EG. Both EG and MW-EG exhibited similarities. However, EG had higher levels of absorbance in comparison to MW-EG. The observed spectra exhibit conformity with the findings of a prior study undertaken by

Cuccarese et al. (2021). The researchers concluded that no distinct peak corresponding to functional groups was detected. Additionally, they confirmed that the structure of EG bears resemblance to that of pure graphitic substances, as reported by Cuccarese et al. (2021).

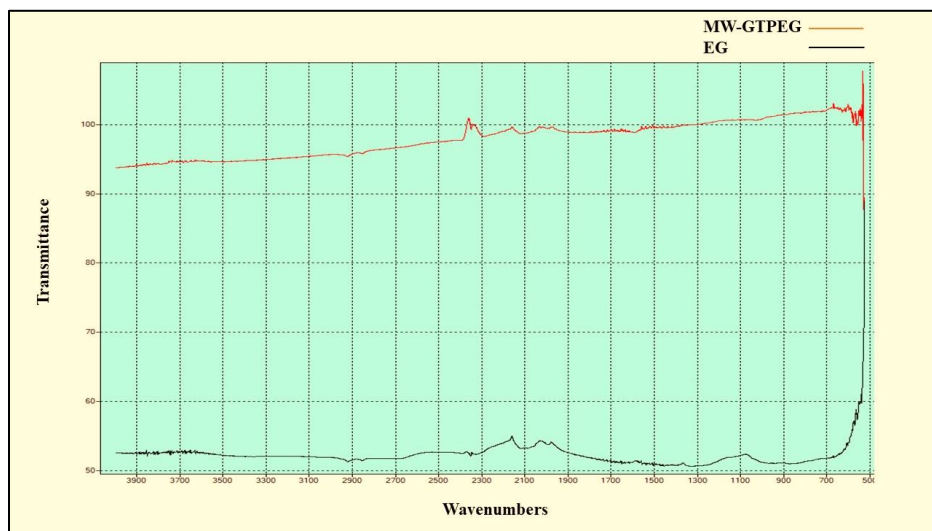


Fig 4.2. FT-IR analysis of MW-EG and EG powder

4.1.4 Chemical characteristics of adsorbent materials

A CHNS analyzer apparatus was utilized to ascertain the proportions of carbon, hydrogen, nitrogen, and sulfur in substances. In addition, the ash content was determined using the process of subjecting 100 mg of the sample to a furnace at a temperature of 650°C for 16 hours. The point of zero charge (pH_{pzc}) value was calculated for both EG and MW-EG by introducing 20 ml of a 0.1 M NaCl into a beaker containing 100 mg of the respective substance. The mixture was then subjected to shaking at a rate of 200 revolutions per minute for three days. Subsequently, the pH was measured. The findings are shown in Table 4.2.

Table 4.2 Chemical characteristics of EG and MW-EG

Material	Carbon %	Hydrogen %	Nitrogen %	Sulphur %	Ash contents %	pH _{pzc}
EG	91.59	0.26	0.05	0.91	1.8	3.0
MW-EG	32.35	4.38	0	0	12.3	5.3

The EG material had a carbon content of over 90%. In contrast, the MW-EG composite showed a reduction in carbon percentage due to the utilization of Na alginate and CaCl₂ during its preparation. The greater ash concentration of MW-EG further demonstrated this phenomenon. Moreover, the proportions of nitrogen and sulfur were found to be insignificant in both materials. However, the hydrogen concentration exhibited an increase in the MG-GTPEG sample. The pH at the pHPzc of the electrolyte solution saw a rise from an initial value of 3.0 to a final value of 5.3 following exposure to MW irradiation. Adsorption of cationic dyes, such as MB, can be facilitated by solution pH values that are greater than the pHPzc, resulting in a negatively charged surface of the adsorbent.

4.2 Preliminary study: Effect of different experimental factors on MB adsorption onto Granular EG

A number of preliminary tests were carried out with a specific emphasis on the elimination of Methylene blue from aqueous solutions. The adsorbent material chosen for this study was G-EG, produced from step one of material preparation. The primary objective of this exploratory study was to provide the groundwork for future research by conducting a comprehensive investigation into the impact of several key variables on the process of adsorption.

4.2.1 Factors Examined in the Preliminary Investigation

4.2.1.1 Contact time: The length of time that the adsorbent and solution containing pollutants are in contact. The examination of the impact of contact time yields valuable insights into the temporal duration necessary for the attainment of equilibrium.

4.2.1.2 Adsorbent dosage: The quantity of G-EG introduced into the solution is a crucial factor that affects the adsorption capacity. The determination of the appropriate dosage facilitates the optimization of the usage of the adsorbent material.

4.2.1.3 Initial concentration: Understanding the concentration of the pollutant in the solution at the beginning facilitates the evaluation of the efficacy of the adsorbent in various pollutant concentrations.

4.2.1.4 Sodium alginate amounts The addition of sodium alginate, a biopolymer, was included in the system to investigate its potential for increasing the adsorption process. The introduction of this additional factor has the potential to impact the adsorbent's level of attraction towards the pollutant. The main aim of this preliminary investigation was to get a thorough comprehension of the initial assumption, which would establish the basis for later research activities. Our objective was to collect crucial data on the adsorption of Methylene blue onto G-EG by adjusting these parameters.

4.2.2 Preliminary results

The investigation focused on examining the impact of contact time on the adsorption of MB by observing the adsorption process at different time intervals (2 hours to 7 days). (The experiment condition consists of $C_i=50 \text{ mg L}^{-1}$, amount of adsorbent=1 g of G-EG, without pH adjustment (pH= 5.7)). The findings of the study indicated a rise to 70 % of removal at the 8 hours of contact period progresses, finally reaching a state of equilibrium. During prolonged contact durations, it was observed that the adsorption capacity reached a plateau of around 80 % of removal after 1 day, indicating the reach of a saturation point (Fig 4.3-Fig 4.5).

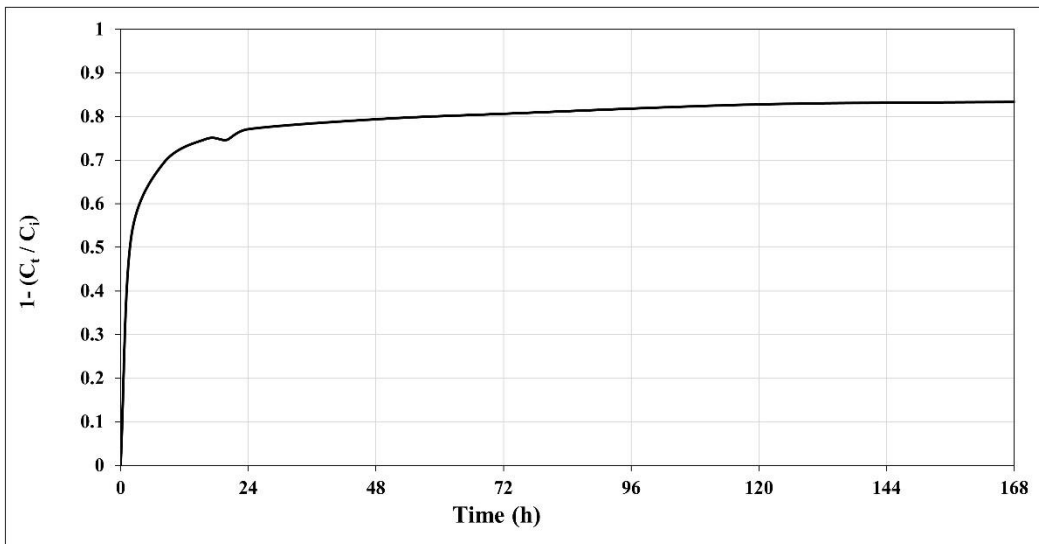


Fig 4.3. Removal efficiency of MB through granular EG (Effect of time)

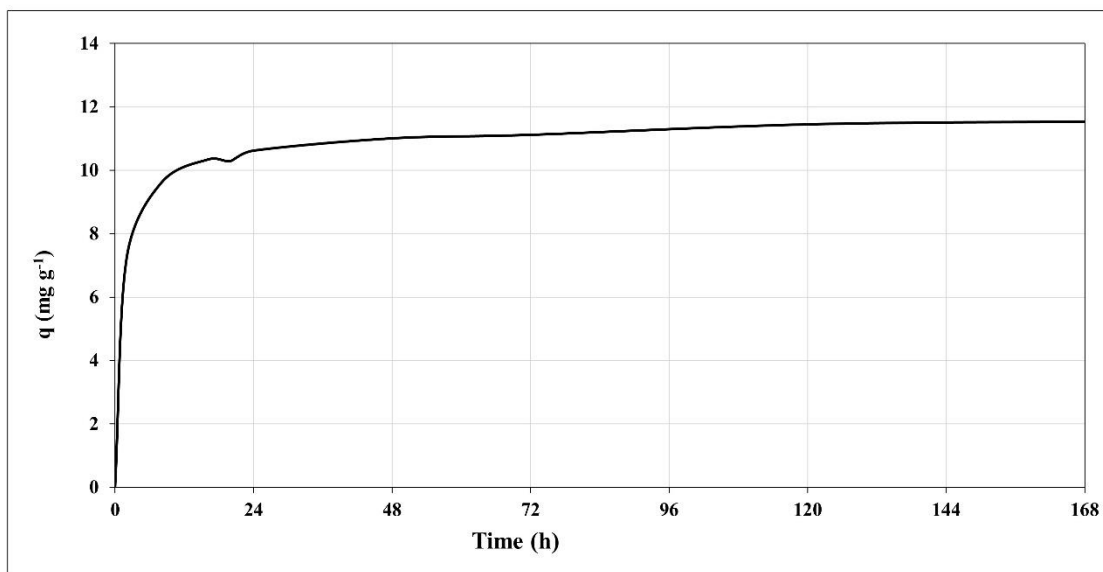


Fig 4.4 Adsorption capacity of granular EG by removing MB (Effect of time)

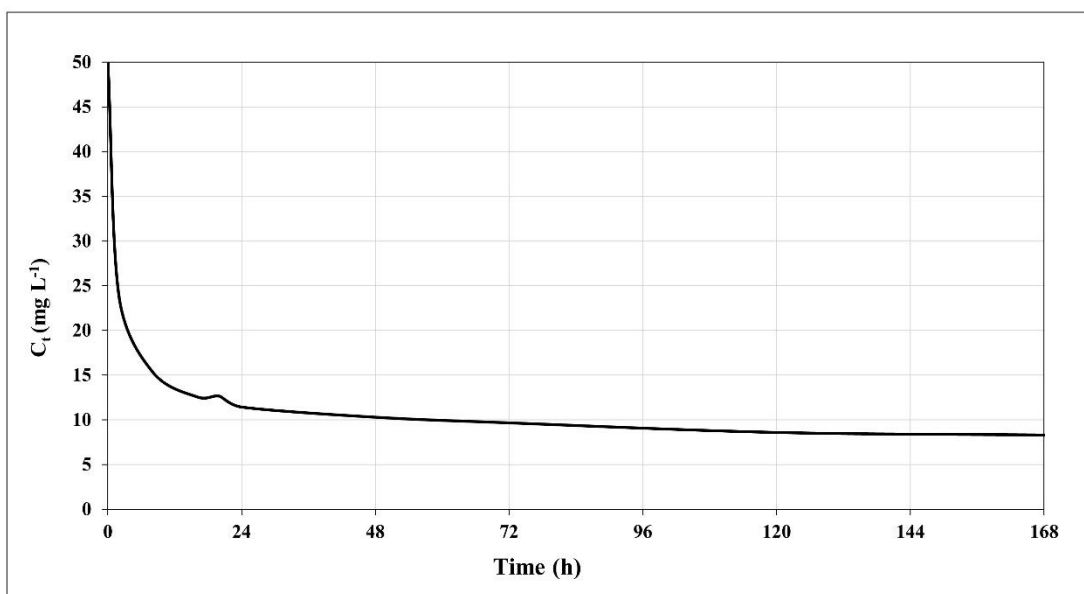


Fig 4.5. The final concentration of MB remained in solution using G-EG (Effect of time)

The Pseudo-first order and Pseudo-second order models were utilized in the preliminary experiments data to characterize the kinetics of the adsorption process. The experimental data were utilized to fit both models in order to assess their capacities in representing the adsorption behavior. The results of our pre-study (Fig 4.6- 4.8) suggested that the Pseudo- second order model demonstrated a more favorable agreement with the empirical observations in situations where the adsorption kinetics were comparatively slow or when chemisorption exerted a substantial influence as well as in these experimental conditions. Table 4.3 provides a comparison between these 3 models.

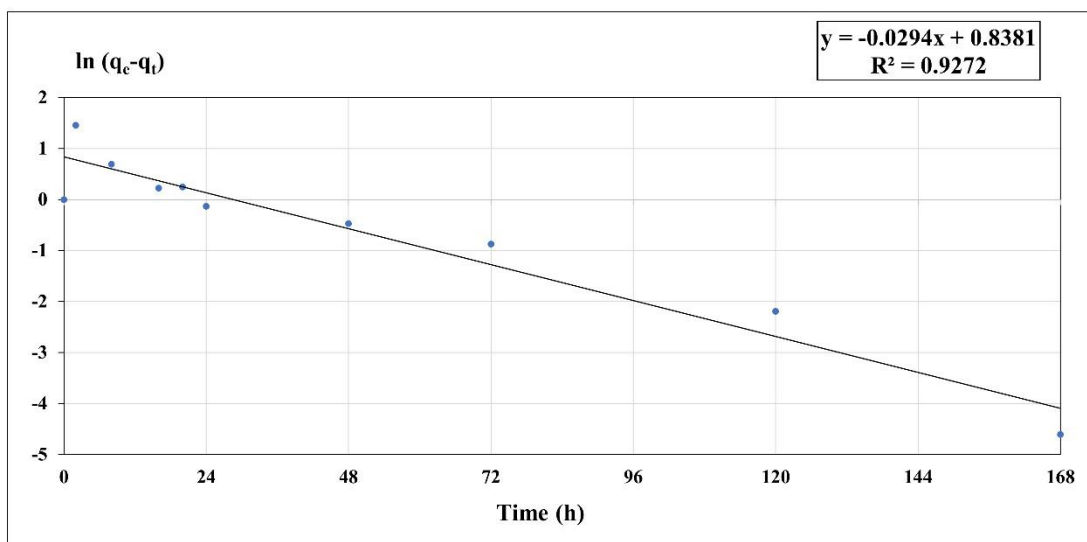


Fig 4.6 Pseudo-first order fitted on experimental data of MB adsorption onto G-EG (effect of time in preliminary study).

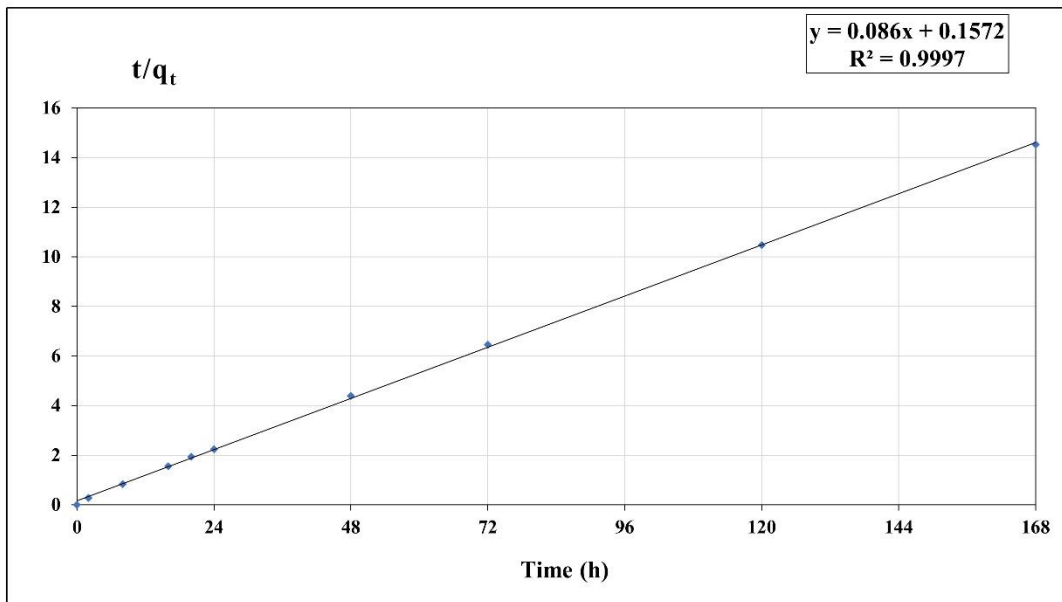


Fig 4.7 Pseudo-2nd-Order model fitted on experimental data of MB adsorption onto G-EG (effect of time in preliminary study).

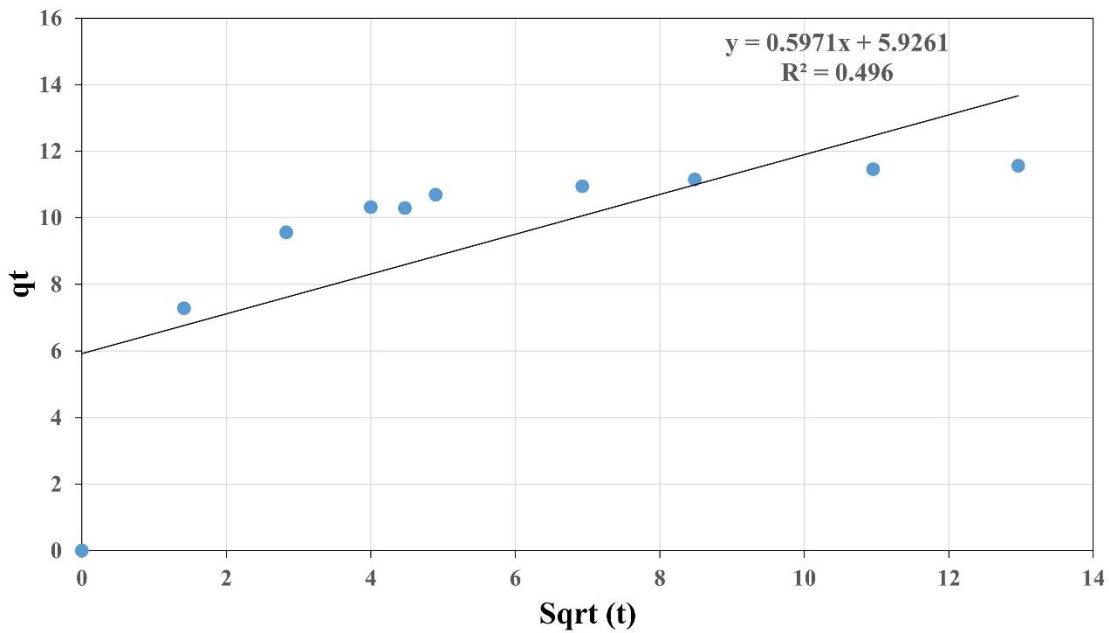


Fig 4.8 Intra-particle diffusion model fitted on experimental data of MB adsorption onto G-EG (effect of time in preliminary study)

Table 4.3. Comparison of Pseudo- second order, Pseudo-first order, and Intra-particle diffusion models in the preliminary study of MB adsorption onto granular EG

Model	q_e	K1	R^2
Pseudo-first order	2.31	-0.00018	0.9272
Pseudo-second order	11.62	0.047048	0.9997
Intra-particle diffusion	$\theta = 5.92$	$K_i = 0.5971$	0.496

The influence of the adsorbent dosage on the adsorption efficiency was investigated by varying the quantity of granular EG added to the MB solution. The increase in adsorbent dosage did not have a significant impact on adsorption percentage. According to Fig 4.9, the removal percentage increased from 73 to 83 percent by changing the adsorbent dose from 0.25 g to 2 g of composite in this experimental condition: initial concentration of MB= 50 (mg L^{-1}), without pH modification, contact time= 1 day). Nevertheless, the adsorption capacity (mg g^{-1}) exhibited a declining trend as the dosage increased, as expected, because of the more adsorbent amount and almost the same pollutant mass. However, these results were obtained in preliminary experiments, emphasizing the need for further investigation in the next steps of study related to adsorbent dose.

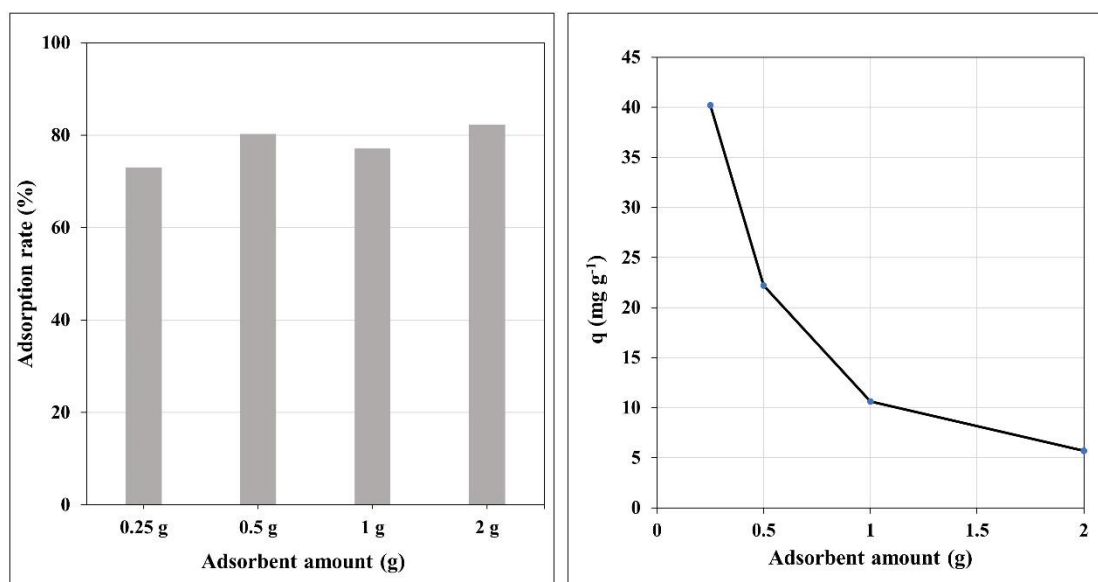


Fig 4.9. Effect of adsorbent dose in preliminary studies of MB removal onto G-EG.

The tests aimed to examine the impact of varying starting MB concentrations on the adsorption behavior (12.5 to 100 mg L^{-1}). The other factors were fixed at 1 day of contact time, amount of adsorbent= 1 g of G-EG composite using, without pH adjustment ($\text{pH} = 5.7$). The experiment

showed a positive correlation between the initial concentration of MB in the solution and the adsorption capacity of granular EG. The results of this study suggest that the adsorbent had a greater affinity for MB when exposed to higher starting concentrations (Fig 4.10). Nevertheless, it is important to acknowledge that the rate of adsorption had the same trend except for a lower concentration of 12.5 (mg L⁻¹).

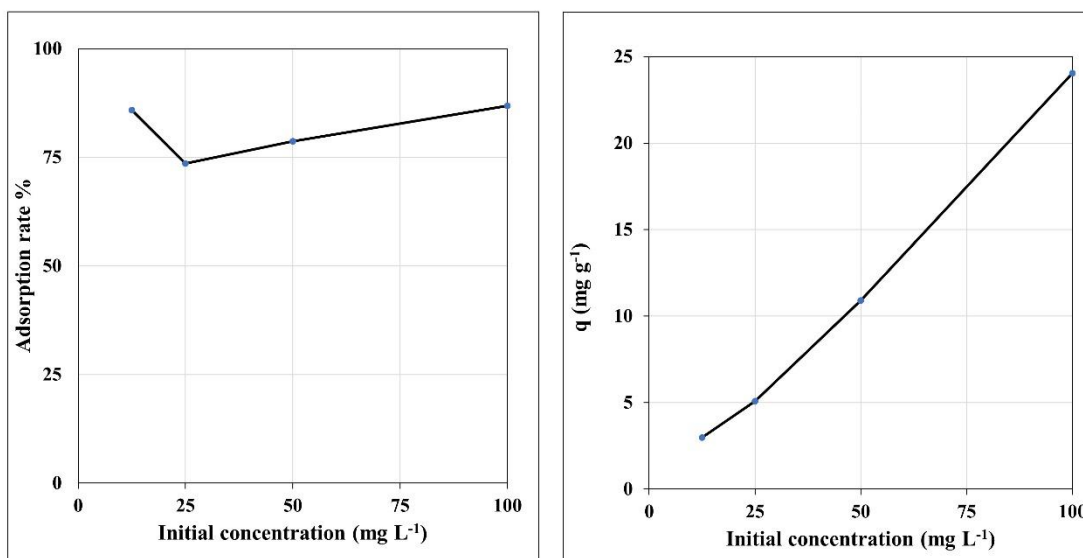


Fig 4.10. Adsorption rate and capacity for the preliminary step of MB removal onto G-EG considering different initial concentrations.

The analysis of the preliminary experimental adsorption data was conducted using several isotherm models. It was found that the Freundlich model yielded the most accurate match to the data, as shown by the greatest coefficient of determination ($R^2=0.80$) (Fig 4.11). This implies the presence of a multilayer adsorption process involving heterogeneous surfaces. The Langmuir model resulted in a less accurate match. The Temkin and Dubinin-Radushkevich models, however, exhibited better goodness-of-fit to the data with a correlation coefficient of 0.57 for both models (Fig 4.12).

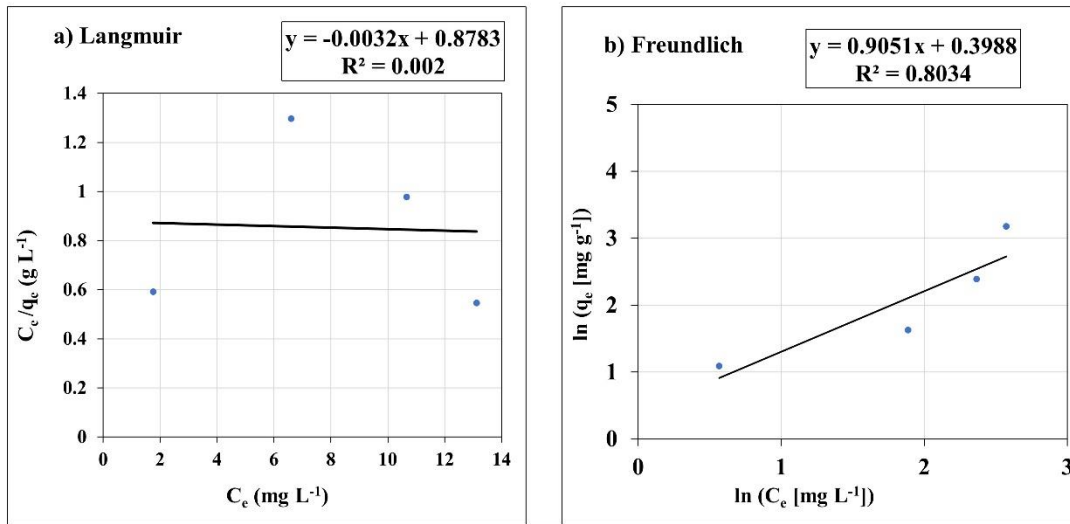


Fig 4.11. Langmuir Freundlich models fitted on the preliminary step of the experiment for MB removal onto G-EG.

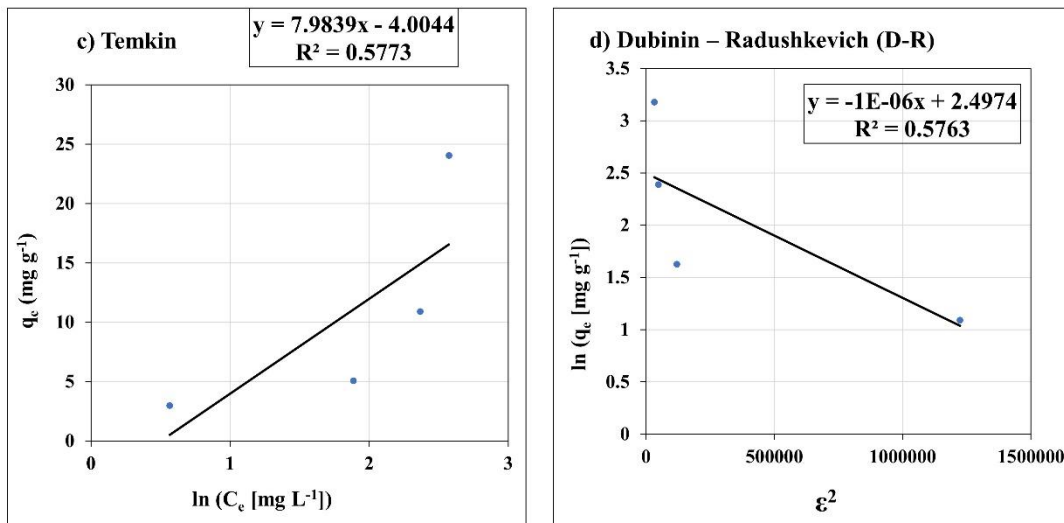


Fig 4.12. Temkin and Dubinin-Radushkevich's models fit the preliminary step of an experiment for MB removal onto G-EG.

Table 4.4. Kinetics' constants

Model	Equation	Parameters
-------	----------	------------

Langmuir		K_L	q_m	R^2
Langmuir linear	$\frac{C_e}{q_e} = \frac{1}{q_m K_L} + \frac{C_e}{q_m}$	-0.00359	-317.1	0.002
Freundlich		n_f	K_f	R^2
Freundlich linear	$\ln q_e = \ln K_f + \frac{1}{n_f} \ln C_e$	1.104	1.489	0.8034
Temkin	$q_e = B_1 \ln A + B_1 \ln C_e$	B_1	A	R^2
		7.98	0.605	0.5773
Dubinin – Radushkevich (D-R)	$\ln q_e = \ln q_s - \beta \varepsilon^2$	β	q_m	R^2
		1.00E-06	12.1	0.5763

Another factor considered in the preparation of G-EG was the amount of sodium alginate. Therefore, different amounts of sodium alginate were introduced to the composition of the granular form (5, 10, and 20 g). Fig 4.13 shows the results for this composition, where increased sodium alginate amounts elevated the adsorption capacity and rate of MB removal onto G-EG.

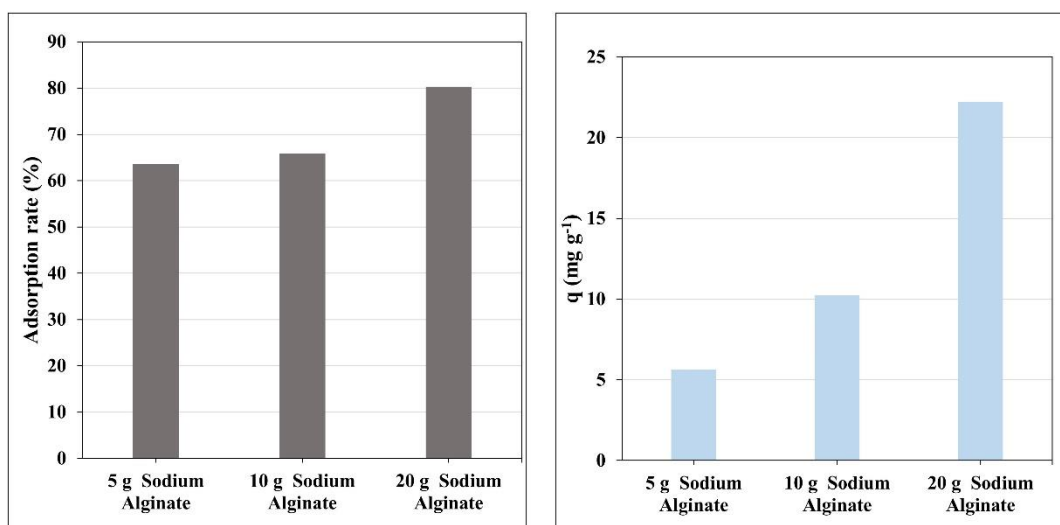


Fig 4.13. The effect of different sodium alginate additions on the adsorption performance of G-EG in MB removal.

4.3 Microwave (MW)-assisted production and regeneration of granular EG for adsorption of MB from aqueous solution

4.3.1 Optimization of adsorption process parameters using RSM

The RSM is a valuable analytical and statistical approach used to evaluate the impact of several independent factors on the response variable. Multiple trials were undertaken using various beginning values, and statistically designed tests were employed to investigate the collective influence of these elements (see Table 4.5). The RSM offers information on the linear impact of the factors on the adsorption response. Additionally, it gives insights into the squared and interaction effects of these parameters. Table 4.6 presents the analysis of variance (ANOVA) conducted for three different response variables. It can be demonstrated that values less than 0.05 indicate significant models.

Additionally, the coefficients for estimating R^2 for reduced quadratic responses are presented in Table 4.7. The observed agreement between the Predicted R^2 and the Adjusted R^2 is quite high, with a difference of less than 0.2. The optimization of experimental conditions was conducted using the adsorption capacity (q) and adsorption rate as parameters. The values of R^2 , which indicate the goodness of fit, were found to be within an acceptable range. This demonstrates the accuracy of the RSM in predicting adsorption behavior and analyzing data.

Table 4.5 Different runs of MB removal

	Factor 1	Factor 2	Factor 3	Factor 4	Response ₂	Response 3
Run	A: Time	B: Initial concentration	C: pH	D: Dose	Q	adsorption rate
Unit	Min	mg L ⁻¹	pH	g L ⁻¹	mg g ⁻¹	%
1	10	50	11	3.6	12.22	90.55
2	30	25	3.6	0.9	24.76	90.35
3	30	50	11	0.9	50.97	94.45
4	10	25	3.6	3.6	5.65	82.42
5	10	50	5.7	0.9	43.2	79.44

6	20	100	11	1.8	52.58	94.64
7	10	100	3.6	1.8	49.54	89.18
8	20	50	3.6	1.8	24.63	91.28
9	20	25	11	1.8	12.37	90.28
10	30	100	5.7	1.8	51.87	93.37
11	20	25	5.7	1.8	12.19	88.93
12	20	50	3.6	1.8	24.6	91.19
13	30	100	3.6	3.6	25.61	92.21
14	20	100	3.6	0.9	97.84	88.06
15	10	50	5.7	0.9	43.8	80.56
16	30	100	11	3.6	25.78	92.82
17	30	50	5.7	3.6	11.98	88.15
18	20	50	3.6	1.8	24.61	91.23
19	20	100	5.7	3.6	25.44	91.6
20	20	50	5.7	3.6	11.93	87.75
21	10	25	3.6	0.9	19.96	72.81
22	20	100	11	1.8	52.85	95.13
23	30	50	5.7	1.8	24.93	91.69

Table 4.6 Analysis of variance for three responses in terms of p-value

Adsorption capacity q (mg g ⁻¹)	p-value	Adsorption rate (%)	p-value
Model	< 0.0001	Model	< 0.0001
A-Time	< 0.0001	A-Time	< 0.0001
B-Initial concentration	< 0.0001	B-Initial concentration	0.0002
C-pH	0.0148	C-pH	0.0136
D-Dose	< 0.0001	D-Dose	0.0060
AB	0.0250	AB	0.0336
AD	0.0012	AD	0.0018

B ²	< 0.0001	B ²	0.0961
D ²	< 0.0001	C ²	0.0854
		D ²	0.0003

Table 4.7 Coefficients of correlation provided by RSM model fitted on experimental data

Response	Adsorption capacity (q)	Adsorption rate (%)
	reduced quadratic model	reduced model
R ²	0.9994	0.9466
Adjusted R ²	0.9991	0.9097
Predicted R ²	0.9983	0.8134

Additionally, the accuracy of the model was assessed by generating a plot (Figure 4.14, 4.15) that compares the actual (experimental) values with the predicted values. These plots demonstrate the potential of RSM for subsequent optimization purposes. The R² values exhibited a high level of excellence, falling within the range of 0.94-0.99.

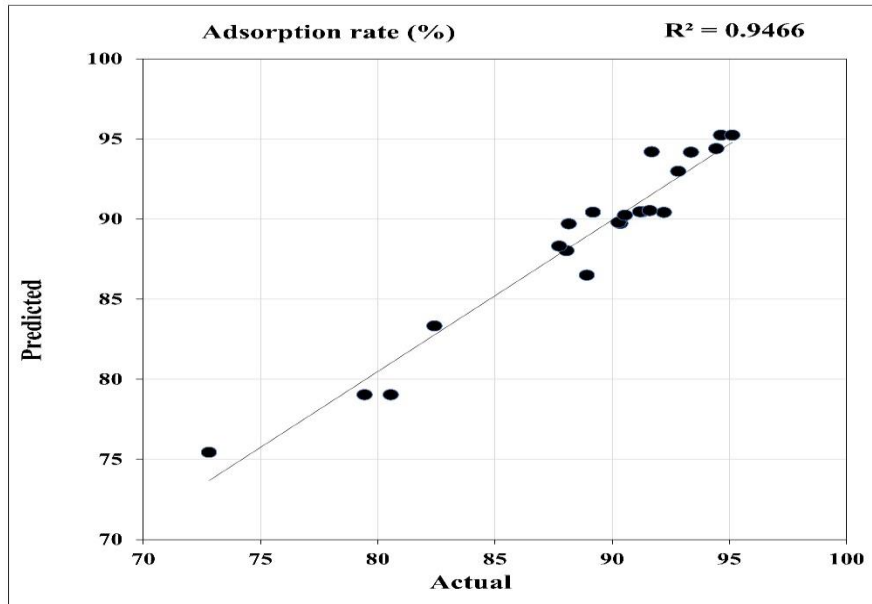


Fig 4.14 Actual (experimental) versus predicted (models) values by RSM for adsorption rate (%) (MW-EG plus MB removal)

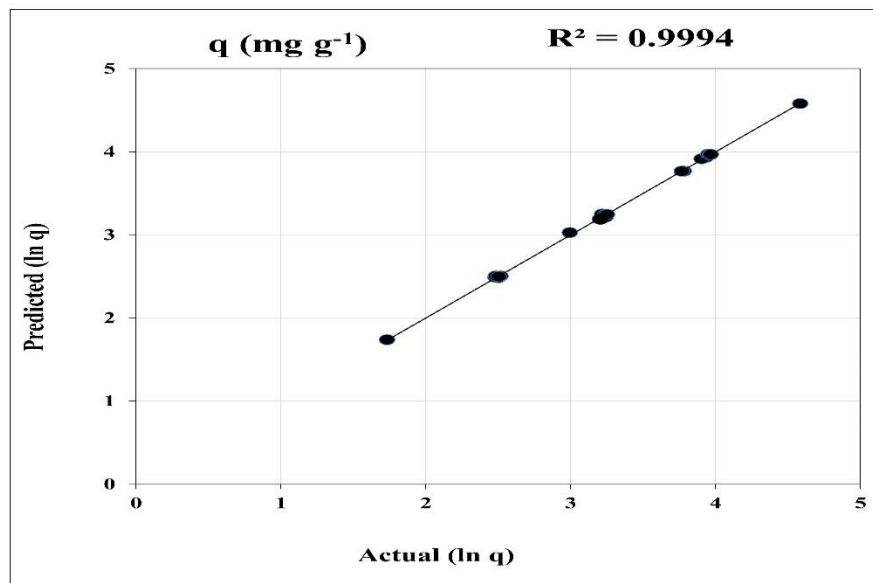


Fig 4.15 Actual (experimental) versus predicted (models) values by RSM for adsorption amount (q) (MW-EG plus MB removal)

4.3.2 Evaluation of the one-factor effect on adsorption features

Figures 4.16 to 4.19 present the impacts of distinct parameters on the variables q and figures 4.20 to 4.23 on the adsorption rate. An upward trend was seen in the q and adsorption rate as the contact duration and starting concentration were increased. This phenomenon can be explained by the increased contact time between MB and MW-EG pores, as well as the larger concentration of adsorbate that can be adsorbed at the pore site. Additionally, it should be noted that both responses exhibited dependence on elevated pH levels. This is because at higher pH values, the adsorbent's surface becomes negatively charged, hence facilitating the adsorption of MB, a cationic dye, within its pores.

Additionally, the adsorption rate reached its maximum at levels of 1.8 and 2.7 (g L^{-1}). In contrast, a clear downward trend was seen for variable q , as it exhibits an inverse relationship with dosage. Specifically, an increase in the amount of doses corresponds to a decrease in the adsorption capacity (q) value.

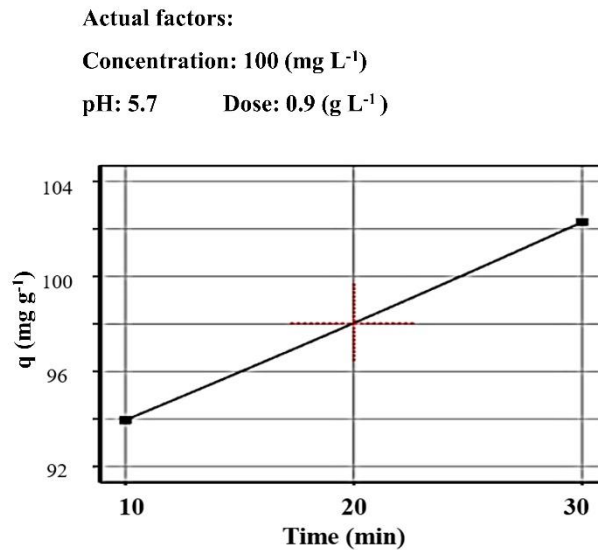


Fig. 4.16 Effects of time on q performance

Actual factors:

Time: 20 min pH: 5.7

Dose: 0.9 (g L⁻¹)

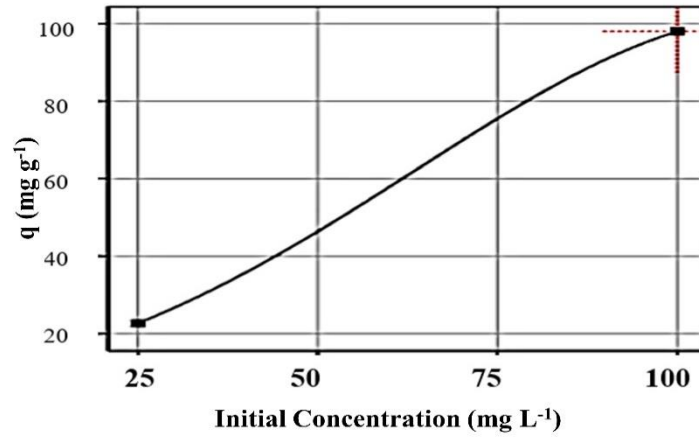


Fig 4.17. Effects of initial concentration on q performance

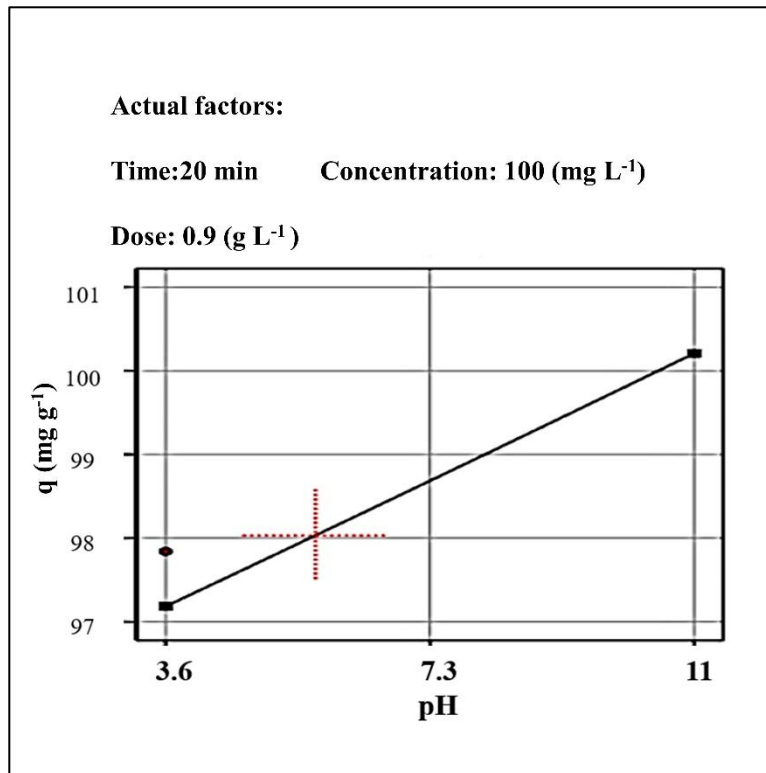


Fig 4.18 Effects of pH on q performance

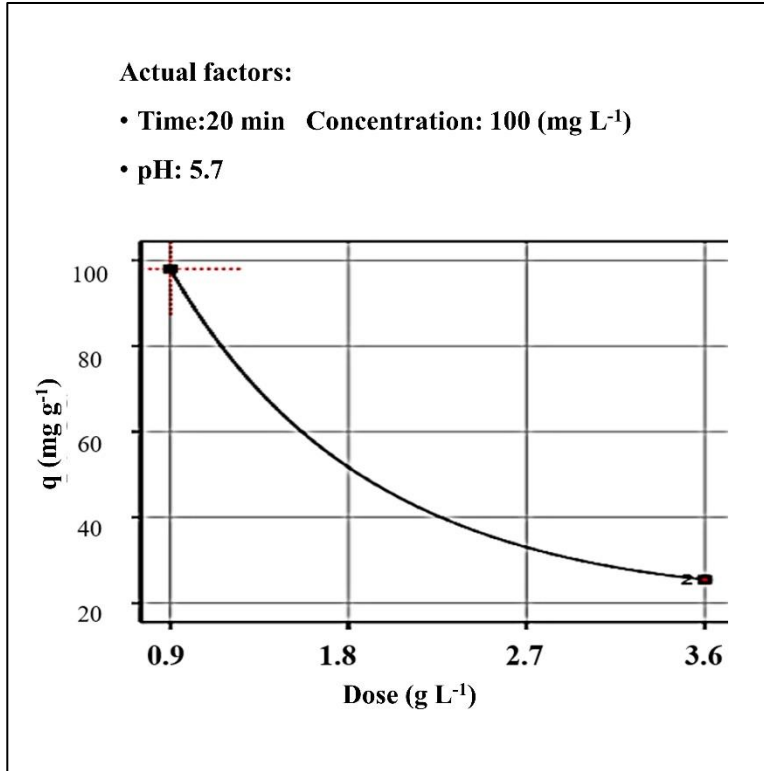


Fig 4.19 Effects of adsorbent dose on q performance

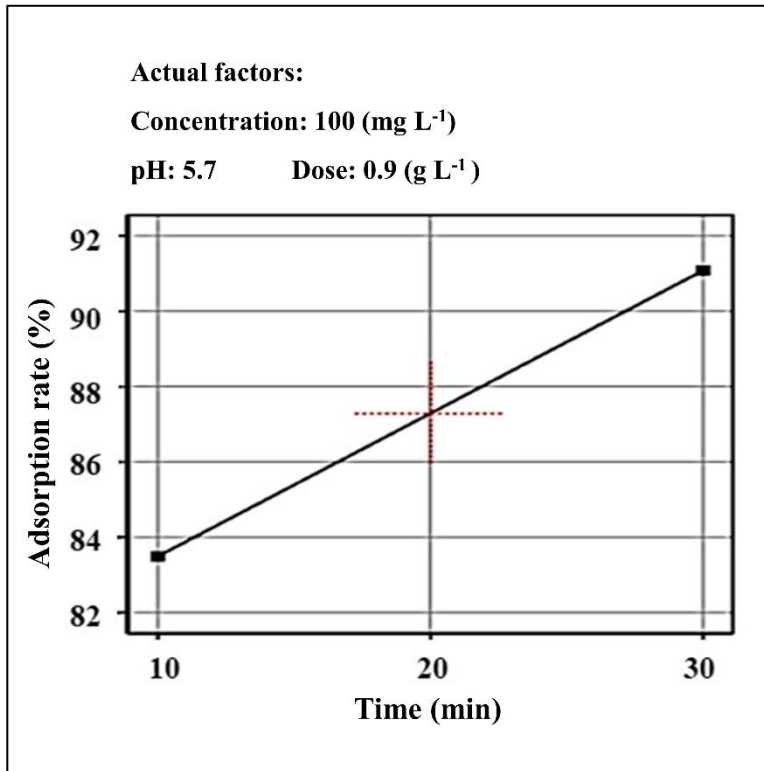


Fig 4.20 Effects of time on adsorption rate

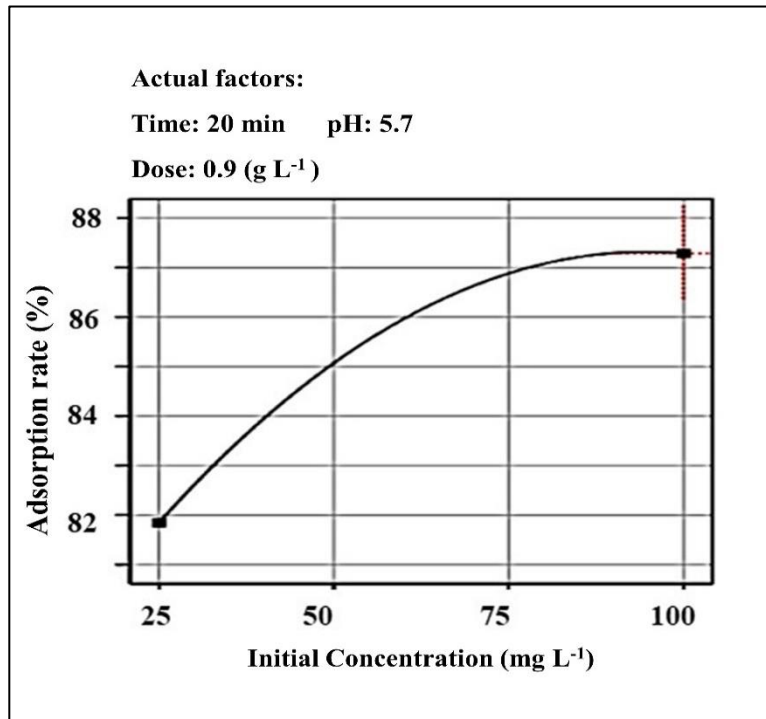


Fig 4.21 Effects of initial concentration on adsorption rate

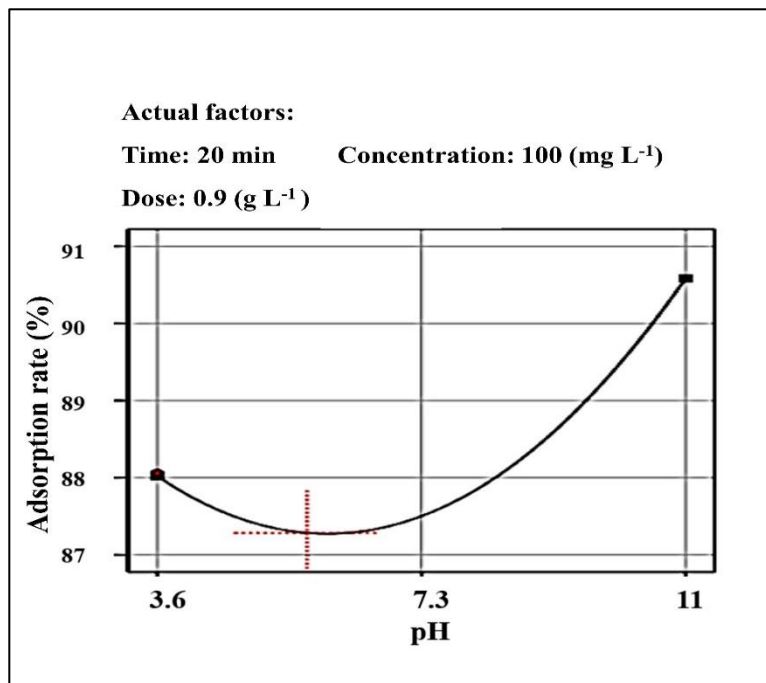


Fig 4.22 Effects of pH on adsorption rate

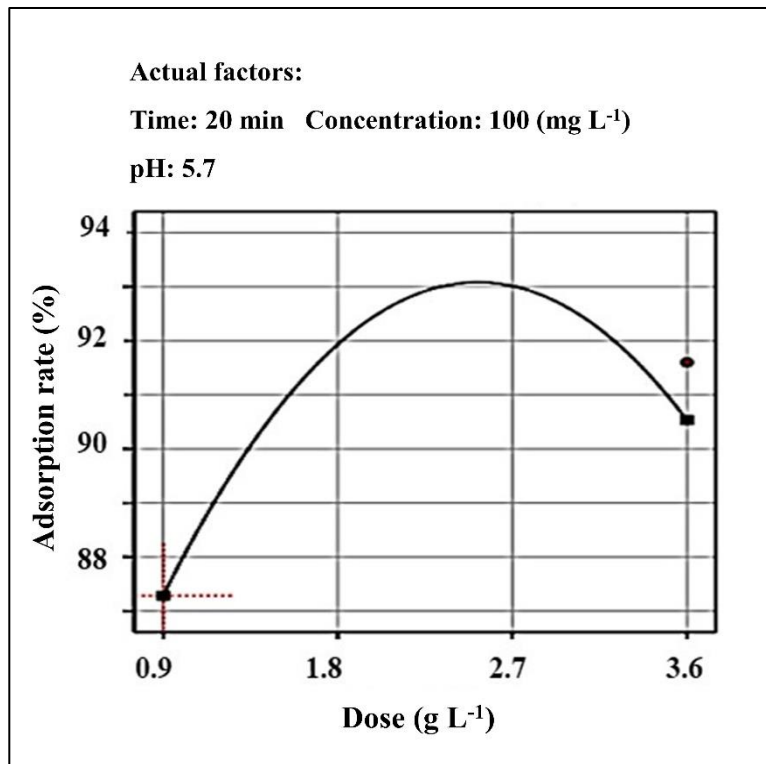


Fig 4.23 Effects of adsorbent dose on adsorption rate

4.3.3 Response surface plots

One notable benefit of RSM is its ability to generate three-dimensional plots of the response surface. These plots facilitate a comprehensive understanding of the interactions between key elements and allow for the exploration of ideal values for all parameters in order to maximize the adsorption rate and amount.

Figures 4.24 to 4.29 provide the graphical representation of the relationship between the contact time, starting concentration, pH, dose, and the rate and adsorption capacity (q) of MB on a 3D surface. The findings presented in Figure 4.24, which illustrates the time-dose interaction, indicate that the plots with a dose of 0.9 g L⁻¹ and a minimum time of 10 minutes, along with other fixed factors at specific levels (pH= 5.7 neutral, concentration 100 mg L⁻¹), exhibit the highest adsorption capacity (indicated by red colors, ranging from 80-100 mg g⁻¹). These results highlight the noticeable influence of the adsorbent dose on the adsorption capacity (q). The experimental results presented in Fig 4.25 demonstrate the relationship between the initial concentration of MB and the contact time. It was observed that when the initial concentration exceeded 75 mg L⁻¹ while

maintaining a constant pH of 5.7 and a dose of 0.9 g L⁻¹ for 10 minutes, the adsorption capacity (q) reached its maximum values, ranging from 80 to 100 mg g⁻¹. This can be attributed to the fact that higher concentrations of the substance result in a greater number of MB molecules being exposed to available adsorption sites. It is noteworthy to notice that, as indicated by Fig 4.26, an increase in pH led to a corresponding increase in q (104 mg g⁻¹). This observation suggests a higher interaction between positive MB ions and the negative charge MW-EG pores. In addition, the impact of initial concentration over contact time (as seen in Fig 4.27) on adsorption rates demonstrates that in order to achieve a greater efficiency level (>90%), a minimum of 30 minutes and a concentration of more than 35 (mg L⁻¹) of MB solution are required, while keeping other parameters constant. The data presented in Fig 4.28 indicate that there is a significant interaction between contact time and the dosage of MW-EG. Specifically, it was seen that a contact duration of 10 minutes and a dosage of 1.8 g L⁻¹ of MW-EG resulted in adsorption rates above 90%, suggesting that these conditions are favorable for achieving greater adsorption rates. The results from the pH and time interactive Fig 4.29 demonstrate that achieving an efficiency of over 90% at lower pH levels necessitates a time exceeding 25 minutes. Conversely, at higher pH levels, this duration is decreased to 18 minutes.

Furthermore, one advantage of RSM is the ability to set a parameter while finding the optimal values for the other parameters, hence achieving the greatest response or desired objective. Table 4.8 presents the optimal parameters required to get the highest response in terms of both the q and adsorption rate, therefore facilitating efficient utilization of resources and time. The outcome mentioned above is achieved by optimizing the dosage and contact time while maintaining a pH level of 5.7. This pH value closely resembles the actual conditions and requires no additional pH adjustments. It is evident that there are other solutions to achieve optimal response rates, with the first solution being prioritized above the alternative solution due to its greater desirability.

Table 4.8 Results of optimization of RSM

Number	Time (min)	Initial concentration (mg L ⁻¹)	pH	Dose (g L ⁻¹)	q (mg g ⁻¹)	Adsorption rate (%)	Desirability
--------	------------	---	----	---------------------------	-------------------------	---------------------	--------------

1	10	100	5.7	0.9	93.95	83.5	0.829
2	10	100	5.7	1.8	50.54	89.7	0.789
3	20	100	5.7	0.9	98.03	87.3	0.755
4	20	100	5.7	1.8	51.73	91.9	0.686
5	20	50	5.7	0.9	46.37	85.1	0.671

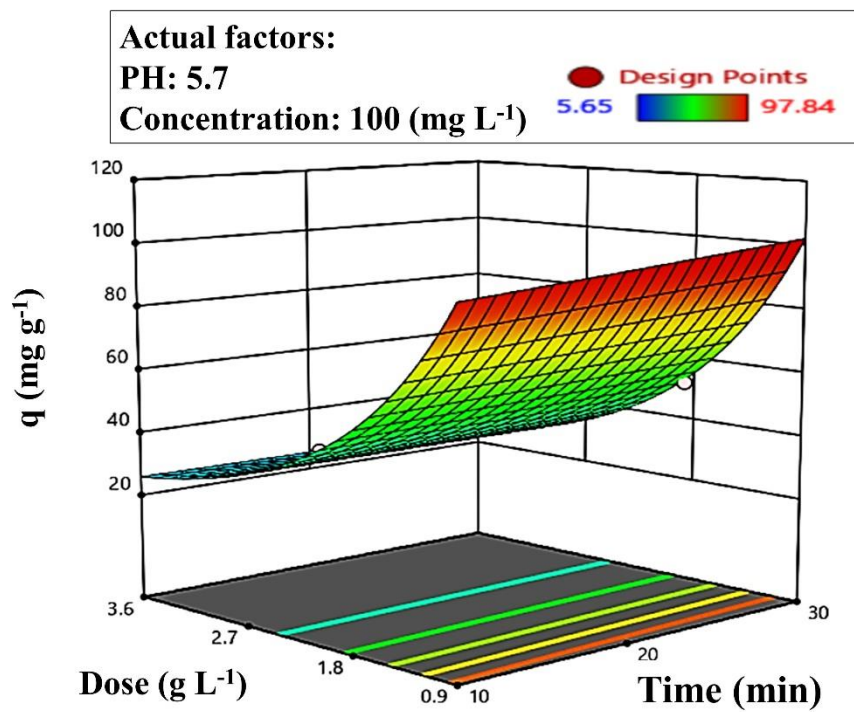


Fig. 4.24. 3D surface of the adsorption capacity (q) of MB versus the contact time and dose

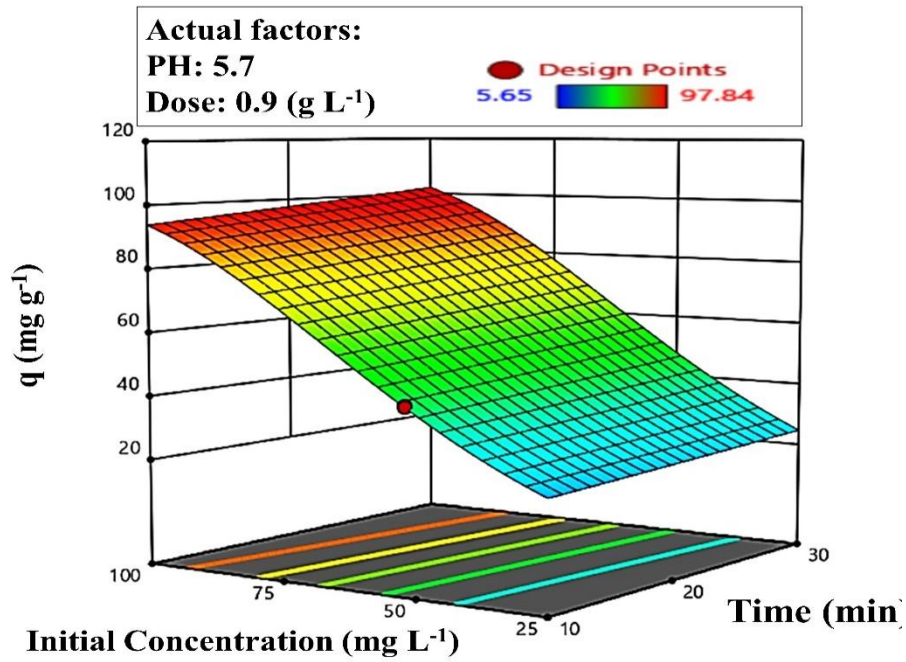


Fig 4.25. 3D surface of the adsorption capacity (q) of MB versus the contact time and initial concentration

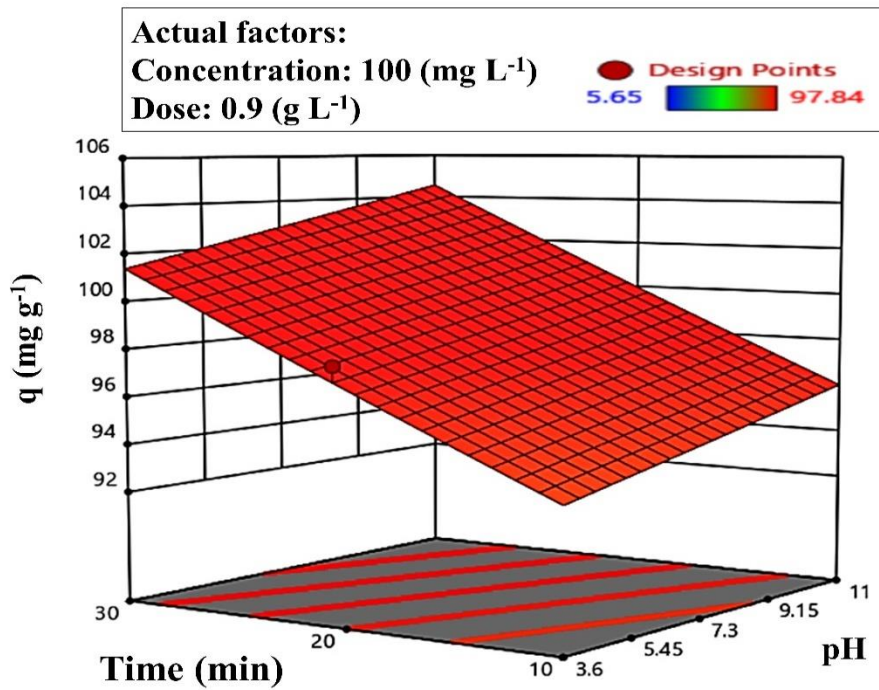


Fig. 4.26. 3D surface of the adsorption capacity (q) of MB versus the contact time and pH

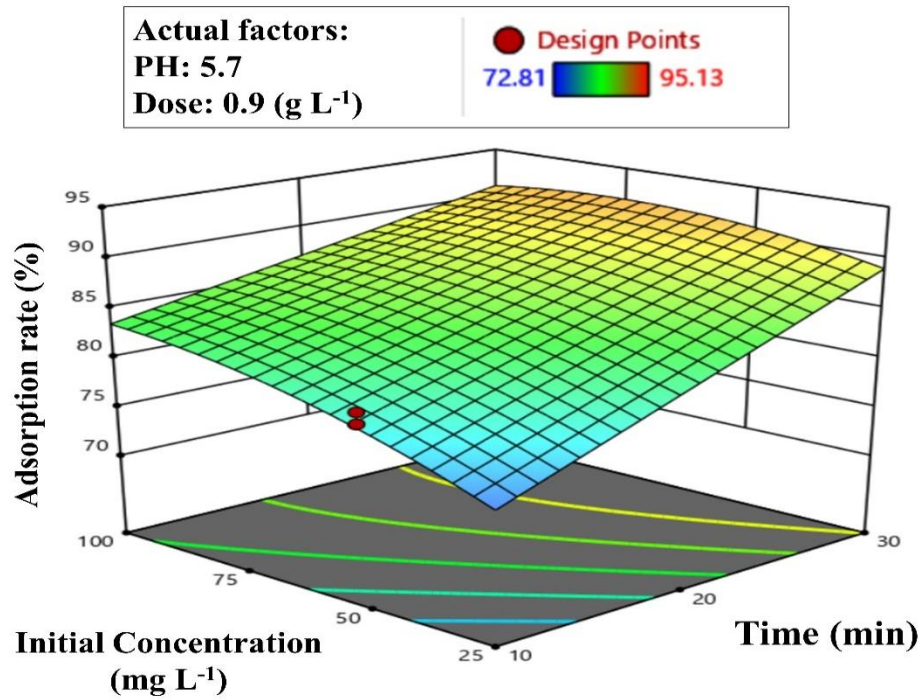


Fig 4.27. 3D surface of the adsorption rate of MB versus the contact time and initial concentration

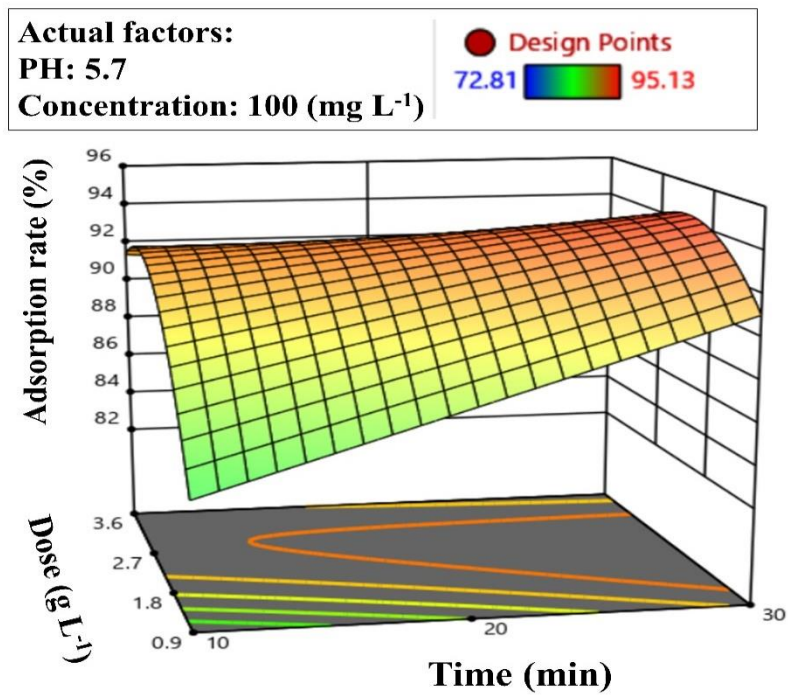


Fig 4.28. 3D surface of the adsorption rate of MB versus the contact time and dose

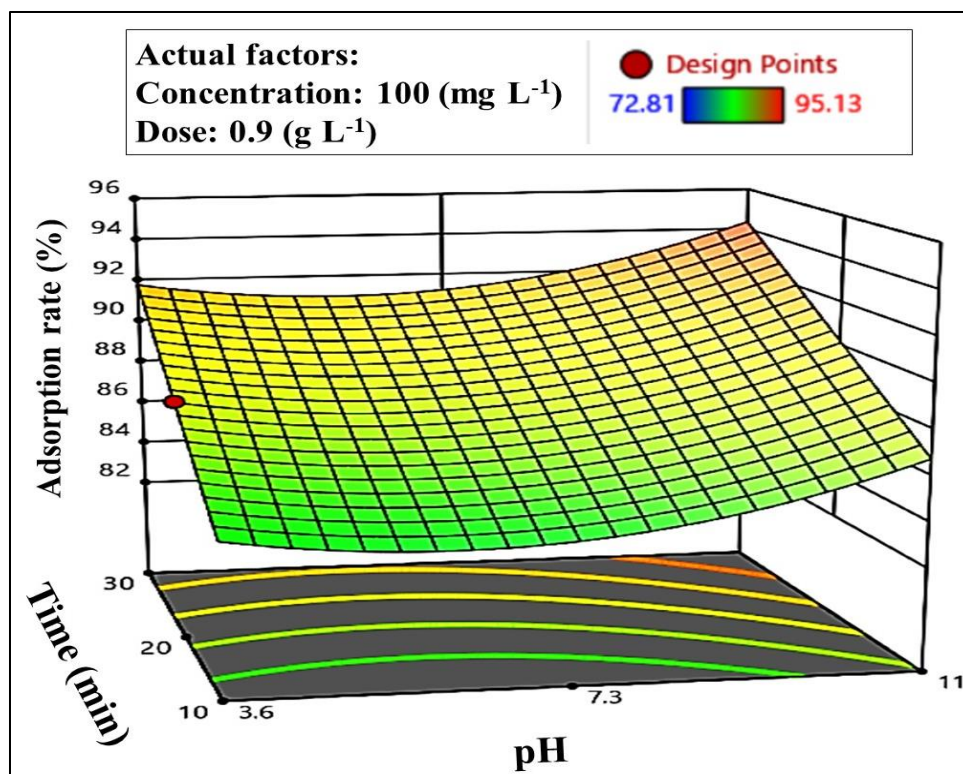


Fig 4.29. 3D surface of the adsorption rate of MB versus the contact time and pH

4.3.4 Adsorption isotherms

Figure 4.30 to 4.32 display the Langmuir, Freundlich, Temkin, and Dubinin-Radushkevich models. Based on the obtained figures and the R^2 value, it can be concluded that the data proved a good fit for the Freundlich model. This observation highlighted the presence of heterogeneous surfaces and the occurrence of adsorption in a multi-layered manner. Furthermore, the active sites and their associated energies were found to be exponentially distributed, indicating that the adsorbent had several nearby sites. Besides, the parameters corresponding to all isotherm models are provided in Table 4.9.

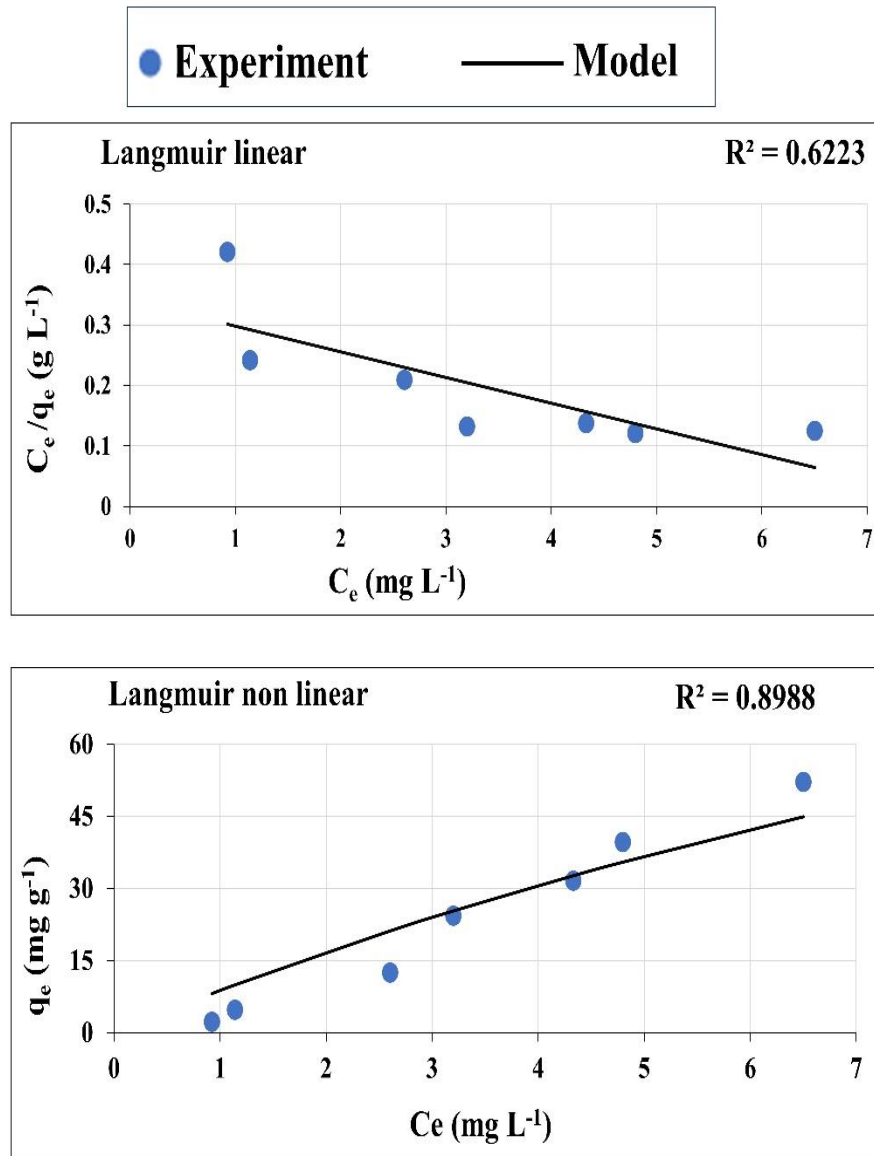


Fig 4.30 Linear and non-linear Langmuir models fitted on experimental data

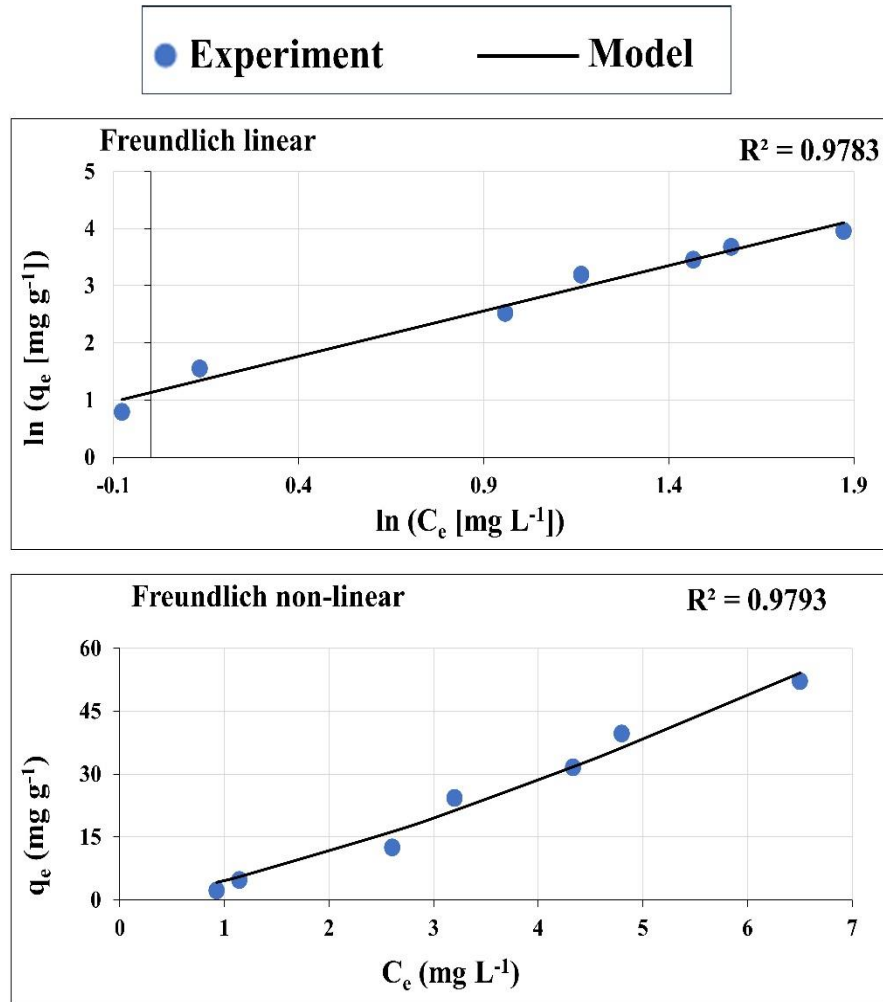


Fig 4.31 Linear and non-linear Freundlich models on experimental data

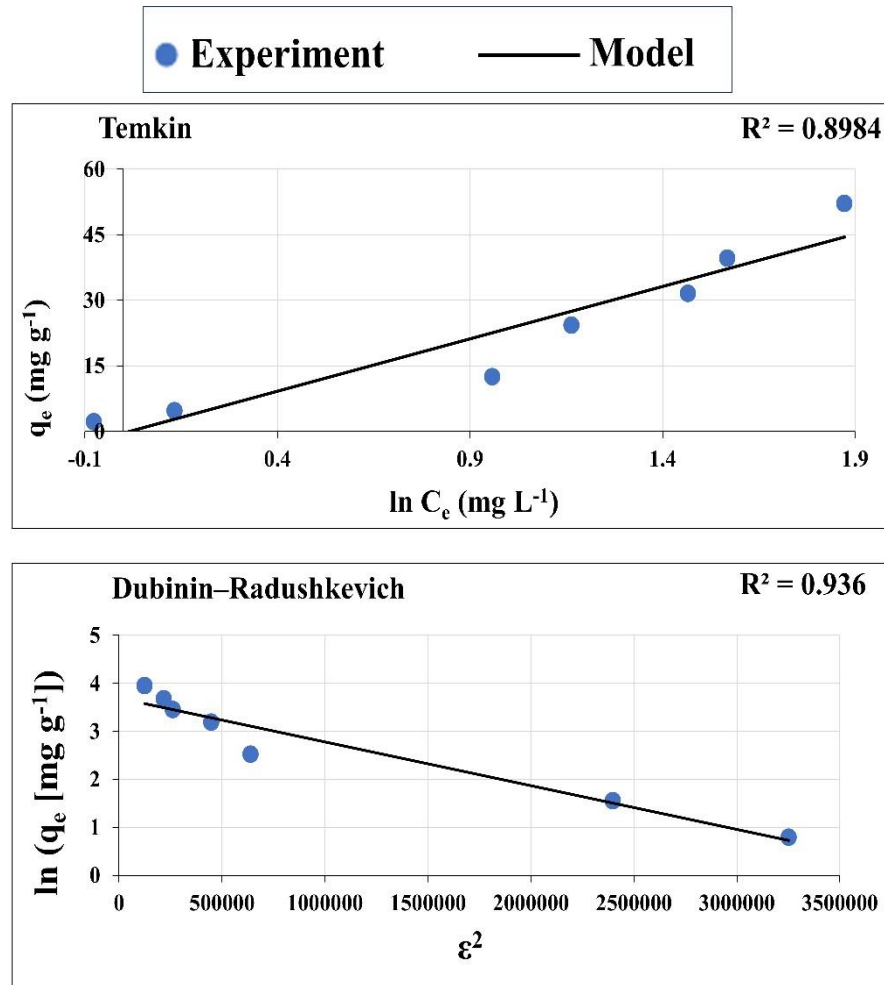


Fig 4.32 Temkin and Dubinin-Radushkevich models on experimental data

Table 4.9 Isotherm parameters by different models

Model	Equation	Parameters		
Langmuir		K_L	q_m	R^2
Langmuir linear	$\frac{C_e}{q_e} = \frac{1}{q_m K_L} + \frac{C_e}{q_m}$	-0.124	-23.48	0.6223
Langmuir non-linear	$q_e = \frac{q_m K_L C_e}{1 + K_L C_e}$	0.051	180.13	0.8988
Freundlich		n_f	K_f	R^2

Freundlich linear	$\ln q_e = \ln K_f + \frac{1}{n_f} \ln C_e$	0.630	3.09	0.9783
Freundlich non-linear	$q_e = K_f C_e^{1/n_f}$	0.760	4.61	0.9793
Temkin	$q_e = B_1 \ln A + B_1 \ln C_e$	B_1	A	R^2
		23.98	0.983339	0.8984
Dubinin – Radushkevich (D-R)	$\ln q_e = \ln q_s - \beta \varepsilon^2$	β	q_m	R^2
		0.001351	40.08571	0.9360

4.3.5 Kinetics studies

Figure 4.33 illustrates the kinetics and equilibrium of the study. The experimental settings employed in this investigation were as follows: pH of the solution was set at 5.7, the dosage used was 1.8 (g L⁻¹), the starting concentration of the MB was 100 (mg L⁻¹), and several time intervals ranging from 5 to 60 minutes were considered. The experimental results indicate that over 90% of the MB solution was adsorbed within the initial 10-minute period of the test and then achieved equilibrium at around 94% after 20 minutes. In addition, Figure 4.34 depicts the kinetics model, namely the pseudo-first order and pseudo-second order models. The R² results indicate that the pseudo-first-order model is not suitable for accurately predicting the kinetics of methylene blue adsorption onto MW-EG. The linear graphs of t/qt vs. t exhibit a high level of agreement between the experimental and estimated q_e values in the context of pseudo-second-order kinetics. The correlation coefficients (R²) for the second-order kinetics model exhibit values exceeding 0.999, suggesting the suitability of this kinetics equation and confirming the second-order characteristics of the methylene blue adsorption process onto the MW-EG. The kinetics variables for models are mentioned in Table 4.10.

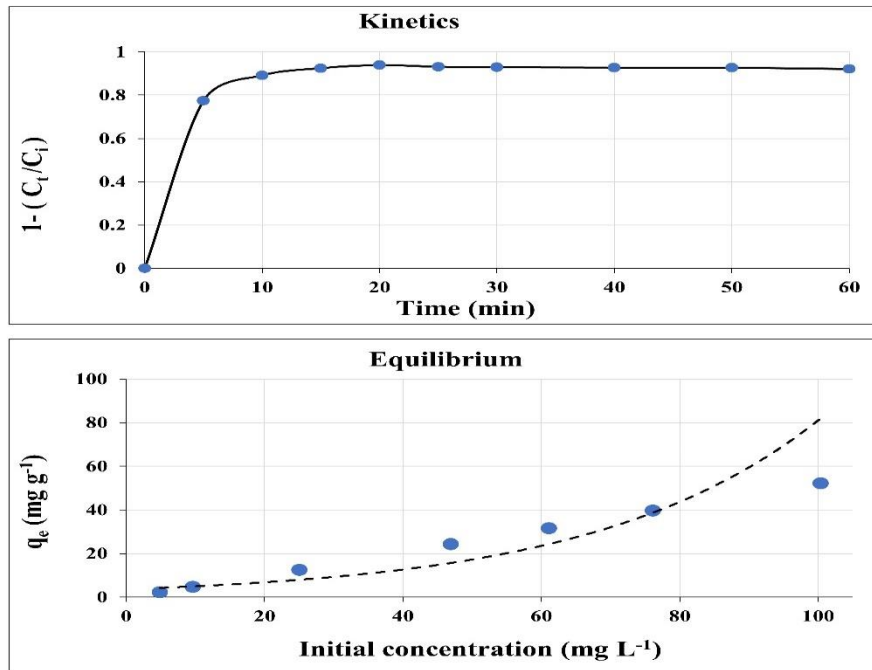
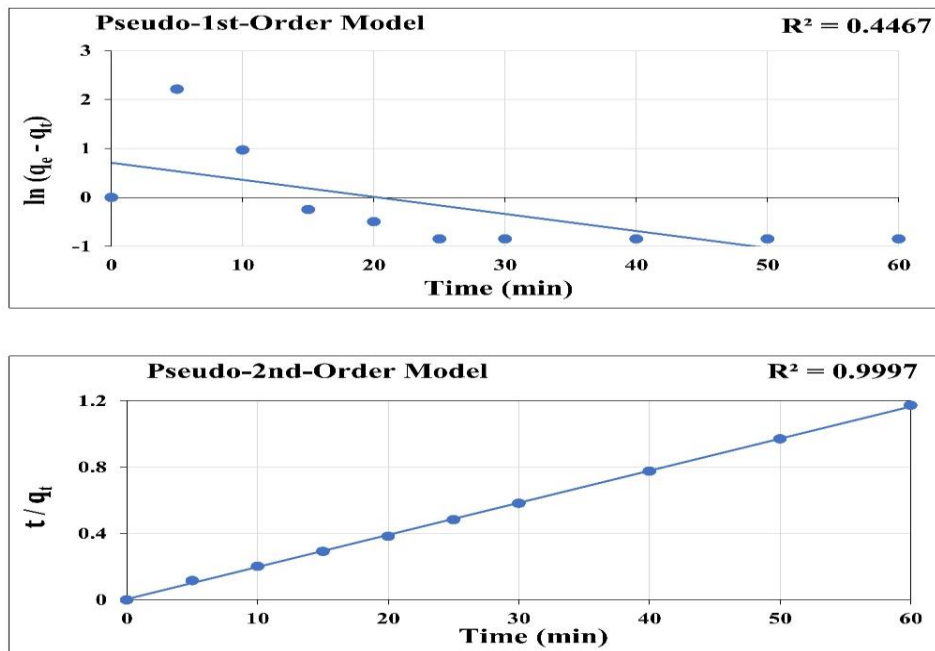


Fig 4.33 Kinetics and equilibrium outlines of MB removal onto MW-EG



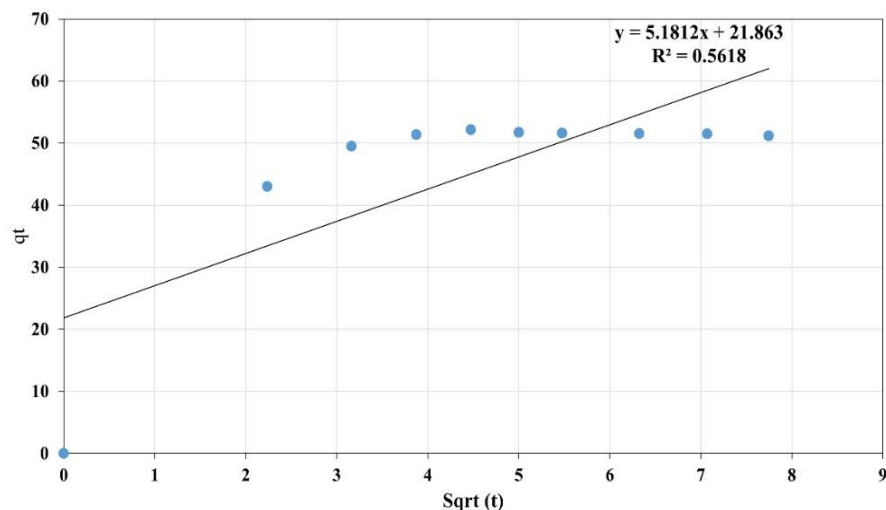


Fig 4.34 pseudo-first-order , pseudo-second-order, and Intra-particle diffusion models of MB removal experiment using MW-EG adsorbent

Table 4.10 Kinetics parameters of different models

Model	q_e (mg g ⁻¹)	Rate constant	R ²
pseudo-first order	2.026419	$k_1 = -0.00058$	0.4467
pseudo-second order	51.67959	$k_2 = 0.08568$	0.9997
Intra-particle diffusion	$\theta = 21.86$	$K_i = 5.1812$	0.5618

4.3.6 Thermodynamics output

Figure 4.35 and Table 4.11 present the thermodynamic characteristics of the adsorption process. The presence of negative values of Gibbs free energy serves as an indication of the thermodynamic feasibility and spontaneity of the adsorption mechanism. Additionally, the observation of negative values for ΔH^0 indicates that the adsorption of MB in MW-EG is characterized by an exothermic process.

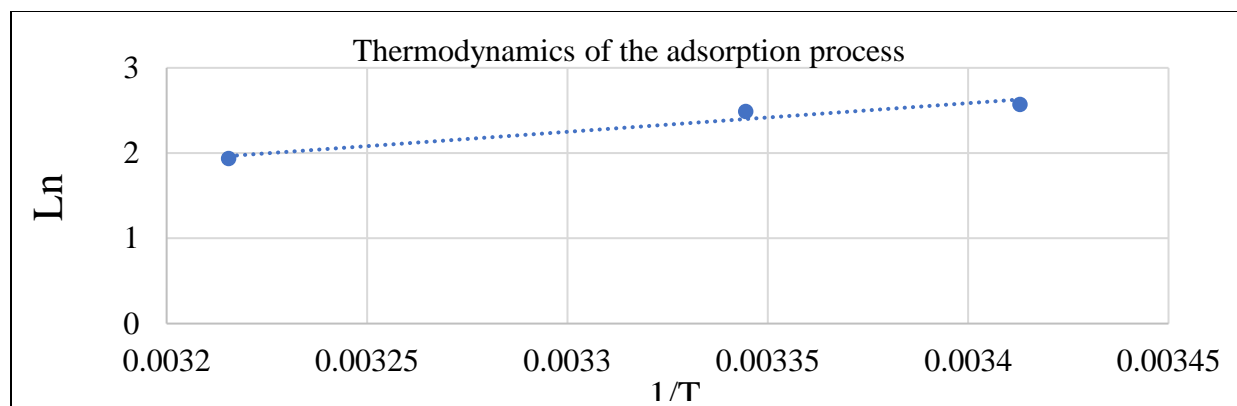


Fig 4.35 Thermodynamics plot of the adsorption process

Table 4.11 Thermodynamics parameters

T (K)	K_L	ΔG^0	ΔH^0	ΔS^0	R^2
293	13.08625	-6.26433	-27.9324	-73.4734	0.9496
299	12.02914	-6.18322			
311	6.92373	-5.00312			

4.3.7 Regeneration studies

The thermal regeneration of MW-EG exhausted by MB was conducted using a commercial microwave device. A power level of 1100 ± 20 W) and an irradiation period of 5 minutes were found to be enough for the removal of MB from the pores of the adsorbent and its subsequent preparation for the next cycle. Regarding energy consumption, each regeneration cycle utilized an average of 0.08 ± 0.01 kilowatt-hours (KWh). The findings from ten regeneration cycles of MW-EG (as seen in Figure 4.36) indicate that there was no observed reduction in both adsorption capacity and rates. This demonstrates the effectiveness of MW irradiation as a means of achieving sustainable recycling. In addition to its fast regeneration procedure, which requires reduced energy usage, MW technology presents an environmentally sustainable alternative to conventional thermal regeneration methods. The weight loss of the adsorbent in this investigation was around

8% after ten cycles, which contrasts with traditional regeneration techniques that often experience significant material loss during cyclic regeneration.

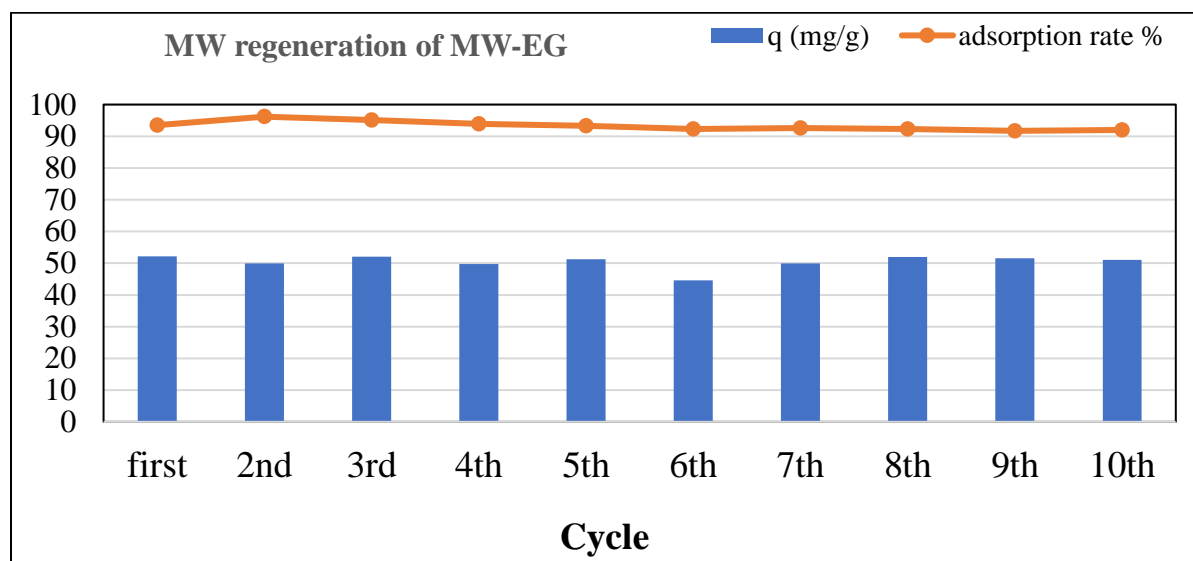


Fig 4.36 Regeneration of MW-EG by MW irradiation (MB removal)

4.3.8 The performance of adsorption of MB from surface water

To assess the suitability of MW-EG for removing MB from a sample of natural surface water obtained from Lake Hartwell in South Carolina (USA), a concentration of 100 mg L^{-1} of MB was introduced into the sample. A quantity of $1.8 \text{ (g L}^{-1}\text{)}$ of MW-EG was introduced into the solution without adjusting the pH level, which was measured at 5.7. The solution was then subjected to shaking for 20 minutes. The surface water sample exhibited a total organic carbon (TOC) concentration of $2 \text{ (mg L}^{-1}\text{)}$, a chloride concentration of 2.7 mg L^{-1} , a phosphate concentration of 11.3 mg L^{-1} , and an alkalinity concentration of 17 mg L^{-1} . The outcome demonstrated that MW-EG, as far as the sample under consideration, can function adsorbing MB in actual contaminated media such as rivers and surface waters since there was no decline in MW-EG's adsorption performance even in the presence of natural organic and inorganic materials. The findings of the replicated study conducted on surface water yielded a value of $51.4 \text{ (mg g}^{-1}\text{)}$, indicating a removal effectiveness of 96%.

Additionally, the analysis conducted in Table 4.12 examined the current body of literature pertaining to modified EG and its efficacy in adsorption. It also included a comparative assessment of the adsorption capacity of these studies in relation to the present investigation.

Table 4.12 Results of various studies on modified EG versus the result of this study

Reference	Material	Adsorption performance	Time	Other conditions
(M. Zhao & Liu, 2009b)	Modified EG powder	Langmuir $q_{\max} = 7.77 \mu\text{g g}^{-1}$ ($q_{\text{exp}} = 2.7 \mu\text{g g}^{-1}$)	180 min	pH: 7 dose: 3.5 g L^{-1}
(Hoang et al., 2019b)	Microwave-assisted EG	Langmuir $q_{\max} = 47.5 \text{ mg g}^{-1}$ ($q_{\text{exp}} = 51 \text{ mg g}^{-1}$)	80 min	pH: 9 dose: 2 g L^{-1}
(Y. Li et al., 2013)	Graphene oxide calcium alginate	Langmuir $q_{\max} = 181 \text{ mg g}^{-1}$	300 min	pH: 5.4 dose: 0.5 g L^{-1}
(Tian et al., 2021)	Magnetic EG $\text{Fe}_3\text{O}_4/3\text{MEG-I}$	($q_{\text{exp}} = 3 \text{ mg g}^{-1}$)	60 min	pH: 7.09 - -
(K.-H. Wu et al., 2021b)	Modified expanded graphite/ Fe_3O_4	Langmuir $q_{\max} = 79 \text{ mg g}^{-1}$	140 min	dose: 3.3 g L^{-1}
This study	MW-EG	Langmuir $q_{\max} = 180.13 \text{ mg g}^{-1}$ ($q_{\text{exp}} = 97.84 \text{ mg g}^{-1}$)	20 min	pH: 5.7 dose: 0.9 g L^{-1} (based on graphene used)

Table 4.13 shows the BET analysis after 10 cycles of adsorption and regeneration. Based on the analysis, the BET surface area witnessed a reduction to an average of 6 after cyclic regeneration.

The mesopore area and total pore volume decreased after the 10th cycle usage as well. Besides, the isothermal linear plot after cyclic regeneration is provided in Fig 4.37.

The decreases in BET values and pore volumes can be because of 10-cycle adsorption/regeneration, where some pollutant particles blocked pores; however, the BET changes were between 40% decreases. One solution for removing this blockage can be a longer regeneration time in MW after several adsorbent uses.

Table 4.13. BET and pore size distribution changes for MW-EG

Material	BET (m ² g ⁻¹)	Total Pore Volume (cm ³ g ⁻¹)	Mesopore volume (cm ³ g ⁻¹)
MW-EG before adsorption	10	0.0195	0.018
MW-EG after 10-cycle regeneration	6.1 (4-8.2)	0.009-0.0159	0.007-0.016

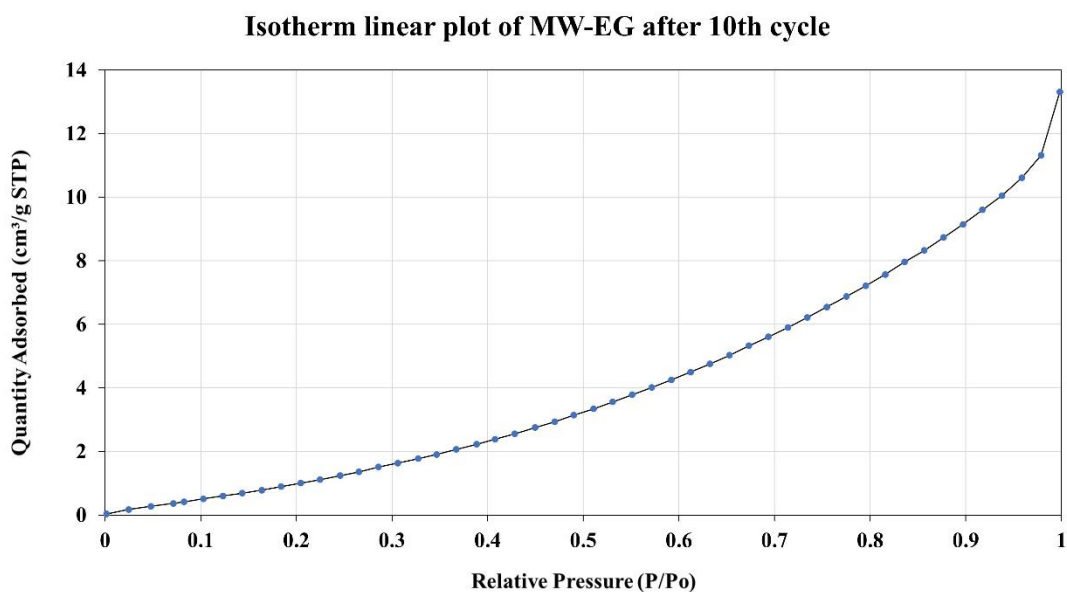


Fig 4.37. isotherm linear plot of MW-EG after 10-cycle regeneration

4.3.9. Conclusion

The MW-EG was prepared from EG to adsorb the methylene blue (MB) as a cationic dye. A commercial microwave system was employed to prepare the MW-EG for regeneration goals. Besides, the RSM was evaluated to optimize the efficient parameters. The adsorption experiments showed that the MW-EG is an efficient adsorbent for removing the MB from an aqueous deionized distilled water (DDW) and surface water. Moreover, applying RSM facilitated the workflow of this study by decreasing the number of runs and consequently triggered the saving of materials and time. It is worth mentioning that MW irradiation was an economical option for regeneration studies because of less energy consumption, excellent recycling performances, and less weight loss of adsorbent. The results of this study showed that:

- MW-EG can be one of the options at an industrial scale, such as dye wastewater adsorption, because of its performance in dye removal on a lab scale and surface water media. The results showed that MW-EG could remove MB from surface water media in less than 20 minutes and achieve 96% removal efficiency.
- RSM applied in this study can overcome the challenges regarding the optimization of experiment conditions by a practical and easy process. This methodology can reduce the number of runs and lead to quick and more accurate optimization of experimental conditions.
- MW irradiation used in the preparation of MW-EG can remove all impurities from pores and facilitate the adsorption process owing to its inside-outside temperature gradient and uniformity of heat transfer.
- BET surface analysis was studied for both EG and MW-EG, emphasizing the importance of pore distribution studies. The result showed that surface area decreased for granular form (MW-EG), while a macropore structure was witnessed for MW-EG.
- Regeneration studies showed that MW irradiation could work for ten consecutive cycles by offering less energy consumption (0.08 KWh), faster process (less than 5 min), and less material losses (around 8 %) in comparison to conventional regeneration.
- Dye removal from a real sample of lake surface water showed the possibility of using MW-EG for real polluted media in the presence of natural organic matter and inorganic compounds.

Removal of oil contents from aqueous solution by Expanded graphite materials.

4.4.1 Adsorption of dissolved oil

4.4.1.1 The Impact of Oil Concentration

The concentration of crude oil in the aqueous solution was studied as the primary variable investigated in this research. Two concentrations (100 and 200 mg L⁻¹) were examined to determine the effect on EG's adsorption effectiveness.

The experimental findings demonstrated a notable difference in the percentage of crude oil removal observed between the two concentrations. At the lower concentration of 100 (mg L⁻¹), it was noticed that the adsorption effectiveness of EG was comparatively lower, resulting in a removal rate of roughly 19 and 73% for 0.1 and 0.2 g L⁻¹ of powder, respectively. However, when the initial oil content was elevated to 200 (mg L⁻¹), the effectiveness of oil removal exhibited an increase to around 70 and 88 % for 0.1 and 0.2 g L⁻¹ adsorbent, respectively. (Fig 4.38)

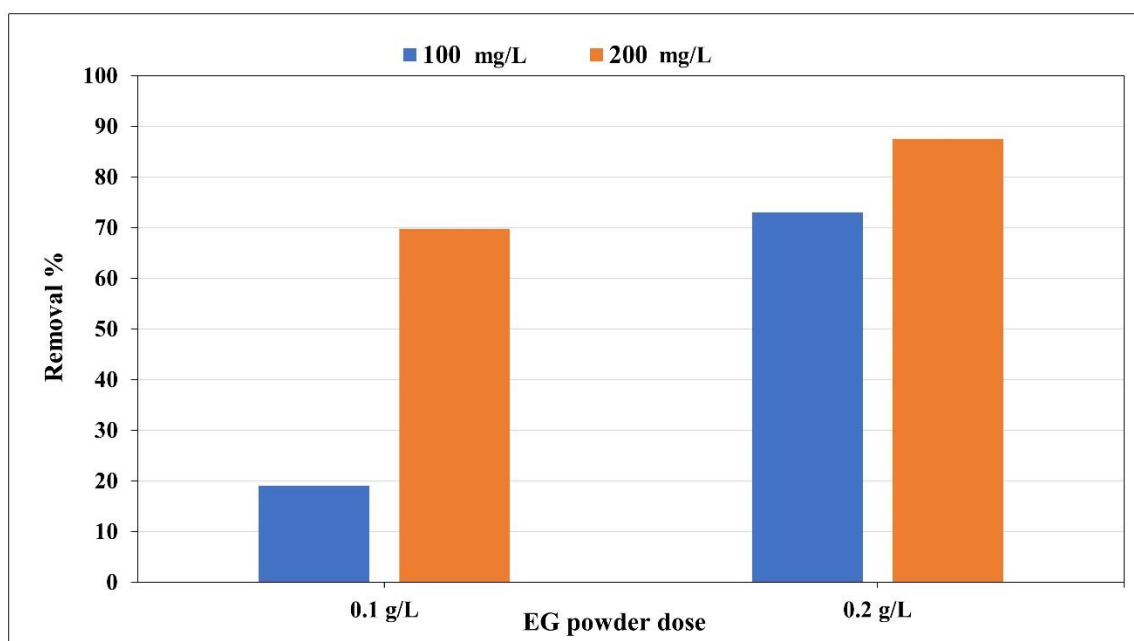


Fig 4.38. The effect of initial concentration on dissolved oil removal

The tendency mentioned above can be attributed to the adsorption capability of EG. At higher quantities of oil, a greater percentage of crude oil molecules can engage with the adsorption

sites present on the worm-like structure of EG. As a consequence, a larger amount of oil is adsorbed, leading to an increased level of removal efficiency.

4.4.1.2 The Impact of Varying Dosages of EG Powder:

The second variable examined in this chapter related to the amount of EG introduced into the crude oil solution. Three different dosages, namely 0.1 g L^{-1} , 0.2 g L^{-1} , and 0.4 g L^{-1} , were used in order to evaluate their impact on the adsorption process.

The findings exhibited a distinct correlation that was depending on the dosage. The degree of crude oil elimination indicated an upward trend with increasing doses of EG. The removal effectiveness at 100 mg L^{-1} of dissolved oil at the lowest dosage of 0.1 g L^{-1} was shown to be around 19%, which exhibited an improvement to almost 73% at the intermediate dose of 0.2 g L^{-1} . The elimination efficiency reached its peak, surpassing around 93%, when the dosage was increased to 0.4 g L^{-1} . Besides, the removal efficiency at 200 mg L^{-1} of dissolved oil increased from 70% to around 88% for 0.1 and 0.2 g L^{-1} of adsorbent (Fig 4.39).

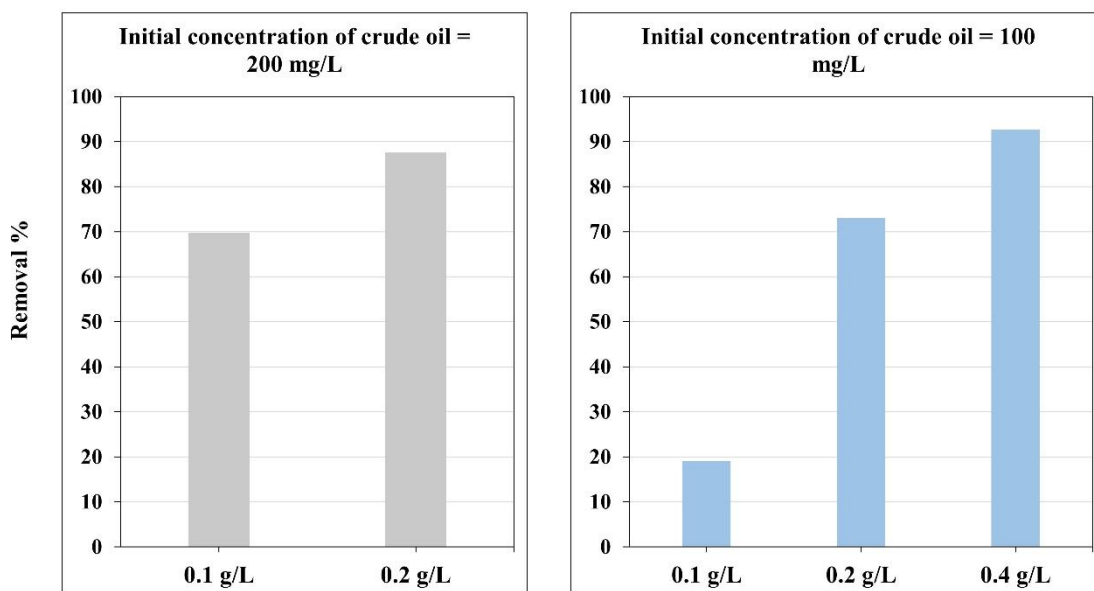


Fig 4.39. Effect of adsorbent dose on dissolved oil removal

The dose-dependent behavior noted in this section can be attributed to the presence of adsorption sites on the surface of EG powder material. With an increase in dosage, a greater number of

adsorption sites become accessible for the attachment of crude oil molecules, leading to enhanced removal efficiency. The increased surface area resulting from adding extra graphite powder added an elevated adsorption capability. Table 4.14 shows the values of removal efficiency. Besides, Fig 4.40 and 4.41 depicted the before adsorption and after-adsorption of 200 mg L⁻¹ solution of dissolved oil in the presence of 0.1 and 0.2 (g L⁻¹) of EG powder.

Table 4.14. Removal efficiency of experimental design for dissolved oil

Absorbent dose (g L ⁻¹)	Initial oil concentration (mg L ⁻¹)	Final concentration (mg L ⁻¹)	Removal %
0.1	100	80.95	19.05
0.2	100	26.98	73.02
0.4	100	7.37	92.63
0.1	200	60.45	69.775
0.2	200	24.93	87.535

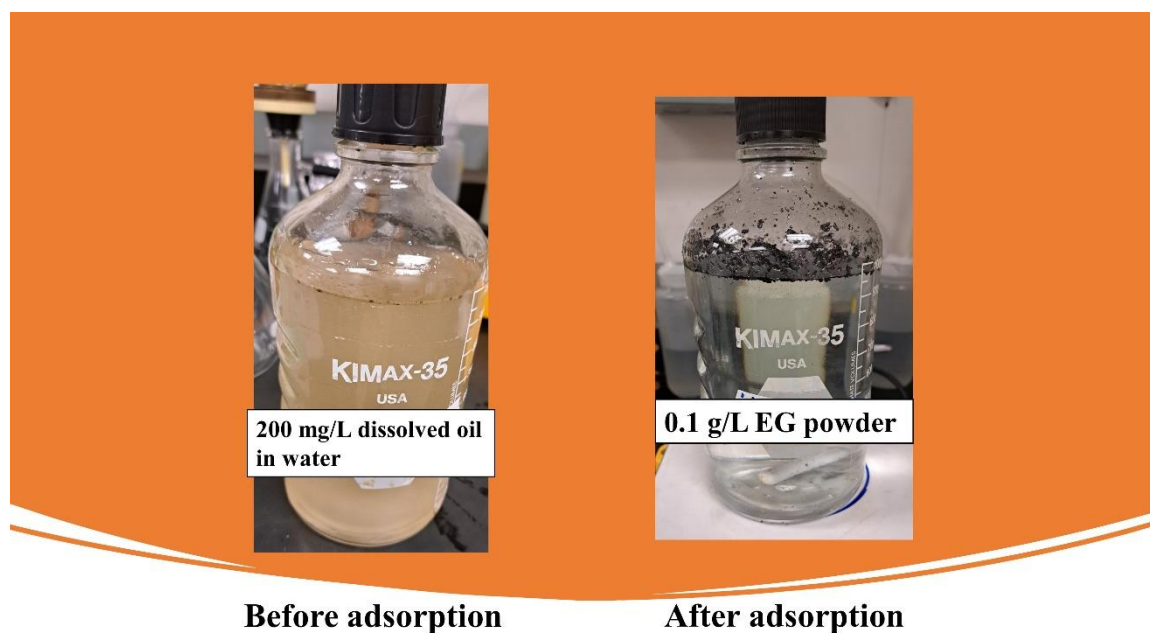


Fig 4.40. Adsorption illustration of EG powder (0.1 g L^{-1}) for 200 mg L^{-1} dissolved oil in water solution

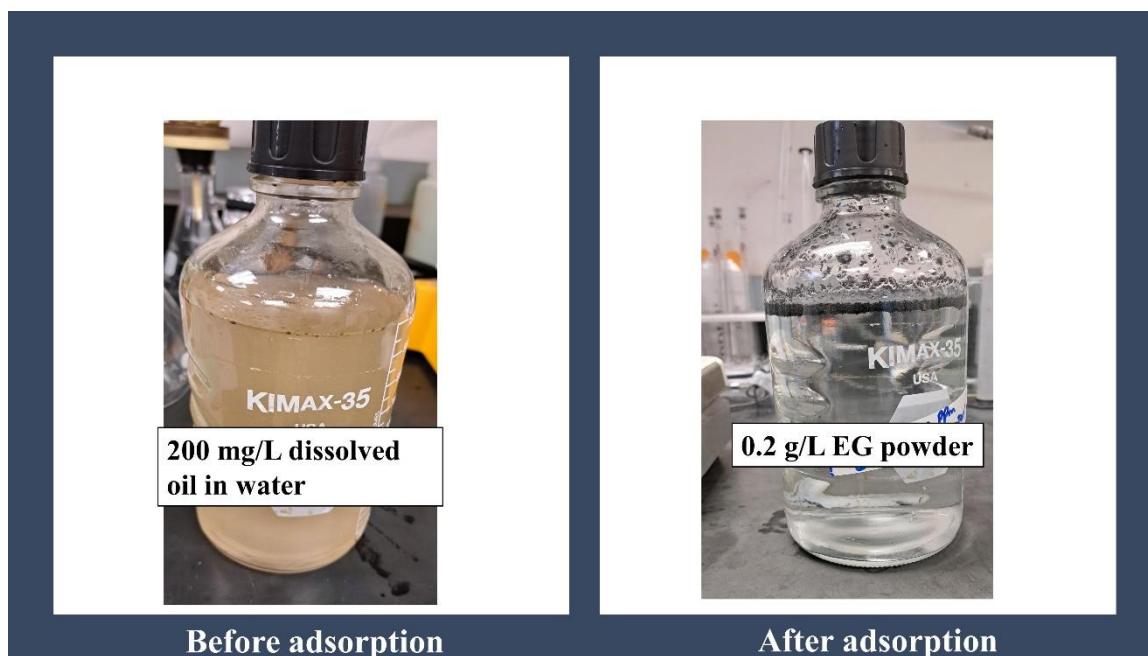


Fig. 4.41. Adsorption illustration of EG powder (0.2 g L^{-1}) for 200 mg L^{-1} dissolved oil in water solution

4.4.1.3 The Mechanism of Adsorption

The adsorption of crude oil on EG is dependent on a combination of physical and chemical interactions. The porous nature of EG powder facilitates the physical adsorption of crude oil molecules by offering places where they may be held through van der Waals forces. Furthermore, the inherent hydrophobicity of EG, together with the hydrophobic constituents present in crude oil, improves the process of adsorption via hydrophobic interactions (Fig 4.42). Furthermore, MW-EG (granular form) showed only 67 % removal of dissolved oil, where a 100 mg L^{-1} solution of dissolved oil was subjected to continuous stirring for 15 h, and the final concentration reached 32.3 mg L^{-1} ; the reason for this can be that granular form of EG is more hydrophilic which prevents the fast reaction with oil molecules as well as with a tendency for water adsorption instead of oil molecules.

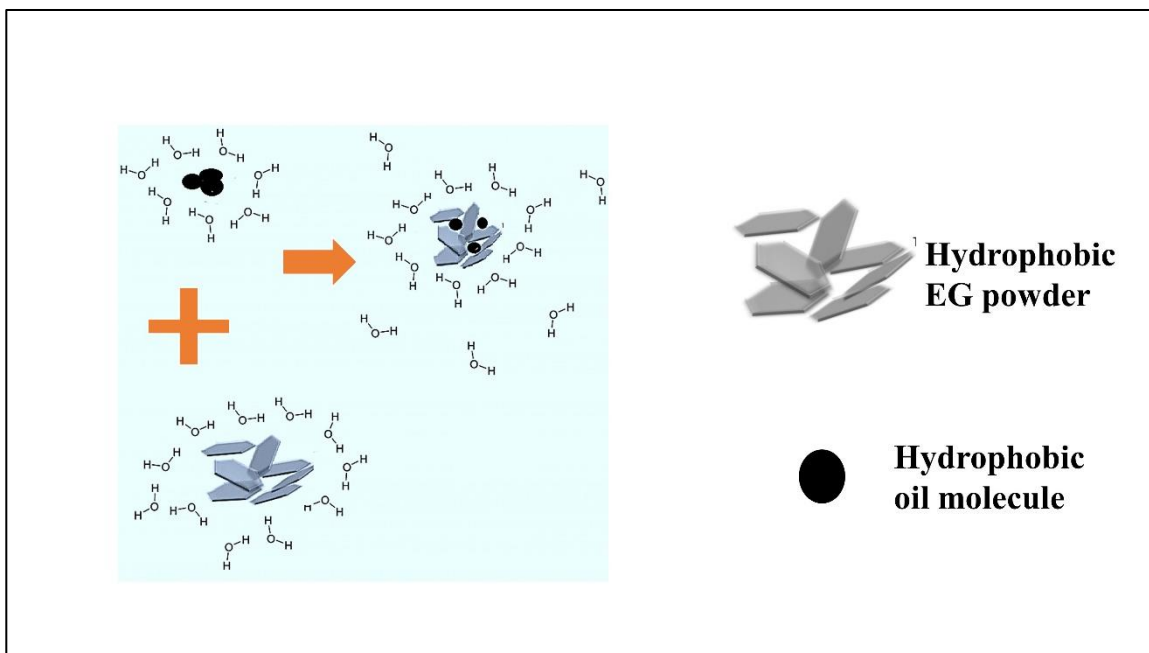


Fig 4.42. Hydrophobic interaction mechanism between oil and EG powder molecules

In summary, the findings of this section indicate that the elimination of dissolved crude oil via the use of EG powder is dependent upon both the initial concentration of oil and the dosage of EG applied. The experimental results indicated that increasing the starting oil concentrations and increasing the dosages of EG led to improved removal efficiency. The process of adsorption encompasses a synergistic interaction between physical and chemical phenomena. The results mentioned above provide significant insights into the possible use of EG powder to tackle the issue of oil contamination in aqueous solutions and PW oily hydrocarbons. Additional investigation can be conducted to examine the optimization technique and practical implementations of this adsorption process.

4.4.2 Adsorption of oil (floating) on the water surface by using powder EG

The first variable investigated in this section was the quantity of floating crude oil present on the water's surface. The study examined the impact of several oil quantities (1 g, 2 g, 4 g, and 6 g) on the adsorption capacity (q) of EG. Fig 4.43 shows the experiment plot of this section.

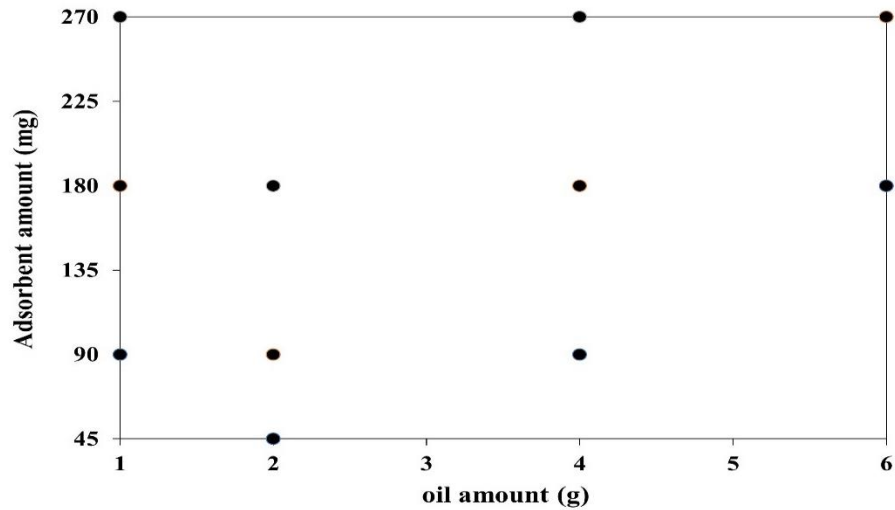


Fig 4.43. Experimental design of floating oil removal by EG powder

The experiment's one-factor effect suggests a clear correlation between the quantity of oil and the adsorption capacity of EG (Fig. 4.44). The increase in the oil amount resulted in a corresponding rise in the adsorption capacity. For example, the adsorption capacity exhibited an initial value of roughly 3.67 g g^{-1} when the oil quantity was at its minimum of 1 g and EG powder at 270 mg. Subsequently, when the starting oil amount went up to 6 g, the adsorption capacity steadily rose to around 22.18 g g^{-1} at the same level as EG powder (270 mg).

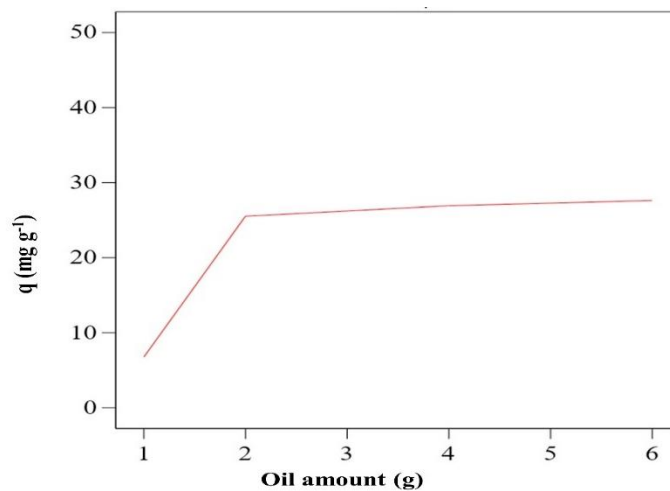


Fig 4.44. The effect of oil amount increases on adsorption capacity (q)

The obtained results can be explained by the presence of crude oil molecules that can undergo adsorption on the surface of EG powder. An increase in the initial quantity of oil results in a larger concentration of oil molecules, thus enhancing the likelihood of interactions occurring with the EG powder. Consequently, an increased amount of oil is adsorbed per unit mass of EG, resulting in an elevated adsorption capacity.

The second variable investigated in this part was the quantity of EG powder placed into the floating crude oil. The effect of four different amounts of EG, 45, 90, 180, and 270 mg, was examined to evaluate their influence on the adsorption process.

The study results indicate a reverse trend between the amount of EG and the adsorption capacity (q) of crude oil. The increase in the quantity of EG resulted in a decrease in adsorption capacity unit g g^{-1} (Fig 4.45). In particular, the adsorption capacity exhibited a value of around 43.87 g g^{-1} when the amount was set at the level of 90 mg for 4 g of oil. This capacity then gradually decreased, reaching a value of almost 14.72 g g^{-1} when the amount was raised to 270 mg of EG at the same level of oil on the water surface.

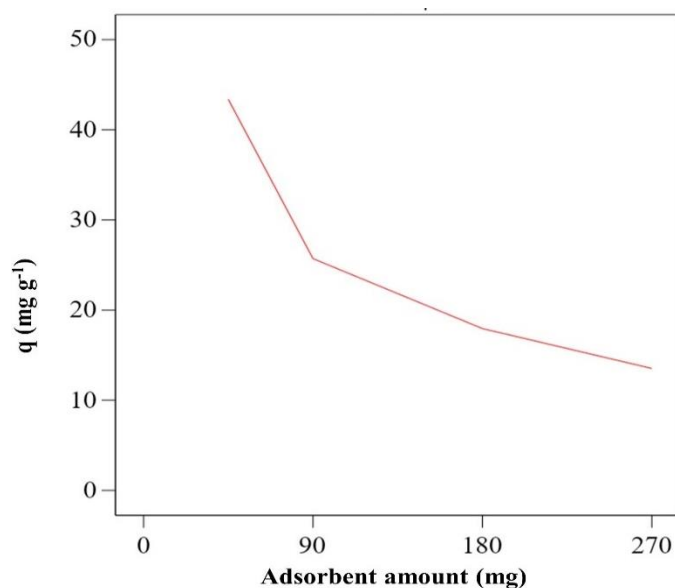


Fig 4.45. One-factor effect of EG powder amount on adsorption capacity (q)

Furthermore, Fig 4.46 shows the 2-factor interaction effects on EG powder adsorption capacity. The experiment figures (4.47-4.49) are also provided.

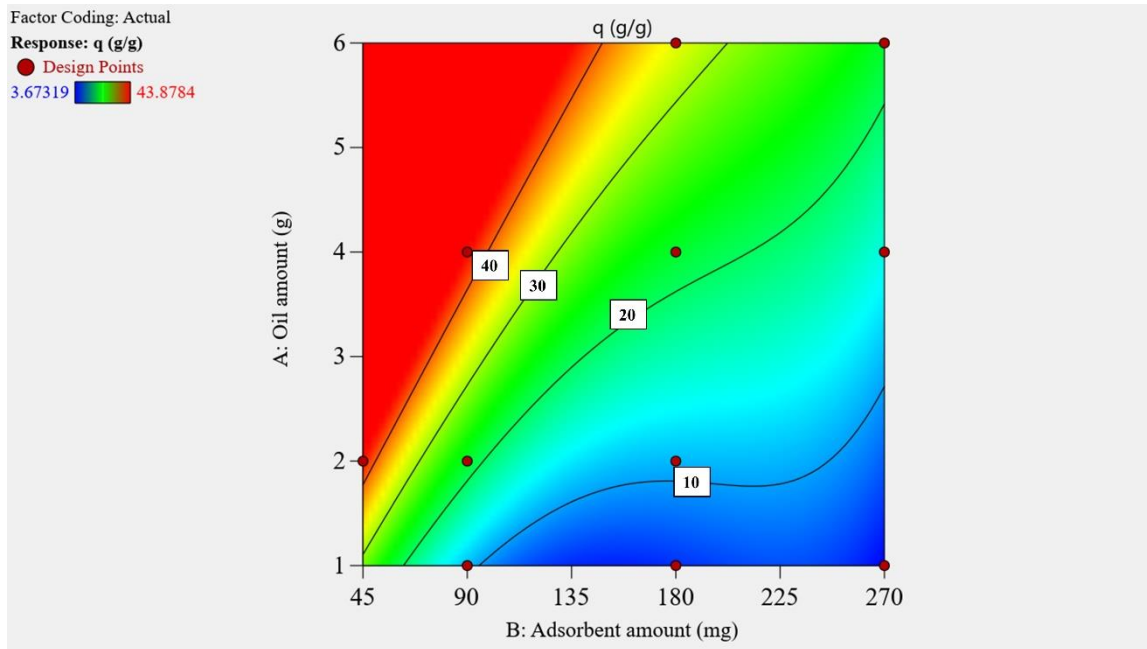
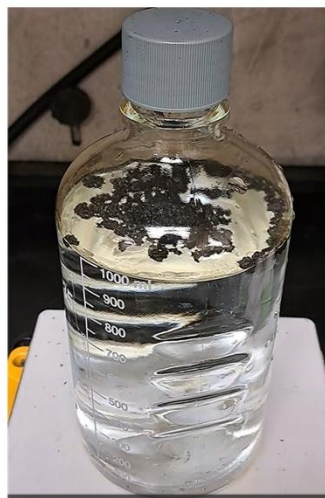
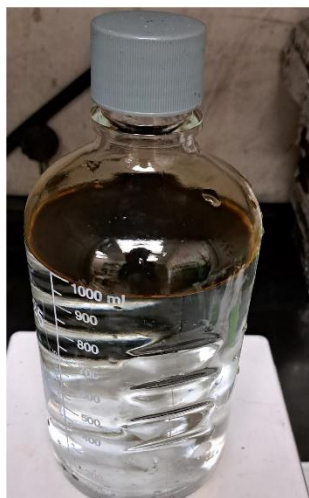


Fig 4.46. Interaction between oil amount and EG powder quantities effects on adsorption capacity (q)



- 6 g of oil on water
- 270 mg EG powder
- $q = 22.1$ g oil/ g EG powder

Fig 4.47. Floating oil removal experiment by EG powder (6 g oil, 270 mg EG)

- 4 g of oil on water
- 90 mg EG powder
- $q = 43.8$ g oil/ g EG powder



Fig 4.48. Floating oil removal experiment by EG powder (4 g oil, 90 mg EG)



- 6 g of oil on water
- 180 mg EG powder
- $q = 33$ g oil/ g EG powder

Fig 4.49. Floating oil removal experiment by EG powder (6 g oil, 180 mg EG)

The process of adsorption for the purpose of eliminating floating crude oil via the use of EG primarily entails physical interactions and hydrophobic forces, as mentioned previously above. The EG powder exhibits a porous configuration that facilitates the presence of physical adsorption sites, enabling the capture and retention of oil droplets.

In addition, the tendency of EG to repel water molecules and the presence of hydrophobic constituents in crude oil facilitate the process of adsorption via hydrophobic interactions, which is discussed above. Aggregating hydrophobic areas of oil molecules around EG particles leads to an effective increase in the adsorption capacity of EG powder.

4.4.3 Column study

The results of column 1 suggested that a 50 mL influent of dissolved oil (100 mg L⁻¹ initial concentration) can be treated to a lower effluent concentration around 5 mg L⁻¹ after 4-5 hours of continuous process (Fig 4.50). Furthermore, a second 50 mL influent was fed to column one to see the possibility of column clogging; the results showed that the column was able to have the same removal efficiency of around 95 % for this sample as well.

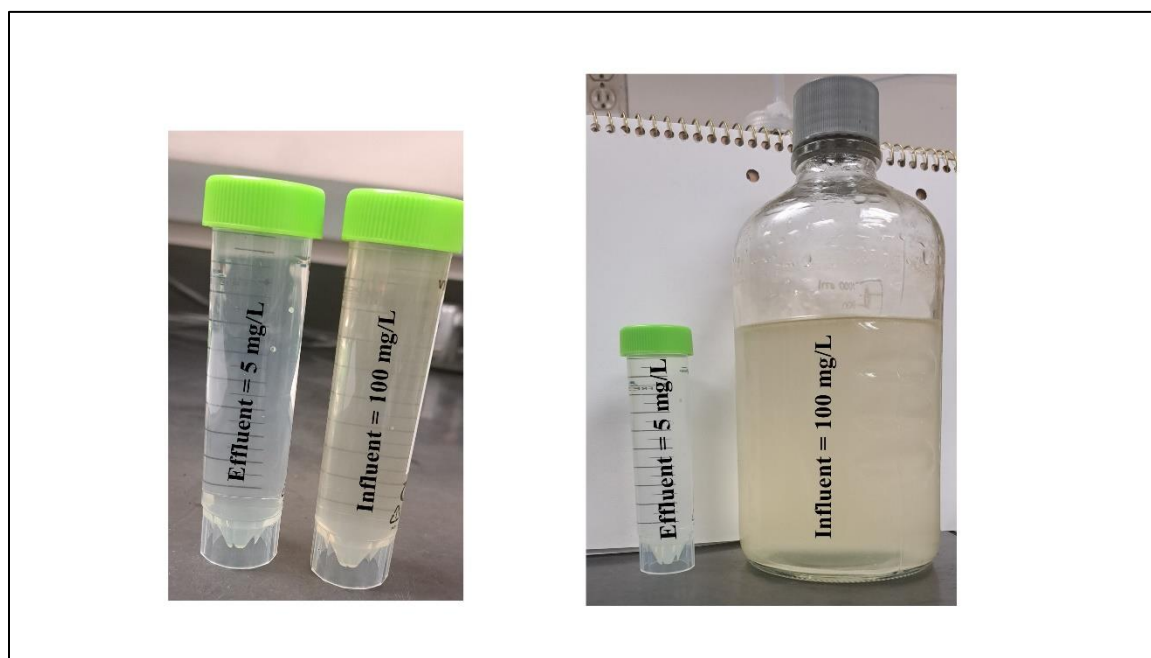


Fig 4.50. Performance of packed column 1 with EG powder

Column 2 showed the faster process of adsorption; since the density of packed EG powder was lower (half the density of column 1), the flow rate was higher and faster. The flow rate diagram is

presented during the experiment in Fig 4.51. The flow rate was faster at the beginning of adsorption (around 4-6 mL/min), then it dropped below 4 mL/min after 80 mins. The reason can be that by the time more oil molecules are adsorbed in the upper layers of EG, it hinders the flow of influent to reach the bottom part of the column, and consequently, a reduction of flow rate happens. Then, the flow rate fluctuated around 3 minutes for the rest of the adsorption time.

The effluent was collected at the end of each time interval; 21 samples were collected, and concentration was measured accordingly. The result of crude oil concentration in column 2 is provided in Fig 4.52. it is apparent that by using column 2, effluent concentration dropped to approximately 5 mg L⁻¹ for all samples taken periodically (Fig 4.53). This result shows the efficient removal of dissolved crude oil by column setup; the removal efficiency is provided in Fig 4.54.

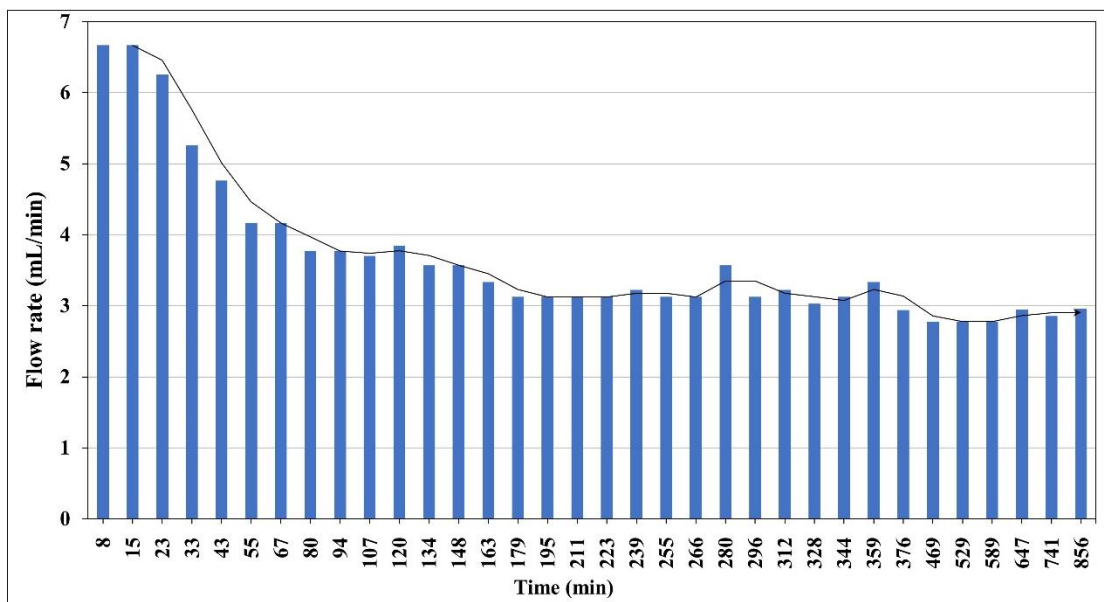


Fig 4.51. Flow rate chart for the column 2 adsorption

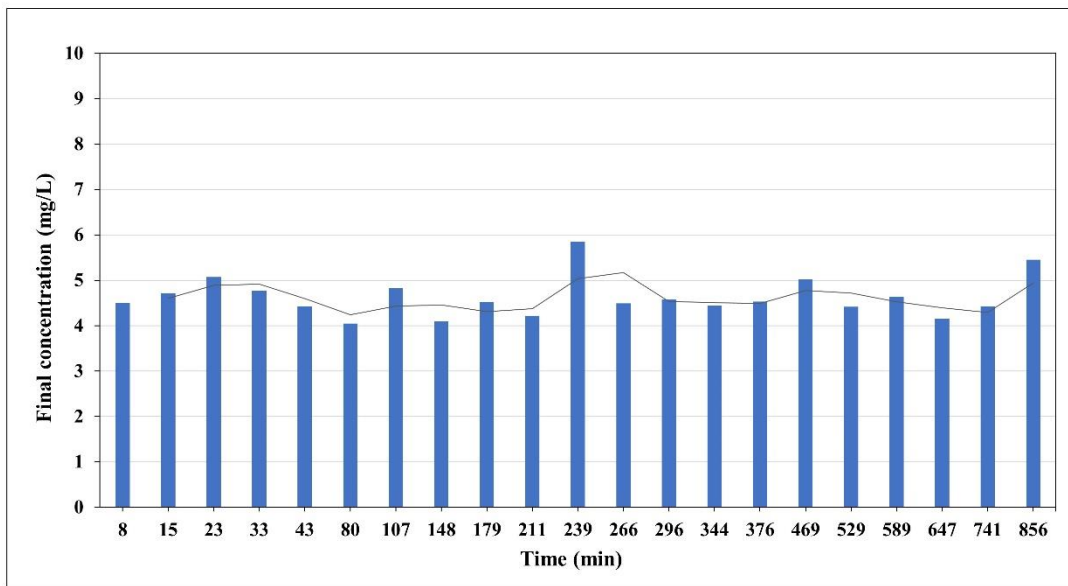


Fig 4.52. The final concentration of collected samples by using column 2 (initial concentration 100 mg L⁻¹)

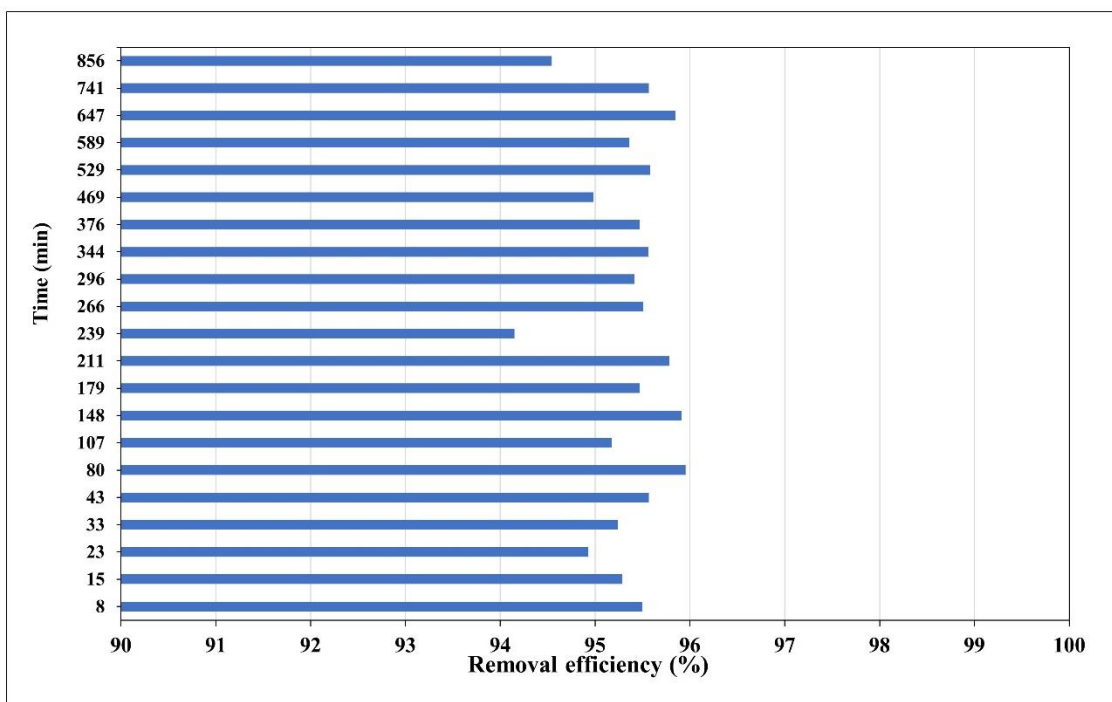


Fig 4.53. The removal efficiency of dissolved crude oil adsorption in fixed bed column 2

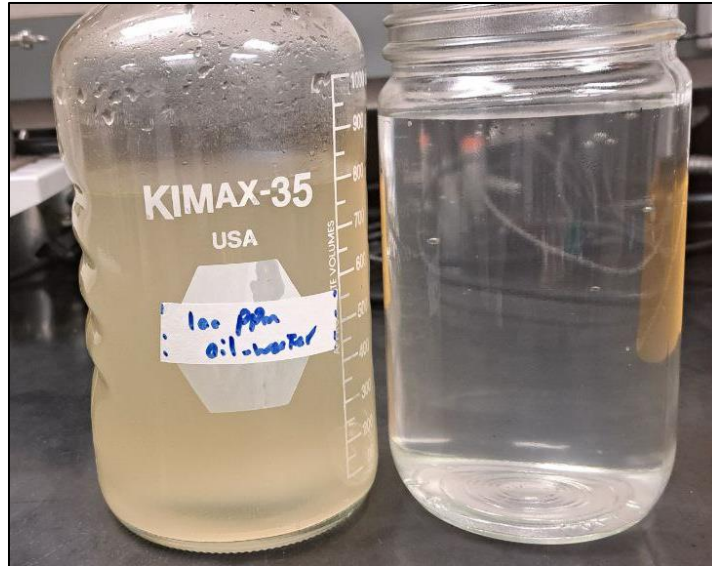


Fig 4.54. Before and after adsorption of dissolved crude oil by column 2 (initial concentration 100 mg L^{-1})

In summary, the findings of this investigation indicate that the adsorption capacity (q) for the removal of floating crude oil from water surfaces via the use of EG is subject to the effect of both the initial amount of oil and the amount of adsorbent introduced. The increase in starting oil quantities and the application of lower dosages of EG result in an improvement in adsorption capacity values in units of g oil/g of EG. Hydrophobic interactions govern the process of adsorption.

4.4.4 Conclusion of oil removal

- Elimination of dissolved crude oil using EG powder with batch mode relies on initial oil concentration and EG dosage.
- Increasing starting oil concentrations and EG doses demonstrated enhanced removal efficiency, indicating a synergistic interaction between physical and chemical phenomena in the adsorption process.
- By adding 0.4 g L^{-1} of EG powder, the removal efficiency was around 93% in batch experiments (the initial concentration of crude oil was 100 mg L^{-1}).
- Column studies proved that the less dense column is efficient for faster and higher crude oil adsorption (column 2).

- With a continuous column adsorption test (14 h), the concentration of the effluent for periodic measurements was around 5 mg L^{-1} , showing a 95 % of crude oil removal (initial concentration 100 mg L^{-1} , the volume of oil in water solution 2.7 liters, flowrate 2.7-6.6 mL/min).
- These findings offer valuable insights into EG powder's potential for addressing oil contamination in aqueous solutions and PW oily hydrocarbons.
- Further research is recommended to explore optimization techniques and practical applications for the adsorption process.

5. Overall conclusion

The extensive exploration conducted in this study regarding MW-EG's potential as an adsorbent, particularly in dye wastewater adsorption, offers compelling insights into its efficacy and applicability. The exceptional performance exhibited in lab-scale scenarios and surface water media highlights its viability as an option for efficient adsorbent. Achieving a remarkable 96% removal efficiency of MB from surface water in less than 20 minutes firmly establishes MW-EG's effectiveness.

The integration of Response Surface Methodology (RSM) has proven its applicability, facilitating experimental optimization, tackling challenges, and ensuring a more precise determination of experimental conditions. This methodology minimizes the number of runs required, expediting the optimization process significantly.

The utilization of MW irradiation in MW-EG preparation emerges as a crucial factor, effectively eliminating impurities from pores and enhancing the adsorption process. The distinct pore structure revealed through BET surface analysis further emphasizes the significance of understanding pore distribution, even as the surface area experiences a reduction in the granular form.

Notably, the regeneration studies' outcomes highlight the potential of MW irradiation, offering ten consecutive cycles with low energy consumption, swift processes, and negligible material losses, outperforming conventional regeneration methods.

Real sample assessments from lake surface water affirm MW-EG's adaptability in treating polluted media, even in the presence of natural organic matter and inorganic compounds, substantiating its practical utility beyond controlled laboratory conditions.

The study illuminates the mechanisms underlying the adsorption process, particularly in eliminating floating crude oil. The porous configuration of EG facilitates physical adsorption, leveraging hydrophobic forces and interactions to capture and retain oil droplets effectively. The hydrophobic nature of EG, coupled with its ability to repel water molecules, highlights its effectiveness in adsorbing oil via hydrophobic interactions.

Column studies reinforce the efficiency of EG, showing its ability to consistently treat influents of dissolved oil, demonstrating promising results in lowering effluent concentrations to around 5 mg L⁻¹ after continuous processing.

However, it is worth noting that the effectiveness of MW-EG in granular form for dissolved oil removal exhibits some challenges, notably a longer removal time, potentially attributed to its increased hydrophilicity.

In summary, this investigation demonstrates that the adsorption capacity of EG for crude oil removal hinges on various factors, including initial oil quantity and adsorbent dosage. The intricate balance between these variables significantly impacts the adsorption process governed by hydrophobic interactions.

These findings not only highlight the promising potential of EG in addressing oil contamination in aqueous solutions but also highlight the need for further research to optimize techniques and ascertain practical applications for the adsorption process. The synergistic interplay between physical and chemical phenomena in enhancing removal efficiency warrants deeper exploration for broader environmental implications and practical implementation.

Future work and suggestions

- It would be a viable option to test different configurations of column studies, such as the Rapid Small Scale column test (RSSCT), for further oily content removal. This test can broaden the knowledge for real case oil removal.
- Further, a study on the pilot scale of EG powder as a filter for post-treatment of produced water can be another viable option.
- Different types of EG material, such as magnetic EG and hydro-soluble EG, can further be studied for the removal of different organic pollutants.

Chapter 4 References

- Allouss, D., Essamlali, Y., Amadine, O., Chakir, A., & Zahouily, M. (2019). Response surface methodology for optimization of methylene blue adsorption onto carboxymethyl cellulose-based hydrogel beads: Adsorption kinetics, isotherm, thermodynamics and reusability studies. *RSC Advances*, 9(65), 37858–37869. <https://doi.org/10.1039/C9RA06450H>
- Avetta, P., Sangermano, M., Lopez-Manchado, M., & Calza, P. (2015). Use of graphite oxide and/or thermally reduced graphite oxide for the removal of dyes from water. *Journal of Photochemistry and Photobiology A: Chemistry*, 312, 88–95. <https://doi.org/10.1016/j.jphotochem.2015.07.015>
- Bayat, A., S.f, A., & A, M. (2008). *OIL SORPTION BY SYNTHESIZED EXFOLIATED GRAPHITE (EG)* (1). 5(1), Article 1.
- Caniani, D., Calace, S., Mazzone, G., Caivano, M., Mancini, I. M., Greco, M., & Masi, S. (2018). Removal of Hydrocarbons from Contaminated Soils by Using a Thermally Expanded Graphite Sorbent. *Bulletin of Environmental Contamination and Toxicology*, 101(6), Article 6. <https://doi.org/10.1007/s00128-018-2395-4>
- Carvallho, M. N., da Silva, K. S., Sales, D. C. S., Freire, E. M. P. L., Sobrinho, M. A. M., & Ghislandi, M. G. (2016). Dye removal from textile industrial effluents by adsorption on exfoliated graphite nanoplatelets: Kinetic and equilibrium studies. *Water Science and Technology*, 73(9), Article 9. <https://doi.org/10.2166/wst.2016.073>
- Cuccarese, M., Brutti, S., De Bonis, A., Teghil, R., Mancini, I. M., Masi, S., & Caniani, D. (2021). Removal of diclofenac from aqueous solutions by adsorption on thermo-plasma expanded graphite. *Scientific Reports*, 11(1), Article 1. <https://doi.org/10.1038/s41598-021-83117-z>
- Ding, X., Wang, R., Zhang, X., Zhang, Y., Deng, S., Shen, F., Zhang, X., Xiao, H., & Wang, L. (2014a). A new magnetic expanded graphite for removal of oil leakage. *Marine Pollution Bulletin*, 81(1), Article 1. <https://doi.org/10.1016/j.marpolbul.2014.01.056>
- Ding, X., Wang, R., Zhang, X., Zhang, Y., Deng, S., Shen, F., Zhang, X., Xiao, H., & Wang, L. (2014b). A new magnetic expanded graphite for removal of oil leakage. *Marine Pollution Bulletin*, 81(1), Article 1. <https://doi.org/10.1016/j.marpolbul.2014.01.056>
- Fan, Z., Yan, J., Ning, G., Wei, T., Qian, W., Zhang, S., Zheng, C., Zhang, Q., & Wei, F. (2010). Oil sorption and recovery by using vertically aligned carbon nanotubes. *Carbon*, 48(14), 4197–4200. <https://doi.org/10.1016/j.carbon.2010.07.001>
- Gagliano, E., Falciglia, P. P., Zaker, Y., Karanfil, T., & Roccaro, P. (2021). Microwave regeneration of granular activated carbon saturated with PFAS. *Water Research*, 198, 117121. <https://doi.org/10.1016/j.watres.2021.117121>
- Hoang, N. B., Nguyen, T. T., Nguyen, T. S., Bui, T. P. Q., & Bach, L. G. (2019a). The application of expanded graphite fabricated by microwave method to eliminate organic dyes in aqueous solution. *Cogent Engineering*, 6(1), Article 1. <https://doi.org/10.1080/23311916.2019.1584939>

- Hoang, N. B., Nguyen, T. T., Nguyen, T. S., Bui, T. P. Q., & Bach, L. G. (2019b). The application of expanded graphite fabricated by microwave method to eliminate organic dyes in aqueous solution. *Cogent Engineering*, 6(1), 1584939. <https://doi.org/10.1080/23311916.2019.1584939>
- Hristea, G., & Budrugaac, P. (2008). Characterization of exfoliated graphite for heavy oil sorption. *Journal of Thermal Analysis and Calorimetry*, 91(3), Article 3. <https://doi.org/10.1007/s10973-006-7465-x>
- Inagaki, M., Konno, H., Toyoda, M., Moriya, K., & Kihara, T. (2000). Sorption and recovery of heavy oils by using exfoliated graphite Part II: Recovery of heavy oil and recycling of exfoliated graphite. *Desalination*, 128(3), Article 3. [https://doi.org/10.1016/S0011-9164\(00\)00035-7](https://doi.org/10.1016/S0011-9164(00)00035-7)
- Inagaki, M., Shibata, K., Setou, S., Toyoda, M., & Aizawa, J. (2000). Sorption and recovery of heavy oils by using exfoliated graphite Part III: Trials for practical applications. *Desalination*, 128(3), Article 3. [https://doi.org/10.1016/S0011-9164\(00\)00036-9](https://doi.org/10.1016/S0011-9164(00)00036-9)
- Inagaki, M., Toyoda, M., Iwashita, N., Nishi, Y., & Konno, H. (2001). Exfoliated Graphite for Spilled Heavy Oil Recovery. *Carbon Letters*, 2(1), Article 1.
- Inagaki, M., Toyoda, M., Iwashita, N., Nishi, Y., Konno, H., Fujita, A., & Kihara, T. (2002). Sorption, Recovery and Recycle of Spilled Heavy Oils Using Carbon Materials. *Tanso*, 2002(201), 16–25. <https://doi.org/10.7209/tanso.2002.16>
- Li, M., Li, J.-T., & Sun, H.-W. (2008). Decolorizing of azo dye Reactive red 24 aqueous solution using exfoliated graphite and H₂O₂ under ultrasound irradiation. *Ultrasonics Sonochemistry*, 15(5), 717–723. <https://doi.org/10.1016/j.ultsonch.2007.10.001>
- Li, Y., Du, Q., Liu, T., Sun, J., Wang, Y., Wu, S., Wang, Z., Xia, Y., & Xia, L. (2013). Methylene blue adsorption on graphene oxide/calcium alginate composites. *Carbohydrate Polymers*, 95(1), 501–507. <https://doi.org/10.1016/j.carbpol.2013.01.094>
- Linh, H. X., Thu, N. T., Toan, T. Q., Huong, D. T., Giang, B. T., Ha, H. K. P., Nguyen, H.-T. T., Chung, N. T. K., Nguyen, T. K., & Hai, N. T. (2019, July 1). *Fast and Effective Route for Removing Methylene Blue from Aqueous Solution by Using Red Mud-Activated Graphite Composites* [Research Article]. *Journal of Chemistry*; Hindawi. <https://doi.org/10.1155/2019/2858170>
- Medjahdi, M., Benderdouche, N., Bestani, B., Duclaux, L., & Reinert, L. (2016). Modeling of the sorption of crude oil on a polyurethane foam-powdered activated carbon composite. *Desalination and Water Treatment*, 57(47), 22311–22320. <https://doi.org/10.1080/19443994.2015.1129511>
- Ordinioha, B., & Brisibe, S. (2013). The human health implications of crude oil spills in the Niger delta, Nigeria: An interpretation of published studies. *Nigerian Medical Journal*, 54(1), 10. <https://doi.org/10.4103/0300-1652.108887>
- Pang, X. Y., Ren, S. X., Di, X., & Sun, S. Y. (2014). Study on the Competitive Adsorption Performence of Direct Deep Blue and Methyl Orange on Expanded Graphite Adsorbent. *Research & Reviews: Journal of Ecology and Environmental Sciences*, 2(1), Article 1.

- Pathania, D., Sharma, S., & Singh, P. (2017). Removal of Methylene blue by adsorption onto activated carbon developed from *Ficus carica* bast. *Arabian Journal of Chemistry*, *10*, S1445–S1451. <https://doi.org/10.1016/j.arabjc.2013.04.021>
- Taherian, R. (2019). 7 - Application of Polymer-Based Composites: Bipolar Plate of PEM Fuel Cells. In R. Taherian & A. Kausar (Eds.), *Electrical Conductivity in Polymer-Based Composites* (pp. 183–237). William Andrew Publishing. <https://doi.org/10.1016/B978-0-12-812541-0.00007-0>
- Takeuchi, K., Fujishige, M., Kitazawa, H., Akuzawa, N., Medina, J. O., Morelos-Gomez, A., Cruz-Silva, R., Araki, T., Hayashi, T., Terrones, M., & Endo, M. (2015). Oil sorption by exfoliated graphite from dilute oil–water emulsion for practical applications in produced water treatments. *Journal of Water Process Engineering*, *8*, 91–98. <https://doi.org/10.1016/j.jwpe.2015.09.002>
- Takeuchi, K., Kitazawa, H., Fujishige, M., Akuzawa, N., Ortiz-Medina, J., Morelos-Gomez, A., Cruz-Silva, R., Araki, T., Hayashi, T., & Endo, M. (2017). Oil removing properties of exfoliated graphite in actual produced water treatment. *Journal of Water Process Engineering*, *20*, 226–231. <https://doi.org/10.1016/j.jwpe.2017.11.009>
- Tian, Y., Ma, H., & Xing, B. (2021). Preparation of surfactant modified magnetic expanded graphite composites and its adsorption properties for ionic dyes. *Applied Surface Science*, *537*, 147995. <https://doi.org/10.1016/j.apsusc.2020.147995>
- Toyoda, M., Aizawa, J., & Inagaki, M. (1998). Sorption and recovery of heavy oil by using exfoliated graphite. *Desalination*, *115*(2), 199–201. [https://doi.org/10.1016/S0011-9164\(98\)00038-1](https://doi.org/10.1016/S0011-9164(98)00038-1)
- Toyoda, M., & Inagaki, M. (2000). Heavy oil sorption using exfoliated graphite: New application of exfoliated graphite to protect heavy oil pollution. *Carbon*, *38*(2), 199–210. [https://doi.org/10.1016/S0008-6223\(99\)00174-8](https://doi.org/10.1016/S0008-6223(99)00174-8)
- Toyoda, M., & Inagaki, M. (2003). Sorption and Recovery of Heavy Oils by Using Exfoliated Graphite. *Spill Science & Technology Bulletin*, *8*(5), 467–474. [https://doi.org/10.1016/S1353-2561\(03\)00131-2](https://doi.org/10.1016/S1353-2561(03)00131-2)
- Toyoda, M., Moriya, K., Aizawa, J., Konno, H., & Inagaki, M. (2000). Sorption and recovery of heavy oils by using exfoliated graphite Part I: Maximum sorption capacity. *Desalination*, *128*(3), Article 3. [https://doi.org/10.1016/S0011-9164\(00\)00034-5](https://doi.org/10.1016/S0011-9164(00)00034-5)
- Toyoda, M., Nishi, Y., Iwashita, N., & Inagaki, M. (2003). Sorption and recovery of heavy oils using exfoliated graphite Part IV: Discussion of high oil sorption of exfoliated graphite. *Desalination*, *151*(2), Article 2. [https://doi.org/10.1016/S0011-9164\(02\)00992-X](https://doi.org/10.1016/S0011-9164(02)00992-X)
- Tuan Nguyen, H. D., Nguyen, H. T., Nguyen, T. T., Le Thi, A. K., Nguyen, T. D., Phuong Bui, Q. T., & Bach, L. G. (2019). The Preparation and Characterization of MnFe₂O₄-Decorated Expanded Graphite for Removal of Heavy Oils from Water. *Materials*, *12*(12), Article 12. <https://doi.org/10.3390/ma12121913>
- Wang, B., Karthikeyan, R., Xiaoying, H. L., Xuan, J., & Leung, M. K. H. (2013). Hollow carbon fibers derived from natural cotton as effective sorbents for oil spill cleanup. *Industrial & Engineering Chemistry Research*, *52*(51), 18251–18261. <https://doi.org/10.1021/ie402371n>

- Wang, G., Sun, Q., Zhang, Y., Fan, J., & Ma, L. (2010). Sorption and regeneration of magnetic exfoliated graphite as a new sorbent for oil pollution. *Desalination*, 263(1), Article 1. <https://doi.org/10.1016/j.desal.2010.06.056>
- Wu, K.-H., Huang, W.-C., Hung, W.-C., & Tsai, C.-W. (2021a). Modified expanded graphite/Fe₃O₄ composite as an adsorbent of Methylene blue: Adsorption kinetics and isotherms. *Materials Science and Engineering: B*, 266, 115068. <https://doi.org/10.1016/j.mseb.2021.115068>
- Wu, K.-H., Huang, W.-C., Hung, W.-C., & Tsai, C.-W. (2021b). Modified expanded graphite/Fe₃O₄ composite as an adsorbent of Methylene blue: Adsorption kinetics and isotherms. *Materials Science and Engineering: B*, 266, 115068. <https://doi.org/10.1016/j.mseb.2021.115068>
- Wu, Z.-Y., Li, C., Liang, H.-W., Zhang, Y.-N., Wang, X., Chen, J.-F., & Yu, S.-H. (2014). Carbon nanofiber aerogels for emergent cleanup of oil spillage and chemical leakage under harsh conditions. *Scientific Reports*, 4(1), Article 1. <https://doi.org/10.1038/srep04079>
- Xu, C., Wang, H., Yang, W., Ma, L., & Lin, A. (2018). Expanded Graphite Modified by CTAB-KBr/H₃PO₄ for Highly Efficient Adsorption of Dyes. *Journal of Polymers and the Environment*, 26(3), Article 3. <https://doi.org/10.1007/s10924-017-1019-0>
- Zaker, A., Chen, Z., Wang, X., & Zhang, Q. (2019). Microwave-assisted pyrolysis of sewage sludge: A review. *Fuel Processing Technology*, 187, 84–104. <https://doi.org/10.1016/j.fuproc.2018.12.011>
- Zeng, Y., Wang, K., Yao, J., & Wang, H. (2014). Hollow carbon beads fabricated by phase inversion method for efficient oil sorption. *Carbon*, 69, 25–31. <https://doi.org/10.1016/j.carbon.2013.11.036>
- Zhang, F., Zhao, Q., Yan, X., Li, H., Zhang, P., Wang, L., Zhou, T., Li, Y., & Ding, L. (2016). Rapid preparation of expanded graphite by microwave irradiation for the extraction of triazine herbicides in milk samples. *Food Chemistry*, 197, 943–949. <https://doi.org/10.1016/j.foodchem.2015.11.056>
- Zhao, B., Zhang, L., Liang, Y., Qiu, H., & Yang, J. (2012). Efficient growth of millimeter-long few-walled carbon nanotube forests and their oil sorption. *Applied Physics A*, 108(2), 351–355. <https://doi.org/10.1007/s00339-012-6884-8>
- Zhao, M., & Liu, P. (2009a). Adsorption of methylene blue from aqueous solutions by modified expanded graphite powder. *Desalination*, 249(1), Article 1. <https://doi.org/10.1016/j.desal.2009.01.037>
- Zhao, M., & Liu, P. (2009b). Adsorption of methylene blue from aqueous solutions by modified expanded graphite powder. *Desalination*, 249(1), Article 1. <https://doi.org/10.1016/j.desal.2009.01.037>
- Zheng, Y.-P., Wang, H.-N., Kang, F.-Y., Wang, L.-N., & Inagaki, M. (2004). Sorption capacity of exfoliated graphite for oils-sorption in and among worm-like particles. *Carbon*, 42(12), 2603–2607. <https://doi.org/10.1016/j.carbon.2004.05.041>
- Bayat, A., S.f, A., & A, M. (2008). *OIL SORPTION BY SYNTHESIZED EXFOLIATED GRAPHITE (EG)* (1). 5(1), Article 1.

- Ding, X., Wang, R., Zhang, X., Zhang, Y., Deng, S., Shen, F., Zhang, X., Xiao, H., & Wang, L. (2014). A new magnetic expanded graphite for removal of oil leakage. *Marine Pollution Bulletin*, 81(1), Article 1. <https://doi.org/10.1016/j.marpolbul.2014.01.056>
- Fan, Z., Yan, J., Ning, G., Wei, T., Qian, W., Zhang, S., Zheng, C., Zhang, Q., & Wei, F. (2010). Oil sorption and recovery by using vertically aligned carbon nanotubes. *Carbon*, 48(14), 4197–4200. <https://doi.org/10.1016/j.carbon.2010.07.001>
- Inagaki, M., Konno, H., Toyoda, M., Moriya, K., & Kihara, T. (2000). sorption and recovery of heavy oils by using exfoliated graphite Part II: Recovery of heavy oil and recycling of exfoliated graphite. *Desalination*, 128(3), Article 3. [https://doi.org/10.1016/S0011-9164\(00\)00035-7](https://doi.org/10.1016/S0011-9164(00)00035-7)
- Inagaki, M., Shibata, K., Setou, S., Toyoda, M., & Aizawa, J. (2000). sorption and recovery of heavy oils by using exfoliated graphite Part III: Trials for practical applications. *Desalination*, 128(3), Article 3. [https://doi.org/10.1016/S0011-9164\(00\)00036-9](https://doi.org/10.1016/S0011-9164(00)00036-9)
- Inagaki, M., Toyoda, M., Iwashita, N., Nishi, Y., & Konno, H. (2001). Exfoliated Graphite for Spilled Heavy Oil Recovery. *Carbon Letters*, 2(1), Article 1.
- Inagaki, M., Toyoda, M., Iwashita, N., Nishi, Y., Konno, H., Fujita, A., & Kihara, T. (2002). Sorption, Recovery and Recycle of Spilled Heavy Oils Using Carbon Materials. *Tanso*, 2002(201), 16–25. <https://doi.org/10.7209/tanso.2002.16>
- Medjahdi, M., Benderdouche, N., Bestani, B., Duclaux, L., & Reinert, L. (2016). Modeling of the sorption of crude oil on a polyurethane foam-powdered activated carbon composite. *Desalination and Water Treatment*, 57(47), 22311–22320. <https://doi.org/10.1080/19443994.2015.1129511>
- Ordinoha, B., & Brisibe, S. (2013). The human health implications of crude oil spills in the Niger delta, Nigeria: An interpretation of published studies. *Nigerian Medical Journal*, 54(1), 10. <https://doi.org/10.4103/0300-1652.108887>
- Takeuchi, K., Fujishige, M., Kitazawa, H., Akuzawa, N., Medina, J. O., Morelos-Gomez, A., Cruz-Silva, R., Araki, T., Hayashi, T., Terrones, M., & Endo, M. (2015). Oil sorption by exfoliated graphite from dilute oil–water emulsion for practical applications in produced water treatments. *Journal of Water Process Engineering*, 8, 91–98. <https://doi.org/10.1016/j.jwpe.2015.09.002>
- Takeuchi, K., Kitazawa, H., Fujishige, M., Akuzawa, N., Ortiz-Medina, J., Morelos-Gomez, A., Cruz-Silva, R., Araki, T., Hayashi, T., & Endo, M. (2017). Oil removing properties of exfoliated graphite in actual produced water treatment. *Journal of Water Process Engineering*, 20, 226–231. <https://doi.org/10.1016/j.jwpe.2017.11.009>
- Toyoda, M., Aizawa, J., & Inagaki, M. (1998). Sorption and recovery of heavy oil by using exfoliated graphite. *Desalination*, 115(2), 199–201. [https://doi.org/10.1016/S0011-9164\(98\)00038-1](https://doi.org/10.1016/S0011-9164(98)00038-1)
- Toyoda, M., & Inagaki, M. (2000). Heavy oil sorption using exfoliated graphite: New application of exfoliated graphite to protect heavy oil pollution. *Carbon*, 38(2), 199–210. [https://doi.org/10.1016/S0008-6223\(99\)00174-8](https://doi.org/10.1016/S0008-6223(99)00174-8)
- Toyoda, M., & Inagaki, M. (2003). Sorption and Recovery of Heavy Oils by Using Exfoliated Graphite. *Spill Science & Technology Bulletin*, 8(5), 467–474. [https://doi.org/10.1016/S1353-2561\(03\)00131-2](https://doi.org/10.1016/S1353-2561(03)00131-2)

Toyoda, M., Moriya, K., Aizawa, J., Konno, H., & Inagaki, M. (2000). sorption and recovery of heavy oils by using exfoliated graphite Part I: Maximum sorption capacity. *Desalination*, *128*(3), Article 3. [https://doi.org/10.1016/S0011-9164\(00\)00034-5](https://doi.org/10.1016/S0011-9164(00)00034-5)

Toyoda, M., Nishi, Y., Iwashita, N., & Inagaki, M. (2003). Sorption and recovery of heavy oils using exfoliated graphite Part IV: Discussion of high oil sorption of exfoliated graphite. *Desalination*, *151*(2), Article 2. [https://doi.org/10.1016/S0011-9164\(02\)00992-X](https://doi.org/10.1016/S0011-9164(02)00992-X)

Tuan Nguyen, H. D., Nguyen, H. T., Nguyen, T. T., Le Thi, A. K., Nguyen, T. D., Phuong Bui, Q. T., & Bach, L. G. (2019). The Preparation and Characterization of MnFe₂O₄-Decorated Expanded Graphite for Removal of Heavy Oils from Water. *Materials*, *12*(12), Article 12. <https://doi.org/10.3390/ma12121913>

Wang, B., Karthikeyan, R., Xiaoying, H. L., Xuan, J., & Leung, M. K. H. (2013). Hollow carbon fibers derived from natural cotton as effective sorbents for oil spill cleanup. *Industrial & Engineering Chemistry Research*, *52*(51), 18251–18261. <https://doi.org/10.1021/ie402371n>

Wang, G., Sun, Q., Zhang, Y., Fan, J., & Ma, L. (2010). Sorption and regeneration of magnetic exfoliated graphite as a new sorbent for oil pollution. *Desalination*, *263*(1), Article 1. <https://doi.org/10.1016/j.desal.2010.06.056>

Wu, Z.-Y., Li, C., Liang, H.-W., Zhang, Y.-N., Wang, X., Chen, J.-F., & Yu, S.-H. (2014). Carbon nanofiber aerogels for emergent cleanup of oil spillage and chemical leakage under harsh conditions. *Scientific Reports*, *4*(1), Article 1. <https://doi.org/10.1038/srep04079>

Zeng, Y., Wang, K., Yao, J., & Wang, H. (2014). Hollow carbon beads fabricated by phase inversion method for efficient oil sorption. *Carbon*, *69*, 25–31. <https://doi.org/10.1016/j.carbon.2013.11.036>

Zhao, B., Zhang, L., Liang, Y., Qiu, H., & Yang, J. (2012). Efficient growth of millimeter-long few-walled carbon nanotube forests and their oil sorption. *Applied Physics A*, *108*(2), 351–355. <https://doi.org/10.1007/s00339-012-6884-8>

Zheng, Y.-P., Wang, H.-N., Kang, F.-Y., Wang, L.-N., & Inagaki, M. (2004). Sorption capacity of exfoliated graphite for oils-sorption in and among worm-like particles. *Carbon*, *42*(12), 2603–2607. <https://doi.org/10.1016/j.carbon.2004.05.041>